Functionalized Single Walled Carbon Nanotube/Polymer Nanocomposite Membranes for Gas Separation and Desalination

By
Anil Kumar Surapathi

Dissertation submitted to the faculty of the Virginia Polytechnic Institute and State University in partial fulfillment of the requirement for the degree of

Doctor of Philosophy
In
Chemical Engineering

Eva Marand, Chair
J. Karl Johnson
Stephen Michael Martin
Richey M Davis

October 26, 2012
Blacksburg, VA

Keywords: Nanocomposite Membrane, Carbon Nanotube, Poly(acrylates), Polyamide, Plasma Etching, Functionalization, Gas Permeation, Gas Adsorption, Desalination.

Functionalized Single Walled Carbon Nanotube/Polymer Nanocomposite Membranes for Gas Separation and Desalination

Anil Kumar Surapathi

ABSTRACT

Polymeric membranes for gas separation are limited in their performance by a trade-off between permeability and selectivity. New methods of design are necessary in making membranes, which can show both high permeability and selectivity. A mixed matrix membrane is one such particular design, which brings in the superior gas separation performance of inorganic membranes together with the easy processability and price of the polymers. In a mixed matrix membrane, the inorganic phase is dispersed in the polymeric continuous phase. Nanocomposite membranes have a more sophisticated design with a thin separation layer on top of a porous support.

The objective of this research was to fabricate thin SWNT nanocomposite membranes for gas separation, which have both high permeability and selectivity. SWNT/polyacrylic nanocomposite membranes were fabricated by orienting the SWNTs by high vacuum filtration. The orientation of SWNTs on top of the porous support was sealed by UV polymerization. For making these membranes, the CNTs were purified and cut into small open tubes simultaneously functionalizing them with COOH groups. Gas sorption of CO_2 in COOH functionalized SWNTs was lower than in purified SWNTs. Permeabilities in etched membrane were higher than Knudsen permeabilities by a factor of 8, and selectivities were similar to Knudsen selectivities.

In order to increase the selectivities, SWNTs were functionalized with zwitterionic functional groups. Gas sorption in zwitterion functionalized SWNTs was very low compared to in COOH functionalized SWNTs. This result showed that the zwitterionic functional groups are kinetically blocking the gas molecules from entering the pore of the CNT. SWNT/polyamide nanocomposite membranes were fabricated using the zwitterion functionalized SWNTs by interfacial polymerization. The thickness of the separation layer was around 500nm. Gas permeabilities in the CNT membranes increased with increasing weight percentage of the SWNTs. Gas permeabilities were higher in COOH SWNT membrane than in zwitterion SWNT membrane. Gas selectivities were similar to the Knudsen selectivities, and also to the intrinsic selectivities in the pure polyamide membrane.

The water flux in SWNT-polyamide membranes increased with increasing weight percentage of zwitterion functionalized SWNTs, along with a slight increase in the salt rejection. Membranes exhibited less than 1% variability in its performance over three days.

Table of Contents

List of Figures

List of Tables

Chapter 1. Introduction

1.1. Problem Statement

Membranes are playing a vital role in replacing some of industry's energy intensive separation processes, such as pressure swing adsorption and cryogenic distillation. Gas separation membranes are widely used for various applications in the chemical industry. For example, membranes are used for nitrogen generation and oxygen enrichment from air, the separation of hydrogen from hydrocarbons in refinery hydrogen recovery, the removal of hydrocarbons from air in pollution control, the removal of H_2S from hydrocarbons in sour gas treating etc[1]. Baker has estimated the membrane market to $350 million in 2010 and predicted to double by 2020 to $760 million, with an average growth rate of 7-8%/year[2]. Gas separation membranes can be made of organic polymers and/or inorganic materials. Some examples of the materials for organic polymers are polysulfone, polydimethylsiloxane, polyimide etc. and for inorganic materials, carbon molecular sieves, zeolites, nanoporous carbon and porous silica. Organic polymers are the dominating material for gas separation membranes because they can be easily processed into membranes. Polymeric membranes are cheaper to produce and also, can be made into hollow fibers, whose configuration provides tremendous surface area for gas separation, thereby decreasing the foot print of a gas separation unit in a chemical plant. However, they have some disadvantages. The membranes cannot operate under harsh conditions and high temperature. For some polymers, performance decreases with time due to plasticization of the membrane by the feed components like heavy hydrocarbons.

More importantly, polymeric membranes are limited in their gas separation performance. In 1991, Robeson plotted all the available data in the literature into a log-log plot with permeability on the x-axis and selectivity on the y-axis[3,4] as shown in Figure 1-1. He observed that an upper bound exists in gas separation capabilities of polymeric membranes for different gas pairs and also described the performance of the upper bound polymers by an empirical equation. Membrane with high gas permeability has very low selectivity. Freeman provided a theoretical foundation for Robeson observation using kinetic theory and proved that an upper bound exists in the performance of polymeric membranes for gas separation[5].

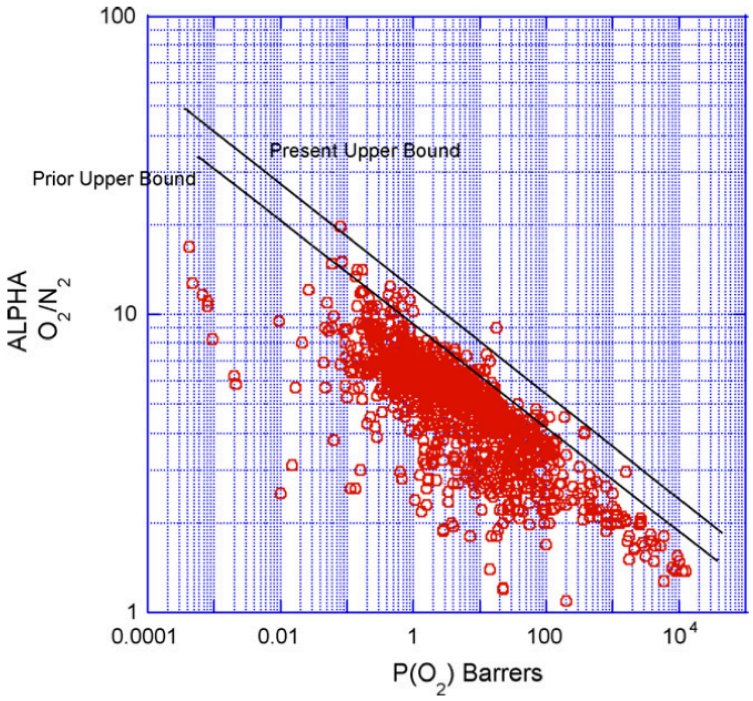

Figure 1-1. Upper bound correlation for O_2/N_2 separation[4].

Solution-diffusion model is the accepted gas transport model for membranes, with diffusivity and solubility as the model parameters[6]. Diffusion and diffusion selectivity are controlled by interchain separation and chain stiffness of polymer respectively. Increasing the interchain separation increases the penetrant diffusion in the polymer. However, the interchain separation cannot be increased to such an extent that the polymer segmental motion looses controls over the penetrant diffusion decreasing the diffusion selectivity[7]. With this limitation in diffusion selectivity, the only way to make membranes that can surpass the Robeson upper bound is by enhancing the solubility and solubility selectivity. Solubility is a thermodynamic factor and represents the interactions between a gas and a polymer. Its value depends on the nature of the gas and the polymer. Thus, it is difficult to improve/control the design of polymers for gas separations. Hence researchers started looking for new ways of fabricating membranes, which have superior performance and transcend Robeson upper bound.

Compared to polymers, molecular sieves like zeolites or carbon molecular sieves show superior selectivity for many gas mixtures due to their well defined pore structures and pore sizes. Hybrid membranes made using these inorganic materials as the dispersed phase and polymers as the continuous phase are termed 'mixed matrix membranes' (MMM)[8]. These materials systematically combine the excellent properties of the dispersed phase with the easy

processibility of the polymeric membranes. However, it is very difficult to make defect-free zeolite mixed matrix membranes. Poor adhesion between the inorganic dispersed phase and the polymer affects the selectivity, which can lead to poor performance[9,10]. Thus it is very important that the filler has good intrinsic properties and dispersability in the polymer matrix to make high performance mixed matrix membranes.

Carbon nanotubes are very interesting material when used as the dispersed phase in mixed matrix membranes. Atomistic simulations of gas transport in carbon nanotubes demonstrated that gas molecules can travel very fast inside them due to the atomically smooth inner surface of the tubes[11]. Simulations by Skoulidas et al.[12] also showed that carbon nanotube membranes have high gas transport rates. Sangil et al.[13,14] fabricated functionalized single walled carbon nanotube (SWNT)/MMMs using polysulfone or poly(imide siloxane) as the matrix material. Later, he fabricated SWNT/polysulfone nanocomposite membranes using a filtration method for alignment of SWNTs[15]. This method is very simple, fast and practical route to fabricate large quantities of SWNT/polymer membranes for gas separation. However, the fabrication procedure has certain aspects that can be improved to make membranes with even better performance. The possible problems with the SWNT/polysulfone nanocomposite membranes are bulleted and briefly discussed in the next paragraph and also the projects accomplished while solving these problems are outlined in the next section.

1. Polysulfone, the matrix material in the nanocomposite membranes, is a glassy polymer (T_g=185^{o}C) at room temperature. Therefore, it is possible that some interfacial defects might form due to the stiffness of the polymers chains, while casting the membrane film[9,16,17].
2. Polysulfone do not form any covalent bonds with the inorganic phase, SWNTs. This may compromise the strength of the interface and reduce the strength and stability of the overall membrane.
3. The thickness of the polymer/SWNT layer in Kim's composite membranes was around 1μm[15]. Decreasing the thickness of the membrane can increase the permeability of the nanocomposite membrane further by decreasing the resistance to gas transport[18,19].
4. Even though the gas permeabilities in the composite membranes were much higher than Knudsen permeabilities, the gas selectivities were almost similar to the Knudsen

selectivities[15]. If the selectivities of gases through these membranes can be altered and improved, then SWNT nanocomposite membranes may become more attractive for gas separations in the chemical industry.

We fabricated two sets of membranes: functionalized (1) SWNT/polyacrylic and (2) SWNT/polyamide nanocomposite membranes and study the gas transport properties of these membranes. It is assumed that the improved fabrication procedure of these membranes will resolve and eliminate the drawbacks of the previous SWNT/polymer nanocomposite membranes reported in the literature[15]. This effort would help in making SWNT/polymer nanocomposite membranes more attractive and economical in producing large amounts of the desired gas with high purity in chemical industries.

1.2. Research Studies

A summary of the various research efforts encompassing this thesis is presented below.

1. **Functionalized SWNTs/polyacrylic nanocomposite membranes** – The fabrication and characterization of COOH functionalized SWNT/polyacrylic nanocomposite membranes is studied. The goal of this investigation is to fabricate membranes employing in-situ polymerization thereby avoiding any interfacial defects and having good dispersion of SWNTs within the polymer matrix without any agglomeration. The thickness of the membrane should be decreased below 1μm to reduce the resistance to gas transport resulting in high gas fluxes.
2. **Role of solubility partition coefficient at the mixed matrix interface in the performance of the mixed matrix membranes** – Diffusivity of gas in a mixed matrix membrane is predicted using the effective medium theory developed by Landauer. This model incorporates K, the solubility partition coefficient of the diffusing gas between the matrix polymer and the inorganic dispersed phase. Model Predictions are compared to experimental results validating the effectiveness of the theory in predicting the gas diffusivity in mixed matrix membrane.
3. **Gas separations: Zwitterion functionalized SWNT/polyamide membranes** – The fabrication and characterization of zwitterion functionalized SWNT-polyamide membranes is studied. SWNTs are functionalized with short

zwitterion groups. Thin SWNT-polyamide membranes are fabricated employing interfacial polymerization. Membranes are tested for their gas permeation properties.

4. **Desalination: Zwitterion functionalized SWNT/polyamide membranes** – The water permeation and salt rejection of thin zwitterion functionalized SWNT-polyamide nanocomposite membranes is investigated. Experiments are conducted to prove the hypothesis that water flux and salt rejection increases by adding functionalized SWNTs into the polyamide layer of the membrane.

1.3. Outline of Chapters

Chapter 2 consists literature review of gas separation membranes. The history of the development of membranes is discussed briefly followed by gas transport in membranes. Transport model called 'solution-diffusion' model, mixed matrix membranes and the properties of carbon nanotubes are discussed along with an extensive review on the development of carbon nanotube membranes.

Chapter 3 describes the fabrication of SWNT/polyacrylic nanocomposite membranes and their gas transport properties. Raw SWNTs were purified by two-step purification method and chemically cut to form small open tubes simultaneously functionalized with COOH groups. Dispersion of COOH functionalized SWNTs was filtered through a porous support partially aligning the SWNTs. Aligned SWNTs were embedded within an acrylate polymer matrix by UV polymerization. Membranes were oxygen plasma etched to remove the excess polymer on top exposing the tips of the CNTs. Sorption studies were performed on raw, purified and purified-cut SWNTs. The concentration of light gases sorbed was higher in purified SWNTs compared to in raw SWNTs. Concentration of CO_2 gas sorbed in COOH functionalized SWNTs was half the concentration in raw SWNTs. Gas permeabilities in 75min etched membrane were higher than Knudsen permeabilities by a factor of 8. However, the gas selectivities were similar to Knudsen selectivities. This chapter laid the foundation for further exploring functionalization of CNTs to improve gas selectivities in CNT membranes.

Chapter 4 describes the gas sorption properties of zwitterion functionalized SWNTs. The chemical conversion of COOH functionalized SWNTs into zwitterion functionalized SWNTs was discussed. Zwitterion SWNTs were characterized by x-ray photoelectron spectroscopy (XPS) and thermogravimetric analysis (TGA). XPS results showed that the atomic percentage of

oxygen and nitrogen was higher in zwitterion SWNTs compared to in COOH SWNTs. TGA graph indicated that zwitterion SWNTs contained loosely bound water, which was removed by heating to 200^{o}C. Gas sorption isotherms showed that the concentration of the gases absorbed in zwitterion SWNTs were much lower compared to in COOH SWNTs. The concentration of CO_2 absorbed in heated zwitterion SWNTs (non-hydrated) was higher than in non-heated zwitterion SWNTs (hydrated). Simulations results showed that zwitterion groups in the ends of SWNTs kinetically blocked the sorption of CO_2 inside the nanotube. This effect was more pronounced in the presence of pre-absorbed water. This result was supported by the potential of mean force graph, which showed that the energy barrier to CO_2 sorption inside the tube was higher in zwitterion SWNTs than in COOH SWNTs.

Chapter 5 discusses the fabrication procedure of thin film zwitterion SWNT-polyamide nanocomposite membranes. Dispersion of functionalized SWNTs was filtered through a porous polyethersulfone support partially aligning the SWNTs. SWNTs were embedded within a thin polyamide layer by interfacial polymerization. The cross-section of the membrane was imaged by scanning electron microscopy. The thickness of the SWNT-polyamide layer in the membrane was around 500nm. Gas transport properties of the membranes with increasing SWNT concentration were studied. Gas permeabilities in zwitterion functionalized SWNT thin film nanocomposite (TFN) membranes increased with increasing weight percentage of the functionalized SWNTs in the separation layer. Gas permeabilities in COOH functionalized SWNT TFN membranes were higher compared to in zwitterion SWNT TFN membranes. However, the gas selectivities were very close to the Knudsen selectivities, which were also very similar to the intrinsic gas selectivities in the neat polyamide membrane. The gas transport results were explained using a proposed three-path diffusion model.

Chapter 6 describes the role of K, the solubility partition coefficient in predicting the diffusivity of gas in mixed matrix membrane (MMM). Effective medium theory was employed to predict the gas diffusivity in a mixed matrix membrane. The effect of partition coefficient, K, volume fraction, ε, ratio of diffusivity in the matrix polymer to in dispersed phase on effective diffusivity in the mixed matrix membrane was studied. Some experimental data on gas permeabilities in MMMs published in literature were explained using this theory. Predictions were made using the diffusivity of gas in matrix polymer and dispersed phase, and also compared to the experimental results.

Chapter 7 describes the water transport results in zwitterion functionalized SWNT-polyamide nanocomposite membranes. Thin film nanocomposite membranes with increasing concentration of functionalized SWNTs were tested for their salt rejection properties. Water flux increased by three times in 20wt% SWNT TFN membrane compared to in neat polyamide membrane, with a slight increase in salt rejection. The membrane performance showed very small variability within the experiment time. Atomistic simulations predicted that the flux of salt ions through membrane with SWNTs functionalized with two zwitterion groups was zero whereas ions passed through COOH functionalized SWNT membrane.

Finally **Chapter 8** and **Chapter 9** present the conclusions of the research efforts and future work aimed at making better membranes.

1.4. References

1. Nunes, S. P. & Peinemann, K. V. *Membrane technology in the chemical industry*. (Wiley-VCH: 2006).
2. Baker, R. W. Future Directions of Membrane Gas Separation Technology. *Ind. Eng. Chem. Res.* **41**, 1393–1411 (2002).
3. Robeson, L. M. Correlation of separation factor versus permeability for polymeric membranes. *Journal of Membrane Science* **62**, 165–185 (1991).
4. Robeson, L. M. The upper bound revisited. *Journal of Membrane Science* **320**, 390–400 (2008).
5. Freeman, B. D. Basis of Permeability/Selectivity Tradeoff Relations in Polymeric Gas Separation Membranes. *Macromolecules* **32**, 375–380 (1999).
6. Wijmans, J. G. & Baker, R. W. The solution-diffusion model: a review. *Journal of Membrane Science* **107**, 1–21
7. Bernardo, P., Drioli, E. & Golemme, G. Membrane Gas Separation: A Review/State of the Art. *Ind. Eng. Chem. Res.* **48**, 4638–4663 (2009).
8. Kulprathipanja, S. *Zeolites in Industrial Separation and Catalysis*. (John Wiley & Sons: 2010).
9. Mahajan, R. & Koros, W. J. Factors Controlling Successful Formation of Mixed-Matrix Gas Separation Materials. *Ind. Eng. Chem. Res.* **39**, 2692–2696 (2000).
10. Li, Y., Chung, T.-S., Cao, C. & Kulprathipanja, S. The effects of polymer chain rigidification, zeolite pore size and pore blockage on polyethersulfone (PES)-zeolite A mixed matrix membranes. *Journal of Membrane Science* **260**, 45–55 (2005).
11. Skoulidas, A. I., Ackerman, D. M., Johnson, J. K. & Sholl, D. S. Rapid Transport of Gases in Carbon Nanotubes. *Phys. Rev. Lett.* **89**, 185901 (2002).
12. Skoulidas, A. I., Sholl, D. S. & Johnson, J. K. Adsorption and diffusion of carbon dioxide and nitrogen through single-walled carbon nanotube membranes. *J. Chem. Phys.* **124**, 054708–054707 (2006).
13. Kim, S., Chen, L., Johnson, J. K. & Marand, E. Polysulfone and functionalized carbon nanotube mixed matrix membranes for gas separation: Theory and experiment. *Journal of Membrane Science* **294**, 147–158 (2007).
14. Kim, S., Pechar, T. W. & Marand, E. Poly(imide siloxane) and carbon nanotube mixed

matrix membranes for gas separation. *Desalination* **192**, 330–339 (2006).
15. Kim, S., Jinschek, J. R., Chen, H., Sholl, D. S. & Marand, E. Scalable Fabrication of Carbon Nanotube/Polymer Nanocomposite Membranes for High Flux Gas Transport. *Nano Lett.* **7**, 2806–2811 (2007).
16. Mahajan, R. & Koros, W. J. Mixed matrix membrane materials with glassy polymers. Part 1. *Polym. Eng. Sci.* **42**, 1420–1431 (2004).
17. Mahajan, R. & Koros, W. J. Mixed matrix membrane materials with glassy polymers. Part 2. *Polym. Eng. Sci.* **42**, 1432–1441 (2004).
18. Pinnau, I. & Koros, W. J. Relationship between substructure resistance and gas separation properties of defect-free integrally skinned asymmetric membranes. *Ind. Eng. Chem. Res.* **30**, 1837–1840 (1991).
19. Henis, J. M. S. & Tripodi, M. K. Composite hollow fiber membranes for gas separation: the resistance model approach. *Journal of Membrane Science* **8**, 233–246 (1981).

Chapter 2. Literature Review

2.1. Introduction

A membrane is a thin layer that acts as a selective barrier between two phases and impermeable to certain molecules, particles or substances under a driving force like temperature, pressure or concentration gradient. It is selectively more permeable to one component compared to the other hence separating the components from each other. Use of membranes for gas separation has started only 30 years back, beginning in 1980 with Permea (now a division of Air Products) by launching its hydrogen separating Prism membrane[1]. Since then, membrane-based gas separation has grown into a million dollar industry. Membrane based separations have the advantage of low operation costs, module design of membranes provide large surface area for separation thereby having smaller foot print in a chemical plant, low energy and labor costs. A schematic of a membrane separating components A and B is shown in Figure 2-1. When component A permeates faster than B, the permeate gets enriched in A and depleted in B.

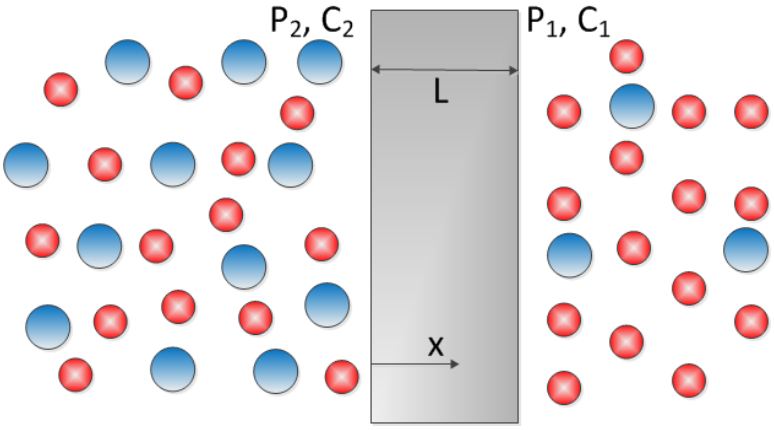

Figure 2-1. Gas separation through a polymeric membrane. Blue circles represent the less permeating gas component B and red circles represent fast permeating gas component A. P_2 and C_2 are the pressure and concentration on the feed side respectively, and P_1 and C_1 on the permeate side.

In 1829, Thomas Graham performed experiments involving transport of gases and vapors in polymeric membranes. Later, in 1866, he proposed the 'solution-diffusion mechanism' for gas permeation. Benchold defined the relationship between physical properties like bubble point, surface tension, pore radius and the performance of membranes. In 1907, Benchold also devised a technique to prepare nitrocellulose membranes of particular pore size and developed an important concept of pore-size distribution. Karplus improved the technique of preparing nitrocellulose membranes. Later, in 1940, cellulose acetate membranes were used in

microfiltration and for filtration of drinking water[2]. The membranes developed by Loeb-Sourirajan for reverse osmosis had transformed the membrane separation from a concept to an industrial process. In the late 1970, separations by membranes became economically competitive and companies like Monsanto made Prism membranes for separation of hydrogen stream from the product stream of ammonia. Cynara and Separex made membranes for separation of carbon dioxide. In 1980, the development and refinement of synthetic polymeric membranes helped in making lot of progress in membrane science and technology[2].

2.2. Gas Transport in Membranes

2.2.1. Polymeric Membranes

Transport in non-porous polymeric membranes is based on 'solution-diffusion' concept. According to this model, permeate first dissolves in the membrane material and then diffuse through this membrane down a concentration gradient. A separation is achieved between different permeates because of difference in the amount of gas that dissolves in the membrane and the rate at which the gas diffuses through the membrane[3].

2.2.1.1. Transport Parameters of Gas Permeation in Membranes

The gas flux through a membrane is given by

$$N = P\left(\frac{\Delta P}{l}\right) \qquad \text{Equation 2-1}$$

So, $P = \frac{N.l}{(p_2 - p_1)}$ Equation 2-2

where p_2 and p_1 is the pressure of the feed stream and the permeate stream respectively as shown in Figure 2-1. The proportional co-efficient in the above equations, P, is defined as the permeability coefficient and l, the thickness of the membrane.

At steady state, Fick's first law gives the gas flux at any point inside the polymer.

$$N = \left(\frac{-D}{1-w}\right)\frac{dC}{dx} \qquad \text{Equation 2-3}$$

where N is the gas flux, C is the gas concentration, x is the distance across the film, w is the mass fraction of gas in the polymer and D is the binary mutual diffusion coefficient of the gas in the polymer.

Combining Equation 2-2 and Equation 2-3,

$$P = -\frac{D}{1-w}\frac{l}{(p_2 - p_1)}\frac{dC}{dx} \qquad \text{Equation 2-4}$$

Integrating the above equation across the film (from x=0, $C=C_2$ to x=l, $C=C_1$)

$$P = \frac{1}{(p_2 - p_1)} \int_{C_1}^{C_2} \frac{D}{1-w}\, dC$$

$$= \frac{(C_2 - C_1)}{(p_2 - p_1)} . \frac{1}{(C_2 - C_1)} \int_{C_1}^{C_2} \frac{D}{1-w}\, dC$$

$$= \frac{(C_2 - C_1)}{(p_2 - p_1)} [D] \qquad \text{Equation 2-5}$$

where $[D] = \frac{1}{(C_2 - C_1)} \int_{C_1}^{C_2} \frac{D}{1-w}\, dC$ Equation 2-6

is called the average effective diffusion coefficient.

When the upstream pressure and concentration (p_2 and C_2 respectively) are much greater than their downstream analogs, the above result simplifies as

$$P = \frac{C_2}{p_2} [D]$$

$$= [S][D] \qquad \text{Equation 2-7}$$

where [S] = C_2/p_2 is the equilibrium solubility coefficient of a gas in a polymer, defined as the ratio of the concentration of gas dissolved in the polymer at equilibrium to the partial pressure of the gas in the continuous phase. P depends upon two factors: (1) a thermodynamic term, S; characterizing the number of gas molecules sorbed into and onto the polymer and (2) a kinetic or mobility term, D; characterizing the mobility of gas molecules as they diffuse through the polymer. Permeability is the pressure and thickness normalized gas flux through the polymer film. P depends upon the product of the number of gas molecules that dissolve in the polymer and their rate of migration through the polymer matrix.

Ideal gas selectivity is defined as $\alpha_{AB} = P_A/P_B$ where P_A and P_B are the permeability coefficient of gases A and B respectively. Ideal selectivity can be partitioned into diffusivity and solubility selectivity.

$$\alpha_{AB} = (D_A/D_B)\,(S_A/S_B) = \alpha_{AB}^{D} \alpha_{AB}^{S} \qquad \text{Equation 2-8}$$

The separation factor, α^*_{AB}, determined from the ability of a membrane to separate feed gas mixture, is defined as

$$\alpha_{AB}^{*} = (y_A/y_B)/(x_A/x_B) \qquad \text{Equation 2-9}$$

where y_A and y_B are the mole fractions of the components produced in the permeate, and x_A and x_B are the corresponding mole fractions in the feed.

2.2.1.2. Robeson Upper Bound

The desirable properties of a synthetic polymer membrane are high permeability and high selectivity. Robeson has systematically plotted all the available gas permeation data of polymeric membranes and observed an upper limit in their separation performance[4,5] as shown in Figure 2-2. These upper bound lines can be predicted from theoretical considerations based on either free volume (or) transition state models, leading to the development of the following correlation[6]

$$\alpha_{AB} = \frac{\beta_{A/B}}{P_A^{\lambda_{A/B}}} \qquad \text{Equation 2-10}$$

where P_A is the permeability of the more permeable gas, $\alpha_{A/B}$ is the selectivity; and $\beta_{A/B}$ and $\lambda_{A/B}$ are model parameters. $\lambda_{A/B}$, slope of the upper bound line can be calculated from the kinetic diameters of the gas molecule

$$\lambda_{A/B} = \left(\frac{d_B}{d_A}\right)^2 - 1 \qquad \text{Equation 2-11}$$

where d_B and d_A are the kinetic diameters of the largest and smallest gas molecules. The position of the upper bound line, $\beta_{A/B}$, depends on gas molecule size and solubility as given in[6].

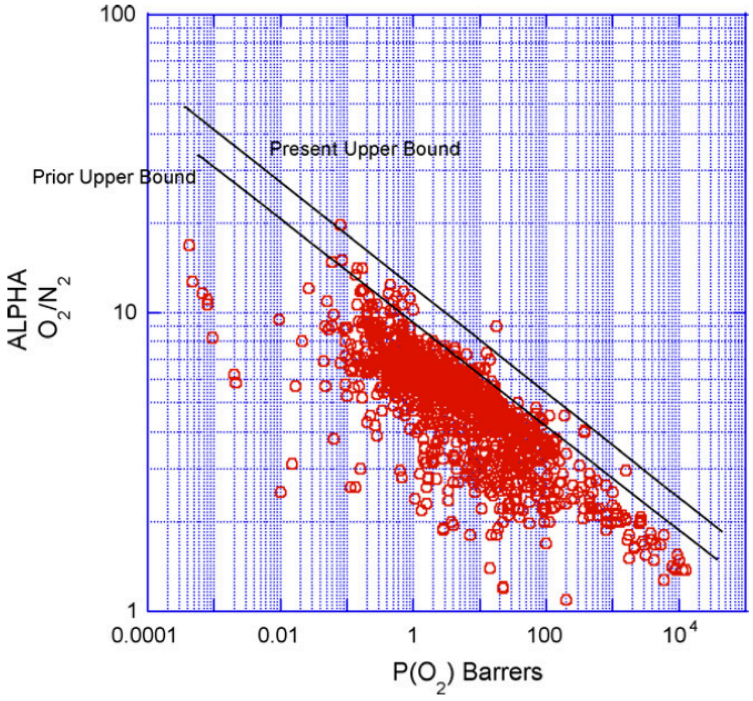

Figure 2-2. Upper bound correlation for O_2/N_2 separation[5].

2.2.2. Mixed Matrix Membranes

Polymeric membranes show an upper limit in their gas separation performance[4,5]. Systematic optimization in the backbone structure of the polymers had increased the performance of polymeric membranes, but could not surpass the Robeson upper bound of important gas separations, such as O_2/N_2. Zeolites, carbon molecular sieves (CMS) and rigid rod polymers have attractive transport properties but they are very difficult and expensive to process. Hence a hybrid approach is necessary to incorporate the properties of molecular sieves with the easy processibility of polymers. A mixed matrix membrane (MMM) has the molecular sieving material embedded within the polymer substrate. The advantages of the MMMs are that they are economical to produce and show good gas separation performance. However, to observe these expected performance in MMMs, it is very important that the membranes do not have any defects at the molecular sieve/polymer interface and also careful matching of the intrinsic permeability and selectivity of the support matrix and molecular sieve domains is necessary[1,7-9]. MMMs were made using zeolites and rubbery or glassy polymers. An increase in the O_2/N_2 selectivities was observed when zeolites were added to the matrix compared to pure polymer[2,10-13]. When using glassy polymers, interfacial voids can form around the molecular sieves and cause failure of the membranes in exhibiting the anticipated O_2/N_2 performance. Composite membranes have the advantage of containing thin dense selective layer on a porous support and hence lower resistance to gas permeation. Using MMM concept and the composite membrane design, nanocomposite membranes can be fabricated containing thin dense selective MMM layer with high loading of molecular sieves on a suitable porous support.

2.2.2.1. Permeability Predictions in MMM

Prediction of permeability of gas penetrants with the nature, characteristics and concentration of molecular sieves and the matrix polymer is necessary for efficient design of the mixed matrix membrane for gas separation[2,14]. The models developed for predicting the permeability of the gases through the MMMs are mainly based on thermal or electrical conductivity approach. A number of theoretical models are available for predicting the permeation properties of MMMs as a function of permeabilities of continuous phase and dispersed phase. Some of the models, which are widely used for predicting gas permeation properties of MMMs, as well as their advantages and limitations are reported in the article[14].

2.3. Carbon Nanotubes (CNT)

Since the discovery of multi-walled and single-walled carbon nanotubes by Iijima in 1991[3,15] and 1993[4,5,16] respectively, many studies and applications of carbon nanotubes in membranes, electronic materials and structured materials have been investigated.

2.3.1. Structure of CNTs

Carbon nanotubes are member of the fullerene family. They are graphene sheets in cylindrical form with the ends covered by half a fullerene molecule. They are sp^2 hybridized. Nanotubes are held by Vander Waals forces, which bundle them together to form ropes. Hydrogen can be reversibly stored in CNTs. Depending on the chirality of the carbon nanotubes, they can behave either as metallic or semi-conductive. This leads to their use in nanoscale devices. Carbon nanotubes demonstrate high strength, flexibility and resilience. They exhibit Young's modulus of about 1 Terapascal.

There are two types of carbon nanotubes – single walled carbon nanotubes (SWNTs) and multi walled carbon nanotubes (MWNTs). MWNT is comprised of 2 to 30 concentric graphitic layers, diameters of which range from 10 to 50nm and lengths of more than 10μm. On the other hand, SWNT has only one graphite layer and typical diameter from 1nm to 1.4nm[6,17]. Carbon nanotubes can be synthesized by various methods: electric arc discharge method, laser ablation method, chemical catalytic vapor deposition method (CVD) and high-pressure carbon monoxide disproportionation (HiPCO) method. The purity and quality of the carbon nanotubes is largely dependent on the synthesis method.

2.3.2. Gas Transport Through SWNTs

Ackerman et al. performed atomistic simulations to compute the self-diffusivity and transport diffusivity of Ar and Ne through single walled carbon nanotubes pores at room temperature[6,18]. The self-diffusivities were one to three orders of magnitude faster in carbon nanotubes than in silicalite, depending on the equilibrium pressure. The transport diffusivities were three orders of magnitude faster in nanotubes than in silicalite over all equilibrium pressures. The fluxes of Ar and Ne were predicted to be four orders of magnitude greater through hypothetical membrane of nanotubes than through silicalite membranes of the same thickness.

Skoulidas et al.[5,19] performed atomistic simulations to compute self and transport diffusivities of light gases like hydrogen and methane in carbon nanotubes and in two zeolites with comparable pore sizes. They found that the transport rate was orders of magnitude higher in

nanotubes compared to the zeolites. They also predicted that membranes made with carbon nanotubes have fluxes orders of magnitude higher than crystalline zeolite membranes. Skoulidas et al.[4,5,20] also performed atomistic simulations to examine the adsorption and transport diffusion of CO_2 and N_2 in single walled carbon nanotubes at room temperature as a function of nanotube diameter. They also calculated the permeance of N_2 through a (40,40) SWNT membrane and compared with experimental results by Hinds et al[21]. They found that the permeance predicted was 30 times larger than the experimental data, which might be due to the imperfections and some blocked nanotubes in the real membranes.

Chen et al.[22] studied the diffusion of CH_4/H_2 mixtures in single walled carbon nanotubes. They found that the self-diffusivities and Fickian diffusivities of CH_4 and H_2 in an equimolar mixture in (10,10) SWNT were very similar to those of the pure components, and extraordinarily large compared to diffusivities in other nanoporous materials (zeolites). However, all the above work done by the various groups did not consider flexibility of the carbon nanotube in their atomistic simulations. Later, Chen et al.[23] examined the influence of nanotube flexibility on the transport diffusion of CH_4 in (20,0) and (15,0) nanotubes. The inclusion of nanotube flexibility reduced the transport diffusion relative to the rigid nanotube by roughly an order of magnitude close to zero pressures, but at pressures above about 1 bar the transport diffusivities for flexible and rigid nanotubes were very similar, differing by less than a factor or two on average. Finally, Chen et al.[24] performed atomistic simulations to predict the binary permeance of CH_4/H_2 mixtures through defect free (10,10) single walled carbon nanotubes at room temperatures. Their results predicted that carbon nanotubes are strongly selective for CH_4 over H_2 when a mixture of these gases permeates through a membrane. Simulations by all these researchers in their respective work predicted that the fluid transport through carbon nanotubes is extremely fast, due to inner atomically smooth surface. Thus CNT use in membranes can help in making high flux membranes.

2.4. Carbon Nanotube/Polymer Membranes

In 2004, Holt et al.[25] had fabricated a carbon nanotube-embedded silicon nitride membrane to study the nanometer-scale mass transport. CNT arrays were grown on Si substrate and infiltrated with low-stress silicon nitride by CVD process. The top surface was etched to remove excess silicon nitride and exposed the tips of CNTs. The measured D_2O diffusive flux through the membrane was 2.4×10^{-8} mol/m^{2}s, which was much lower than the value calculated

by hydrodynamics, 1.91 mol/m^2s. This decrease in flux was believed to be due to the 'bamboo' structure of the CNTs. Then, the CNTs were removed by oxidation to make nanoporous silicon nitride membranes and the N_2 permeance was measured again. From the pore density value and assuming the diffusion to be Knudsen inside the nanopores, the pore diameter was calculated, which was compared with the diameter value of MWNTs obtained from TEM images. The values agreed with each other and hence it was concluded that for pores of 60 nm diameter, Knudsen diffusion is the mode of gas transport inside the pores of carbon nanotubes.

In 2004, Hinds et al. fabricated aligned MWNT membranes[21]. An array of MWNTs grown by CVD on quartz substrate was spin-coated by polysulfone. Hydrofluoric acid was used to remove the membrane film from the quartz substrate. The top excess polymer layer was etched by plasma oxidation process and opened the tips of CNTs. The membrane was treated with HCl to remove the iron catalyst. The N_2 permeance in the membrane is 2.6 μmol/(m^2 s Pa), which is comparable with the value calculated using the Knudsen diffusion transport model and pore diameter of 7.5nm. Plasma oxidation functionalized the tips of the CNTs with COOH groups, which were subsequently functionalized with biotin and streptavidin. The membranes functionalized with biotin-streptavidin showed a reduction in $Ru(NH_3)_6^{+3}$ flux by factor of 15. Thus, Hind's group demonstrated the feasibility of functionalizing CNTs with certain groups and altering the selectivity of CNT membranes.

In 2007, Sangil et al. fabricated carbon nanotube/polymer nanocomposite membranes by filtration method[26]. The author used filtration to orient the carbon nanotubes on a filter support. Polystyrene was spin coated on top to seal the structure. They found that the gas permeabilities in these membranes were higher than Knudsen permeabilities. The selectivities of single gas permeation fell on the same trend as the Knudsen selectivities. However, for mixed gas permeation, selectivity of CO_2/CH_4 was higher than the single gas permeation selectivities. This might be due to the strong adsorption of CO_2 inside the CNT and also pore entrance/exit effects may play a role in molecular sorption.

2.5. References

1. Baker, R. W. Future Directions of Membrane Gas Separation Technology. *Ind. Eng. Chem. Res.* **41**, 1393–1411 (2002).
2. Pandey, P. & Chauhan, R. S. Membranes for gas separation. *Progress in Polymer Science* **26**, 853–893
3. Wijmans, J. G. & Baker, R. W. The solution-diffusion model: a review. *Journal of Membrane Science* **107**, 1–21

4. Robeson, L. M. Correlation of separation factor versus permeability for polymeric membranes. *Journal of Membrane Science* **62**, 165–185 (1991).
5. Robeson, L. M. The upper bound revisited. *Journal of Membrane Science* **320**, 390–400 (2008).
6. Freeman, B. D. Basis of Permeability/Selectivity Tradeoff Relations in Polymeric Gas Separation Membranes. *Macromolecules* **32**, 375–380 (1999).
7. Mahajan, R. & Koros, W. J. Factors Controlling Successful Formation of Mixed-Matrix Gas Separation Materials. *Ind. Eng. Chem. Res.* **39**, 2692–2696 (2000).
8. Mahajan, R. & Koros, W. J. Mixed matrix membrane materials with glassy polymers. Part 1. *Polym. Eng. Sci.* **42**, 1420–1431 (2004).
9. Mahajan, R. & Koros, W. J. Mixed matrix membrane materials with glassy polymers. Part 2. *Polym. Eng. Sci.* **42**, 1432–1441 (2004).
10. Paul, D. R. & Kemp, D. R. The diffusion time lag in polymer membranes containing adsorptive fillers. *J. polym. sci., C Polym. symp.* **41**, 79–93 (1973).
11. Kulprathipanja, S., Neuzil, R. W. & Li, N. N. Separation of fluids by means of mixed matrix membranes. **95/51**, (1988).
12. Süer, M. G., Baç, N. & Yilmaz, L. Gas permeation characteristics of polymer-zeolite mixed matrix membranes. *Journal of Membrane Science* **91**, 77–86 (1994).
13. Duval, J. M. *et al.* Preparation of zeolite filled glassy polymer membranes. *J. Appl. Polym. Sci.* **54**, 409–418 (1994).
14. Shimekit, B., Mukhtar, H. & Murugesan, T. Prediction of the relative permeability of gases in mixed matrix membranes. *Journal of Membrane Science* **373**, 152–159 (2011).
15. Iijima, S. Helical microtubules of graphitic carbon. *Nature* **354**, 56–58 (1991).
16. Iijima, S. & Ichihashi, T. Single-shell carbon nanotubes of 1-nm diameter. *Nature* **363**, 603–605 (1993).
17. Tanaka, K., Yamabe, T. & Fukui, K. *The science and technology of carbon nanotubes*. (Elsevier: 1999).
18. Ackerman, D., Skoulidas, A., Sholl, D. & Johnson, J. K. Diffusivities of Ar and Ne in Carbon Nanotubes. *Mol. Simulation* **29**, 677–684 (2003).
19. Skoulidas, A. I., Ackerman, D. M., Johnson, J. K. & Sholl, D. S. Rapid Transport of Gases in Carbon Nanotubes. *Phys. Rev. Lett.* **89**, 185901 (2002).
20. Skoulidas, A. I., Sholl, D. S. & Johnson, J. K. Adsorption and diffusion of carbon dioxide and nitrogen through single-walled carbon nanotube membranes. *J. Chem. Phys.* **124**, 054708–054707 (2006).
21. Hinds, B. J. *et al.* Aligned Multiwalled Carbon Nanotube Membranes. *Science* **303**, 62–65 (2004).
22. Chen, H. & Sholl, D. S. Rapid Diffusion of CH_4/H_2 Mixtures in Single-Walled Carbon Nanotubes. *J. Am. Chem. Soc.* **126**, 7778–7779 (2004).
23. Chen, H., Johnson, J. K. & Sholl, D. S. Transport Diffusion of Gases Is Rapid in Flexible Carbon Nanotubes. *J. Phys. Chem. B* **110**, 1971–1975 (2006).
24. Chen, H. & Sholl, D. S. Predictions of selectivity and flux for CH_4/H_2 separations using single walled carbon nanotubes as membranes. *Journal of Membrane Science* **269**, 152–160 (2006).
25. Holt, J. K., Noy, A., Huser, T., Eaglesham, D. & Bakajin, O. Fabrication of a Carbon Nanotube-Embedded Silicon Nitride Membrane for Studies of Nanometer-Scale Mass Transport. *Nano Lett.* **4**, 2245–2250 (2004).

26. Kim, S., Jinschek, J. R., Chen, H., Sholl, D. S. & Marand, E. Scalable Fabrication of Carbon Nanotube/Polymer Nanocomposite Membranes for High Flux Gas Transport. *Nano Lett.* **7**, 2806–2811 (2007).

Chapter 3. Fabrication and Gas Transport Properties of SWNT/Polyacrylic Nanocomposite Membranes

3.1. Introduction

There has been a rising interest in carbon nanotube, CNT membranes, since Sholl et al.[1] has reported simulation results predicting extremely high gas diffusivity in carbon nanotubes. Their work hypothesized that vertically aligned CNTs forming a membrane should have gas transport properties transcending Robeson's upper bound[1,2]. Indeed, recent experimental work has confirmed the high permeability in CNT membranes[3-6]. Holt et al.[4] have constructed nanotube-Si_3N_4 composite membranes using chemical vapor deposition. They used aligned double walled carbon nanotubes having a diameter of about 1.6 nm and confirmed that gas flow through narrow carbon nanotubes is orders of magnitude faster than would be expected for flow through a traditional nanoporous material. They also found that liquid water flow through their nanotube membranes was more than three orders of magnitude faster than predicted by hydrodynamic flow models. However, no selectivity for gas mixtures was demonstrated.

In related work, Hinds and coworkers[6] constructed polymer-nanotube composite membranes using multiwall carbon nanotubes having much larger diameters (6-7 nm) than those used by Holt et. al. They have also verified that transport of liquids (alkanes, water) is orders of magnitude faster than can be accounted for by conventional hydrodynamic flow[7].

More recently, Lin et al. [8]have fabricated vertically aligned multi-walled carbon nanotubes supported by porous α-alumina by a multi-step method consisting of growing vertical CNTs by chemical vapor deposition, filling the inter-CNT gaps with polystyrene and removing the PS over-layer by polishing and acid treatment . The average CNT pore dimensions were 6.3 nm. As expected the resulting CNT membranes exhibited gas diffusivity values about four times larger than the values predicted by the Knudsen diffusion model. However, the H_2/N_2 selectivity was 3.8, which is order of magnitude lower than what can be achieved by polymeric membranes. For example, polyamide and polyimide membranes have H_2/N_2 selectivity of about 200.

The gas selectivity of carbon nanotube membranes have been difficult to achieve, because the CNT pore sizes employed have been too large to effectively separate gases with kinetic diameters on the order of 3 Angstroms by size exclusion.

A key to developing carbon nanotube membranes that show high selectivity as well as high flux is the control of the diameter of the nanotubes. Recent studies suggest that single

walled carbon nanotubes, SWNT, can be synthesized with pore diameters down to 0.4 nm[9-11] and that multi-walled carbon nanotubes, MWNTs, can be made with inner tubes having about this same diameter[12]. Alternatively, the effective CNT pore sizes can be adjusted by introducing functional groups on the tips of CNTs with larger pore diameters[13].

Another challenge is the fabrication of defect-free, large-scale CNT membranes with highly ordered vertical orientation of densely packed small-diameter pores. A common method to fabricate CNT membranes is to employ chemical vapor deposition that relies on precise catalyst patterning and expensive substrate materials[3-5]. Because the area of CVD-prepared CNT membranes is constrained by the size of the reactor, scale up costs are prohibitive. To date, the CNT pore sizes obtained by the CVD method are much too large to be effective in gas separations. To overcome this challenge, we have developed a method of fabricating vertically oriented carbon nanotubes on a porous support using hydro-dynamically driven self-assembly of the carbon nanotubes[14]. The carbon nanotubes can be obtained commercially or synthesized specifically for a given application with the desired pore size. Furthermore, the CNTs can be purified and their pore size and pore-size distribution can be characterized before they are assembled into a CNT membrane.

In this work we describe a complete SWNT purification and characterization approach, which is part of the CNT membrane preparation process. The membrane formation involves encapsulation of the oriented CNTs in an in-situ polymerized polyacrylic matrix that has to be systematically removed to expose the carbon nanotubes pores on the feed-side of the membrane. Specifically, we compare the transport properties of CNT membranes prepared under different polymer etching conditions.

3.2. Experimental

3.2.1. Purification, Cutting and Functionalization of SWNTs

HiPCO single walled carbon nanotubes (SWNTs, as-received) were purchased from Unidym, California. The reported individual SWNT diameter and length were 0.8-1.2nm and 100-1000nm respectively. The catalyst (Fe) content was less than 15wt%. SWNTs were purified of Fe catalyst, amorphous carbon and other carbonaceous impurities. Then, the long entangled ropes of SWNTs were cut into small open tubes by employing the cutting method. While cutting and opening the SWNTs, they were also functionalized with COOH groups on the sidewalls and

the terminal ends of the nanotubes. The detailed procedure for purification, cutting and functionalization of SWNTs with COOH groups are given in the following sections.

3.2.1.1. Purification

As-received SWNTs were purified using a two-step purification method as described by Cinke et al.[15] In the first step, 100 mg of SWNTs were suspended in a solvent mixture of 200 ml dimethylformamide and 100 μl ethylenediamine. The mixture was stirred for 18 h followed by 6.5 h sonication. The solution was filtered using a 0.45 μm pore diameter hydrophobic filter (Millipore, Fluoropore membrane) and washed with methanol twice. SWNTs were collected and air-dried overnight. The entire procedure was repeated once more. In the second step, the treated SWNTs were sonicated in 250 ml of 37% HCl for 30 min and stirred at 45 ^{o}C for 2 h. The solution was filtered using a 0.45 μm pore diameter hydrophilic filter (Millipore, LCR Membrane) and washed with deionized water. Again, SWNTs were air-dried overnight. Then, they were placed inside a quartz tube, which was fed with a stream of wet air. The tube was maintained at 225 ^{o}C for 18 h and then, SWNTs were cooled to room temperature. The acid cleaning step and oxidation using wet air was repeated three more times but the oxidation temperatures were different each time (325 ^{o}C for 1.5 h, 425 ^{o}C for 1 h). Finally, the purified SWNTs were vacuum dried at 80 ^{o}C.

3.2.1.2. Cutting and COOH Functionalization

The purified carbon nanotubes were shortened in length by chemical cutting. The procedure for cutting is similar to as described by Liu et al[16]. 2 mg of SWNTs were added to every 1 ml of acid mixture consisting of sulfuric acid and nitric acid (3:1, v/v), and sonicated for 4 h at 50 ^{o}C. After sonication, they are filtered using 0.1 μm pore size filter (Millipore, Isopore membrane) and thoroughly washed with deionized water. Cutting introduces carboxylic acid functional groups (COOH) on the sidewalls and the openings of the cut tubes as shown in Figure 3-1[17,18].

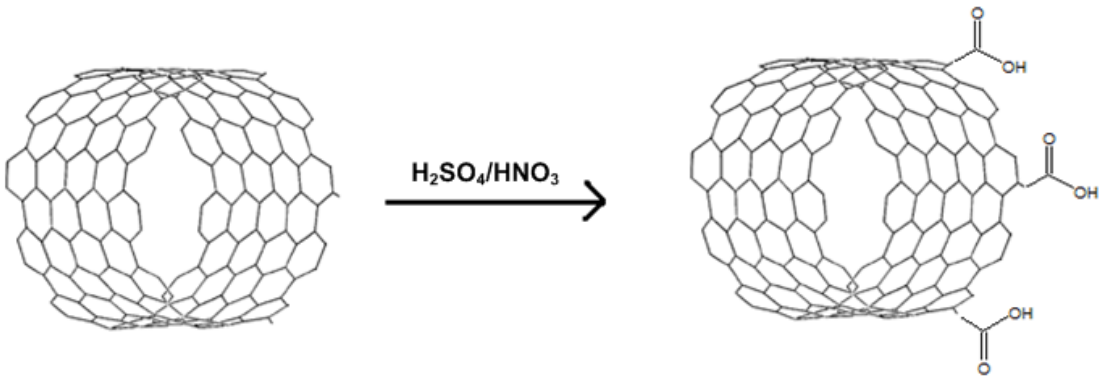

Figure 3-1. Schematic of functionalization of SWNTs.

3.2.2. Membrane Fabrication

5 mg of cut SWNTs were dispersed in 15 ml of anhydrous THF. The solution was sonicated for 2 h and filtered using a 0.45 μm filter (PTFE, hydrophilic, Millipore). A copolymer of butyl methacrylate (BMA) and butyl acrylate (BA) (90:10, w/w) was prepared by free radical polymerization. 5 g of BMA and BA monomer mixture were added to 10 g of n-methyl pyrrolidone. 0.0577 g of azobisisobutyronitrile, thermal initiator was added to it. The mixture was heated to 65 ^{o}C for 24 hours under nitrogen protection. The polymer was collected through precipitation in 100% ethanol and dried at 80 ^{o}C under vacuum in an oven for 24 h. 0.3 g of poly(n-butyl methacrylate)/poly(butyl acrylate) blend was dissolved in 3 ml of anhydrous THF and 5.57 μl of 2-hydroxy-2-methylpropiophenone (Darocur 1173), the initiator for the ultraviolent (UV) polymerization was added to the mixture.

A Millipore PTFE filter disc with an oriented carbon nanotube layer prepared by hydrodynamic[19] assembly was placed upside down in a Teflon plate prefilled with the monomer/initiator solution mixture. The polymer/SWNTs were UV polymerized using a 365 nm wavelength light for 4 h under nitrogen environment. After curing, the membrane was dried at room temperature for 24 h and removed from the plate.

In order to expose the terminal end of the SWNTs, excess polymer on top of the membrane was etched-off using a PE-100 Benchtop Plasma Etcher. Ultra high-grade purity oxygen gas was used for etching the membrane. The flow rate of the oxygen gas inside the plasma etcher was 15 sccm and the vacuum level inside the chamber was in the range 1.5-3.0 Torr. The membranes were etched for 30, 45, 60 and 75 min.

3.2.3. Characterization Methods

Field emission scanning electron microscopy (FESEM, LEO 1550) was performed on as-received, purified and purified-cut SWNTs. The sample for FESEM was prepared by suspending a small amount of SWNTs in DMF, putting a drop of the suspended liquid on clean silicon wafer and allowing it to dry for 2 days. Silicon wafers were cleaned by sonication in acetone for 1 h and then, washing them with deionized water.

Sorption studies on purified and purified-cut SWNTs samples were performed using Intelligent Gravimetric Analyzer (IGA 002), Hiden Analytical Inc., UK. High vacuum ($P<10^{-4}$ mbar) was applied for degassing the samples, chamber and tubing. While degassing the sample, in addition to applying high vacuum, it was also heated to 200 ^{o}C for 8 h. This would remove any dissolved/sorbed gases in the sample. IGA measures the change in the weight of the sample with change in pressure and calculates the moles of gas adsorbed per gram of the sample at a particular temperature, producing an isotherm. For the sorption runs, around 40 mg of the sample was used so that significant amount of sorption takes place in the sample and less error in measurements. In the analysis of the data on the IGA software, the weight of the sample at zero mbar (lowest pressure) was always automatically chosen as the weight to be subtracted from the weights of the sample at higher pressures to calculate the moles of gas absorbed in the sample.

Permeability of gases through the nanocomposite membranes was measured using a constant volume varying pressure apparatus. All the runs were performed with 2 atm feed pressure at room temperature. Membranes were masked using an aluminum tape. The diameter of permeating area of a masked membrane was 1 cm. The edge of the permeating area on the masked membrane was sealed with epoxy on both sides. The whole permeation setup was degassed for 2 h. The permeate pressure was monitored and recorded real time in the computer using Lab View. Data was collected until the permeate pressure reaches the maximum 10 cm of Hg. Then, permeate pressure vs. time data was analyzed to calculate the permeability of gas through the membrane. The gases used in the experiment were hydrogen (H_2), oxygen (O_2), nitrogen (N_2), methane (CH_4) and carbon dioxide (CO_2). Each gas was tested three times and the average was reported.

Raman spectra were collected with Nicolet Almega XR dispersive micro-Raman spectrometer using 633 nm excitation length. X-ray photoelectron spectroscopy (XPS, PHI Quantera SXM) was employed to observe the COOH groups on the SWNTs. Sample for this

analysis was prepared by spreading CNT powder on a copper tape and blowing away any loose powder by air duster. A pore and surface analyzer (PSA, Quantachrome, Autosorb 1C) was used to measure the N_2 isotherm of the SWNTs at 77 K. The CNT sample was degassed for 24 h at 200 ^oC before any measurement. The water contact angle was measured using a goniometer (Kruss DSA-100). A small drop of DI water was placed on the film using a syringe. The drop was viewed using a camera and a picture was taken for analysis. Drop shape analysis software was employed to measure the contact angle from the picture using best-fit method.

3.3. Results and Discussion

3.3.1. Characterization of Single Walled Carbon Nanotubes

3.3.1.1. Purification

The as-received HiPCO SWNTs contained catalyst particles, amorphous carbon and other carbonaceous impurities as can be seen in Figure 3-2(a) and (b). The SWNTs are entangled and covered with amorphous carbon, which showed as bright particles. It was necessary to remove these impurities from the SWNTs prior to their use in membrane fabrication. The two-step purification method purified the SWNTs as can be seen in Figure 3-3(a). The SWNTs are still entangled but do not exhibit any brighter areas in the micrograph indicating that all or most of the amorphous carbon was removed and the SWNTs are clean. The first step in the purification process dispersed the bundles of SWNTs by allowing the amine groups in ethylendiamine and amide groups in dimethylformamide to interact with the π-electrons of SWNTs, leading to intercalation[15]. The second step of the purification process removed the Fe catalyst by reacting it with HCl to form $FeCl_2$ in solution with the release of hydrogen gas. Exposing CNTs to wet air at different temperatures removed the amorphous carbon and all other carbonaceous impurities. This step also exposed the catalyst particles covered by amorphous carbon[15].

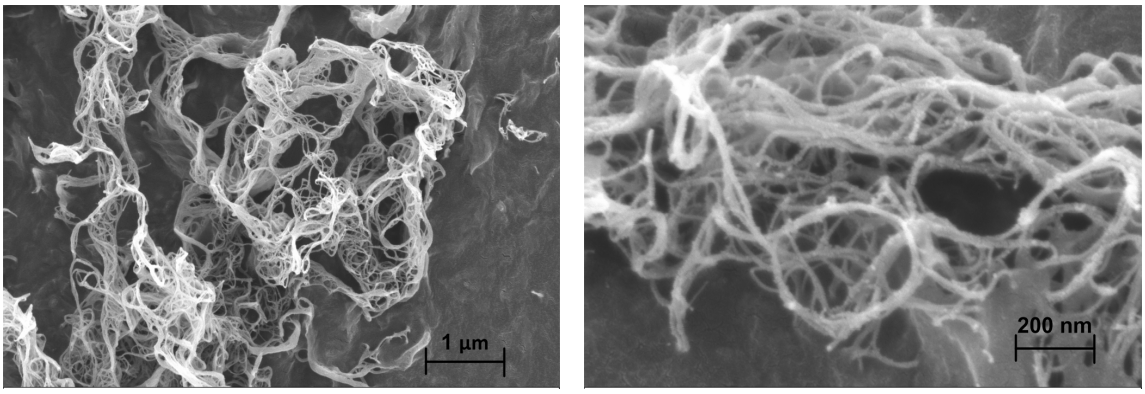

(a) (b)

Figure 3-2. (a) and (b) SEM micrographs of as-received HiPCO SWNTs at different magnifications

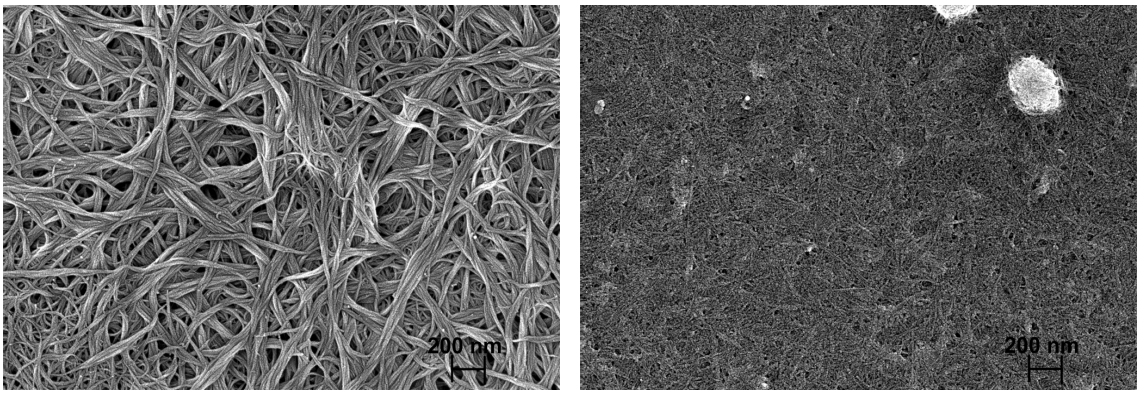

(a) (b)

Figure 3-3. SEM micrograph of (a) the purified SWNTs and (b) purified-cut SWNTs

3.3.1.2. Cutting and Functionalization

After purifying SWNTs, the long ropes of SWNTs were cut into small open tubes. Sonication of the purified SWNTs in the oxidizing mixture cut the SWNTs into small tubes[16] of length approximately 100 nm from an initial length of 1000 nm as seen in Figure 3-3(b). Cutting procedure also introduced carboxylic acid groups on the ends and sidewalls of the cut SWNTs. This has been verified by XPS analysis on both purified and functionalized SWNTs. XPS is a quantitative spectroscopic technique that measures the elemental composition, empirical formula, chemical state and electronic state of the elements that exist within a material. It is a surface chemical analysis technique that can be used to analyze the surface chemistry of the material. XPS spectra is obtained by irradiating a material with a beam of X-rays while simultaneously measuring the kinetic energy and number of electrons that escape from the top of 1 to 10 nm of the material being analyzed.

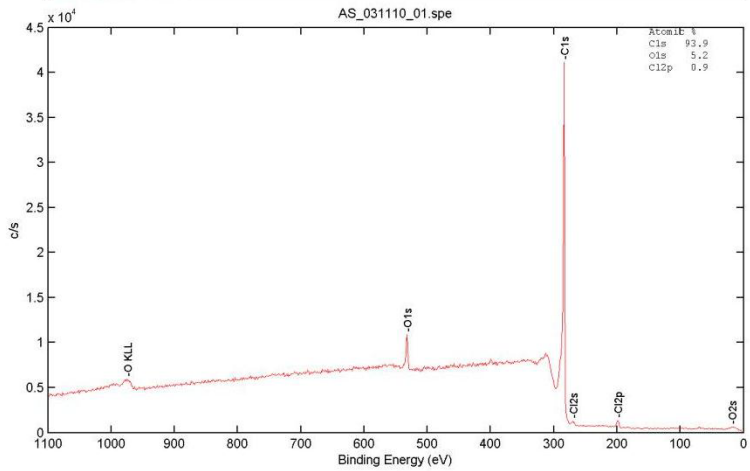

Figure 3-4. XPS survey spectrum of purified SWNTs. (A survey spectrum is a spectrum having peaks for all of the elements within an energy range.)

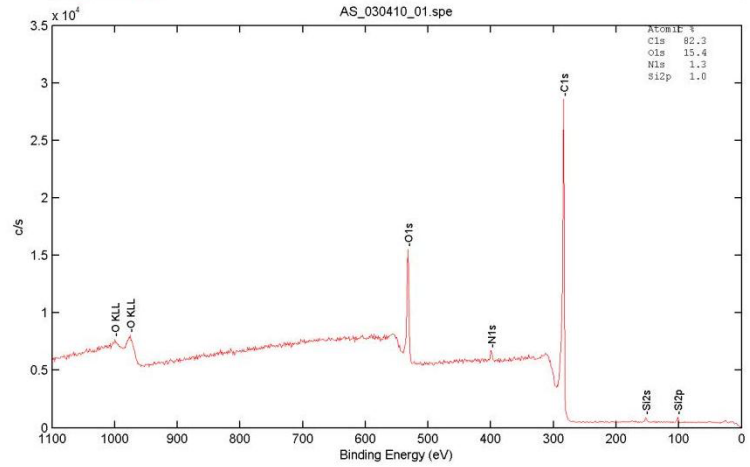

Figure 3-5. XPS survey spectrum of COOH functionalized (purified-cut) SWNTs.

Figure 3-4 and Figure 3-5 are the survey spectrums of purified and COOH functionalized SWNTs. The atomic composition of the material can be calculated from the height and area under the peak representing each element. Table 3-1 shows the percentage of carbon and oxygen in both samples. An increase in percentage of oxygen and decrease in carbon from sample (i) to (ii) indicated that cutting introduced COOH groups on the SWNTs[20].

Table 3-1. Percentage of C1S and O1S in the purified and purified-cut SWNTs samples.

Sample	**Type of SWNTs**	**C1S%**	**O1S%**
(i)	Purified	93.9	5.2
(ii)	Purified and Cut	82.3	15.4

Table 3-2. Samples of SWNTs with their respective *G/D* ratio.

Sample	***G/D* ratio**
Manufacture	16.4
As-received	10.6
Purified-cut	3.6

Cutting of SWNTs may also introduce defects on the SWNTs. Figure 3-7 compares the Raman spectra of the as-received and functionalized samples with the spectrum provided by the manufacturer, Unidym. Table 3-2 specifically compares the *G/D* ratio of the various samples. A typical Raman spectrum of carbon nanotubes is shown in Figure 3-6[21]. It shows the possible wavenumber ranges in which different modes of resonance in SWNTs are observed. 'Radial breathing modes' (RBM) are the modes in which all the atoms of the CNTs vibrate radially. These are low energy modes typically observed at Raman shifts between 150 and 350 cm^{-1}. The energy of these vibrational modes only depends on the diameter *d* of the SWNTs. The tangential modes are the intensive high-energy modes of SWNTs and form the G-band, which is observed at around 1600 cm^{-1}. *G/D* ratio is the ratio of the intensity of the G+ peak and the defect induced D-band peak (around 1300 cm^{-1}) in a Raman spectrum. This ratio depends on the concentration of the defects in the SWNTs assuming (i) the intensity of the G-band is independent of the defect concentration and (ii) the intensity ratio does not depend on any other effects[22].

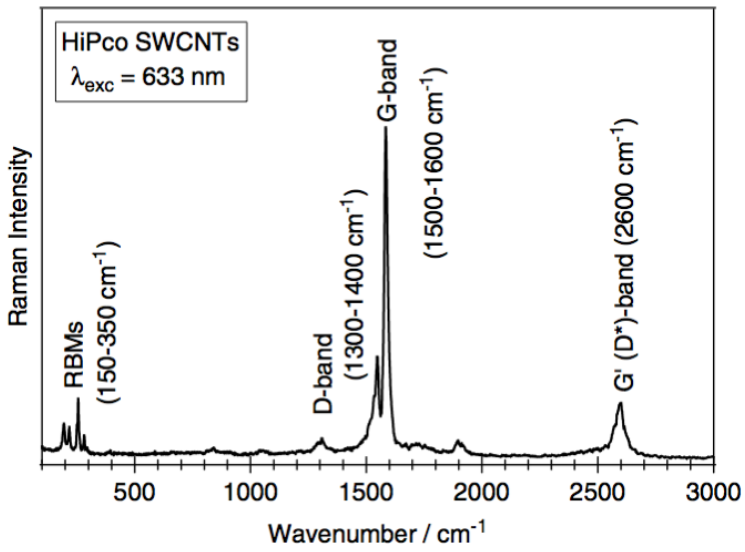

Figure 3-6. Raman spectrum of HiPCO SWNTs using a laser wavelength of λ_{exec}=633 nm[21] [used with permission].

The *G/D* ratio of the SWNTs measured by Unidym was 16.4 compared to our measurement of 10.6 on the as-received SWNTs. After functionalization, the *G/D* ratio decreased to 3.6. Although this indicates that some defects had formed during functionalization, this suggests that the quality of the functionalized SWNTs remained relatively high[21].

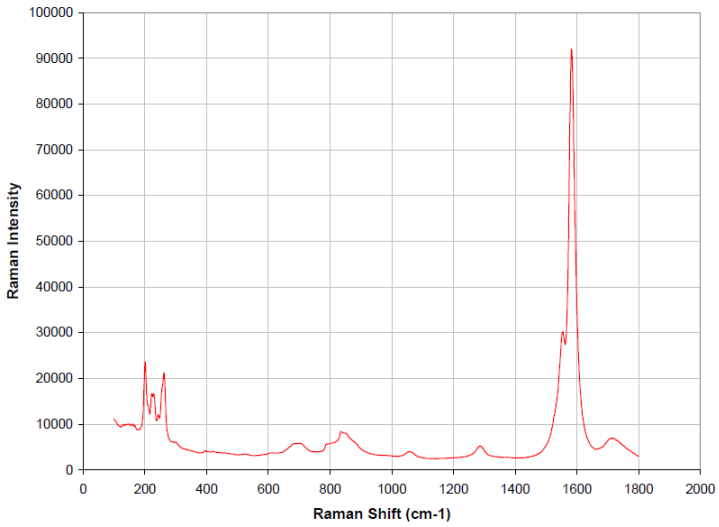

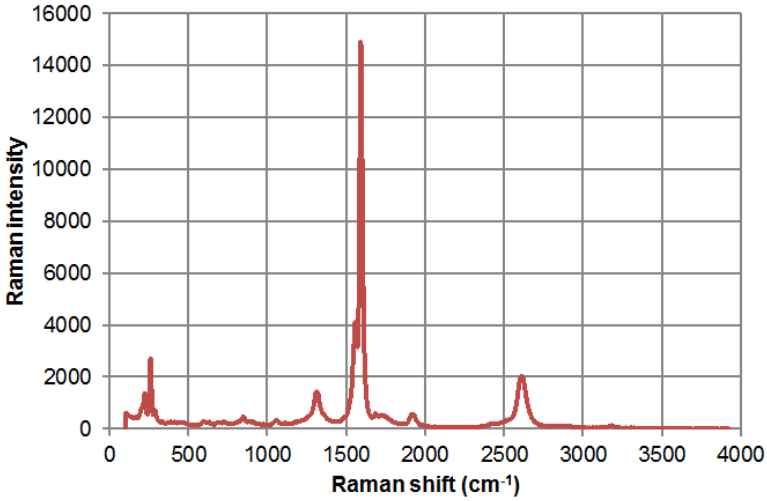

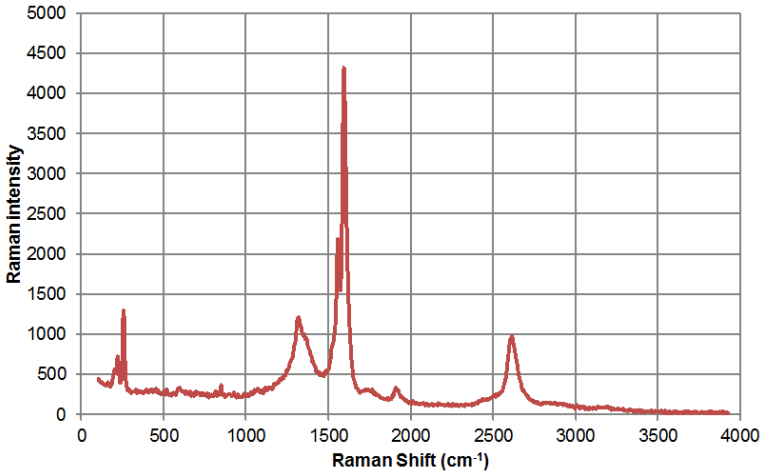

Figure 3-7. Raman spectra of SWNTs (a) Manufactured (Unidym) (b) purified and (c) purified-cut (COOH) functionalized SWNTs.

It is possible that purification destroys small diameter carbon nanotubes. To verify that the average diameter of the CNT has not changed during purification, the CNT samples were characterized by BET analysis. The pore size and pore-size distribution of the purified-cut SWNTs were obtained from BET analysis of an N_2 isotherm. Figure 3-8 shows the pore size distribution of purified SWNTs, which is centered at 8 Å. This result is consistent with the pore diameter reported by the manufacturer. Furthermore, analysis of the Raman spectral region (for all samples) has resulted in pore sizes around 9 Å. As discussed before, the 'radial breathing mode' (RBM) of SWNTs in a Raman spectrum can be used to calculate its diameter. When the diameter is in the range of 0.9-1.3 nm, the relation d (nm)=248/ω (cm^{-1}), where d is the diameter and ω is the RBM frequency, can be used to calculate the diameter[23]. The RBM frequency (ω) of the pristine and functionalized SWNTs was 259 cm^{-1} and 255 cm^{-1} respectively. The diameter, calculated using the above relation for both samples was 0.96 nm and 0.97 nm respectively, which is consistent with the pore sizes measured by Porosimetry. These results further demonstrated that the purification and functionalization method preserved the small diameter SWNTs.

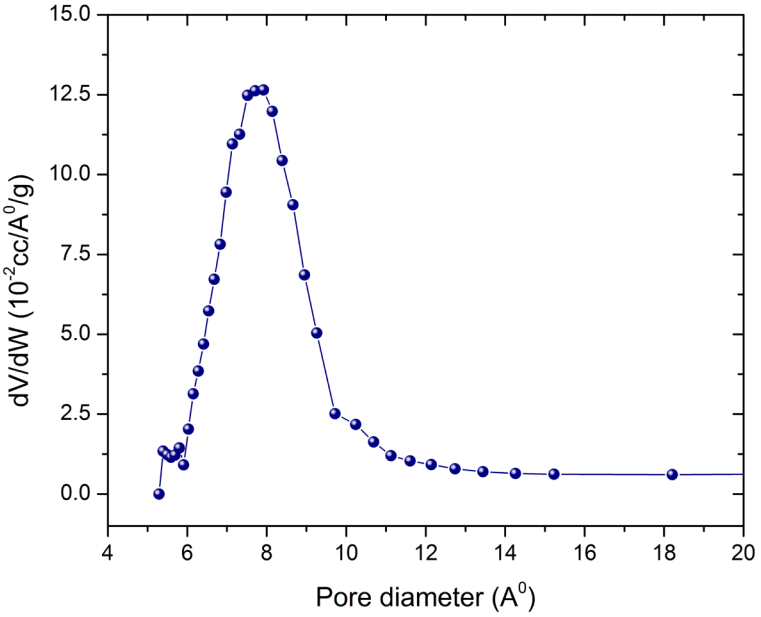

Figure 3-8. Pore size distribution of purified SWNTs.

3.3.1.3. Gas Sorption Isotherms

It is very important that the dispersed phase in a mixed matrix membrane have desirable intrinsic properties to observe similar properties for the overall membrane. In simpler words, the permeability of gases through CNTs should be high in order to make high gas permeability CNT nanocomposite membranes. Since permeability happens in two phases, sorption and diffusion, it is very important that CNTs have both high gas diffusivity and sorption. Simulations by Sholl et al. showed that CNTs have high diffusion and sorption of gases[1,2,24,25]. Gas sorption studies were performed on as-received (sample 1), purified (sample 2) and purified-cut (sample 3) SWNTs using the following gases: hydrogen (H_2), oxygen (O_2), nitrogen (N_2), methane (CH_4) and carbon dioxide (CO_2). The results from this study help in observing any change in the sorption properties of CNTs between as-received, purified and COOH functionalized SWNTs.

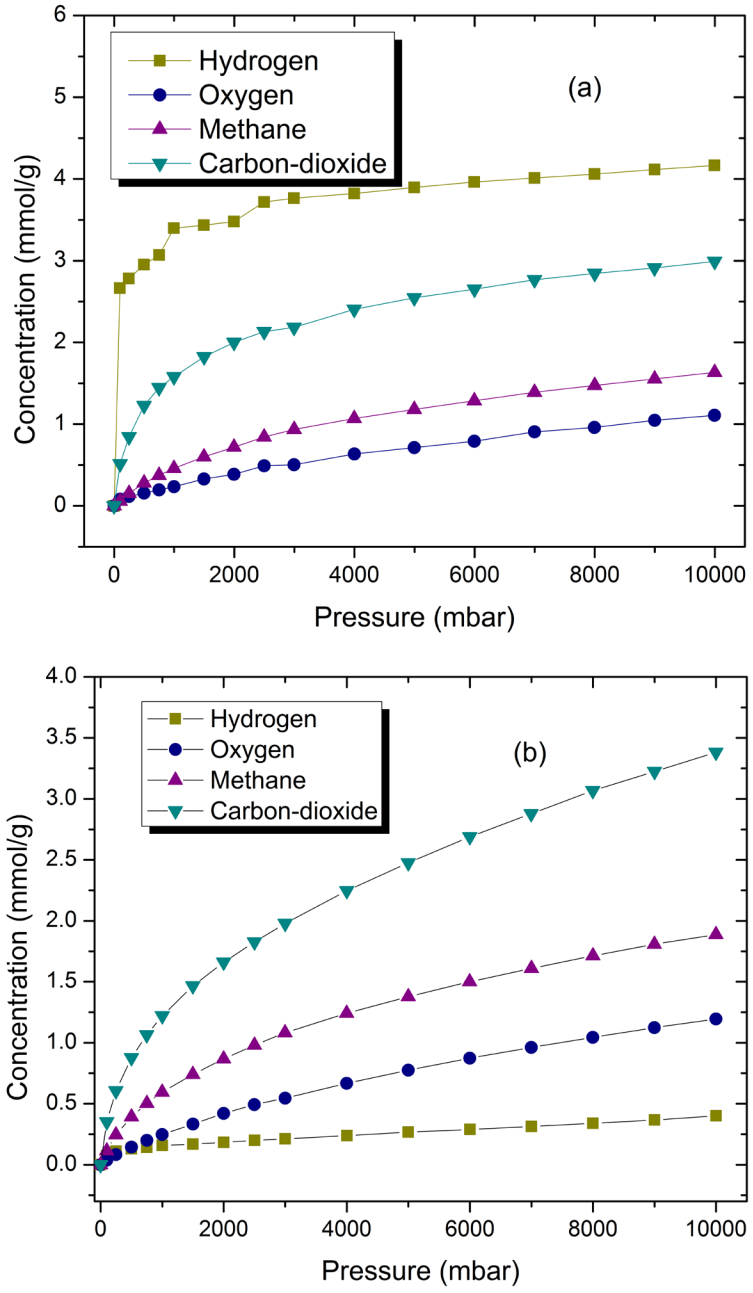

Figure 3-9. Gas Sorption isotherm of samples (a) as-received sample 1 and (b) purified sample 2

All runs were performed at 308 K. Comparison of gas sorption isotherms except that of hydrogen between sample 1 shown in Figure 3-9(a) and sample 2 shown in Figure 3-9(b) indicate that the concentration of gases adsorbed in sample 2 (purified) at any pressure was higher than in sample 1 (as-received). Because the two-step purification process de-bundled the SWNTs and increased the available surface area, the sorption of gases in sample 2 increased. The catalyst particles in sample 1 led to an undesirable sorption of H_2 in the as-received sample

due to favorable interaction between H_2 gas and Fe particles. These catalyst particles might even block the pore of CNT tube and decrease the amount of gas sorbed in it. These results point to the necessity of purifying the SWNTs prior to their use in membrane fabrication. Otherwise, unwanted sorption and blocking of inside of tube for diffusion of gas will reduce the performance of the membrane for gas separation.

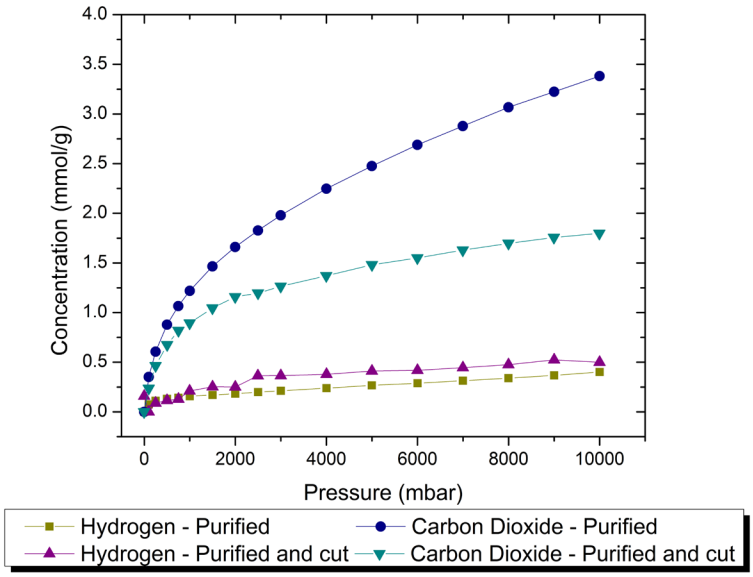

Figure 3-10. Comparison of sorption of hydrogen and carbon dioxide gases for sample 2 and 3.

The effect of opening the SWNTs by cutting and functionalization with COOH groups on gas sorption was also examined. The gas sorption isotherms of H_2 and CO_2 for uncut sample 2 and functionalized sample 3 are compared in Figure 3-10. While the concentration of H_2 gas adsorbed in sample 3 increased slightly in comparison to sample 2 within the pressure range of 0-10 bar, the concentration of carbon dioxide in sample 3 decreased to nearly half the value of sample 2 at higher pressures. This effect can be explained by a combination of size exclusion and molecular-molecular interactions between the COOH functional groups and the carbon-dioxide molecule. While the COOH functional groups can partially block the entry to the CNT pores by virtue of their molecular size, they can also interact with CO_2 via quadrupole-dipole, thus increasing the associated complex in size and exclude additional CO_2 from the SWNT pore. This effect would limit the adsorption of gas to the exterior walls of the SWNTs. On the other hand, the kinetic diameter of hydrogen is very small and has no dipole moment and so, the interactions with the SWNT tips are not significant enough to affect its sorption in the SWNTs.

3.3.2. Gas Transport Properties of SWNTs/Polymer Composite Membrane

SWNT/polymer nanocomposite membranes were fabricated with variable composite structure. The different samples that allow the comparison of gas transport in cut vs. uncut(closed) SWNTs are described in Table 3-3.

Table 3-3. Samples used in the study of transport properties of nanocomposite membranes

Name of the Sample	Description of the sample
Sample A	Polyacrylic layer supported by PTFE filter disc
Sample B	CNT composite membrane with uncut (closed) SWNTs and polyacrylic coating
Sample C	CNT composite membrane consisting of COOH functionalized (open) SWNTs and polyacrylic coating
Sample D	Sample C etched for 60 min
Sample E	Sample C etched for 75 min

The sample gas permeabilities are compared with Knudsen permeabilities and selectivities graphically in Figure 3-11 and Figure 3-14 respectively. The gas flow rate in Knudsen flow regime can be estimated from Equation 3-1[5]:

$$Q = \frac{2}{3}\sqrt{\frac{8\pi}{MRT}}\left(\frac{d}{2}\right)^3 V_m \frac{\Delta P}{L}\sigma A \qquad \text{Equation 3-1}$$

where Q is the flow rate, M is molecular weight of penetrant, R is the universal gas constant, T is absolute temperature, d is the inner diameter of nanotube, V_m is the molar volume, ΔP=2 atm is the pressure difference between permeate and feed side, L=50μm is the thickness of the membrane, $\sigma = 7.0 \times 10^9$ nanotubes/cm^2 is the area density[14], and A=0.786cm^2 is the effective membrane area.

Since, the permeability is defined as

$$P = \frac{Q \times L}{A \times \Delta P} \qquad \text{Equation 3-2}$$

then

$$P_{Knudsen} = \frac{2}{3}\sqrt{\frac{8\pi}{MRT}}\left(\frac{d}{2}\right)^3 V_m \sigma \qquad \text{Equation 3-3}$$

Knudsen permeability was calculated using Equation 3-3 for all the gases tested.

Table 3-4. Permeabilities of various gases through different composite membranes

Name of the Gas	Permeability [10^{-10} cc(STP).cm/cm^2 sec atm]					
	Knudsen	*Sample A*	*Sample B*	*Sample C*	*Sample D*	*Sample E*
Hydrogen	1501	714	1095	1078	527	11884
Helium	1067	-	-	-	-	8069
Oxygen	377	197	112	318	188	3433
Nitrogen	403	59	-	92	97	3716
Methane	533	124	81	175	134	5449
Carbon-dioxide	322	1129	457	1683	745	3712

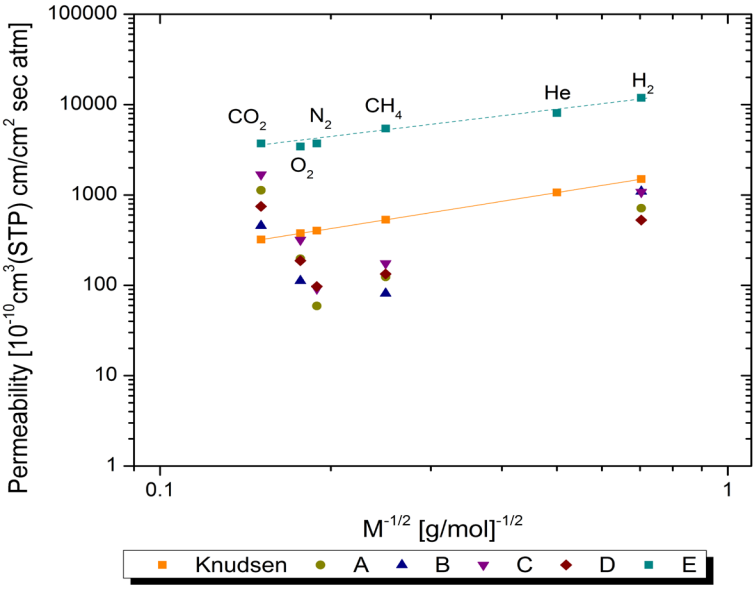

Figure 3-11. Permeability of gases through different SWNT/nanocomposite membranes. (Error bars are approximately the same size as the symbols.)

Sample A is the control for the gas transport study. The butyl acrylate polymer with its relatively low permeability of gases is a good material for the membrane matrix since it acts as a barrier in between the carbon nanotubes. This sample exhibited low permeability as seen in Figure 3-11 and Table 3-4. Thus, the permeation in nanocomposite membrane is expected to take place predominantly through the open SWNTs rather than through the polymer matrix.

Sample B is a SWNT/polymer nanocomposite membrane made with as-received SWNTs. Gases have a rapid transport through SWNTs due to their smooth inner atomic surface. So, it can be hypothesized that (in the absence of defects) any increase in permeability of gases through this nanocomposite membrane in comparison to the control is due to the gases diffusing through SWNTs inside the membrane. However, in comparison to the control sample A, the permeability of all gases except that of hydrogen has decreased in sample B. This seems reasonable, since the as-received SWNTs are not cut, the tubes are closed and gas molecules cannot permeate through the inner pores. In fact, the un-cut SWNTs acts more as filler, increasing the tortuosity of the permeation path. The observed decrease in permeability is also an indication of good interface compatibility between SWNTs and the polymer within the membrane. The small increase in permeability of hydrogen in the un-cut SWNT membranes is due to the enhanced sorption of gas by the catalyst present along with the CNTs in the membrane.

Sample C membrane was fabricated using purified-cut SWNTs. The cutting opens the SWNTs allowing the gas to diffuse in them and thus, increases the gas permeabilities. The gas permeabilities had increased in sample C as seen in Figure 3-11 and Table 3-4. In this membrane, a thin layer of polymer above the open-SWNTs layer was still contributing to the total resistance to gas permeation. Hence, etching this excess polymer layer and exposing the tips of the SWNTs is expected to further increase the gas permeabilities.

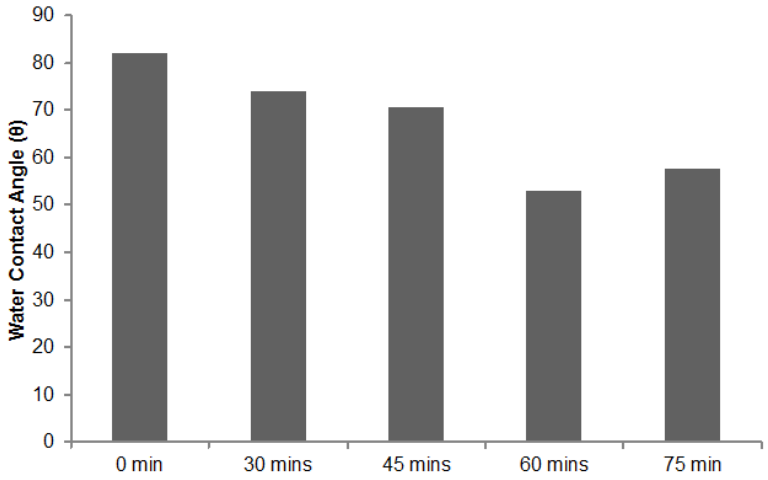

Figure 3-12. Water contact angle on sample C membrane etched for different times

Sample C was etched for etching times of 30, 45, 60 and 75 min and water contact angle was measured after each step. The results are shown in Figure 3-12. Therefore, etching the membrane for at least 60 min removed the excess top polymer layer and exposed for two

different times, 60 min (sample D) and 75 min (sample E) were chosen for further transport studies.

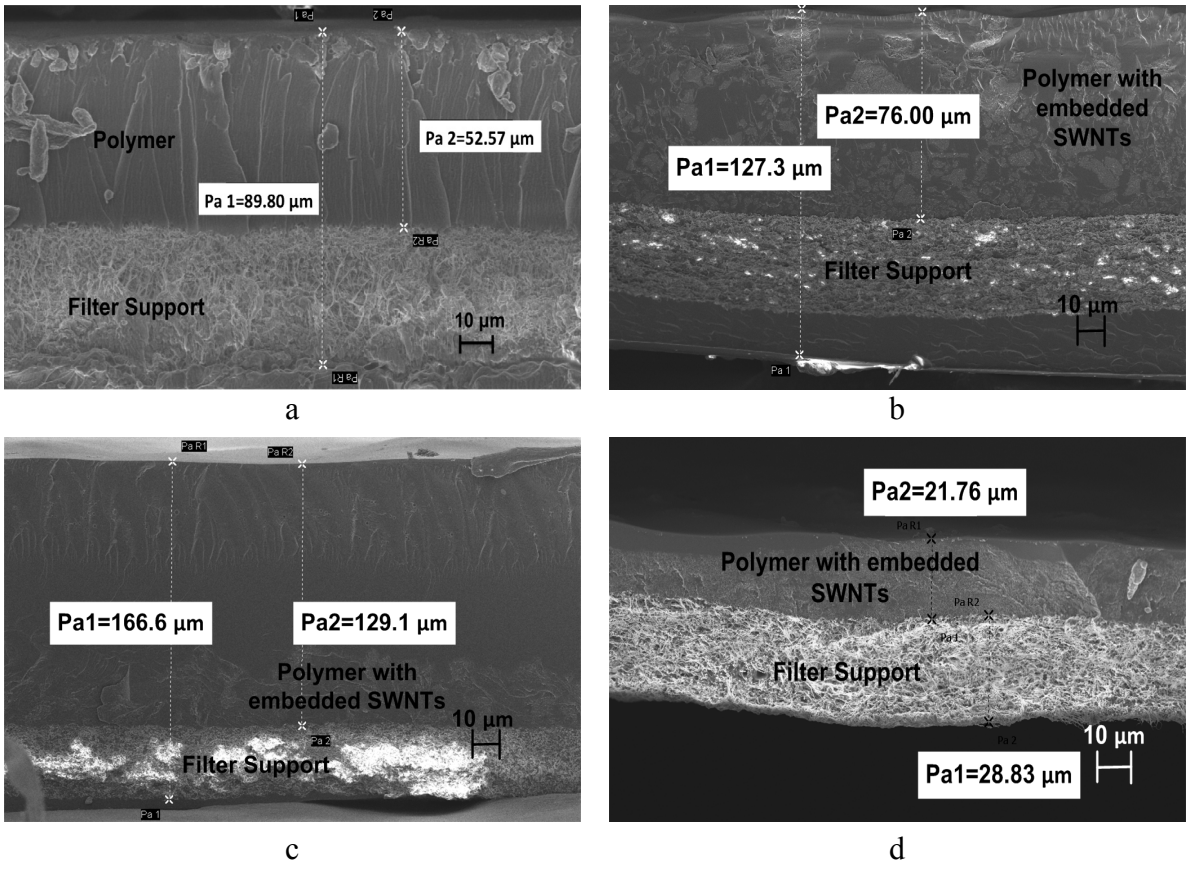

Figure 3-13. SEM images of the four membranes studied (a) sample A (b) sample B (c) sample C (d) sample D. Length of different layers of each membrane are marked.

As seen in Figure 3-11 and from Table 3-4, the gas permeabilities in sample D had decreased somewhat compared to sample C. One possible explanation is that plasma etching of polymer created radicals that cross-linked top of the membrane[26,27] and decreased the free fractional volume (FFV) of the polymer. Such decrease in FFV led to a decrease in gas permeabilities. Results also indicate that 60 min etching did not expose the SWNTs completely and hence no increase in gas permeability was observed. However, the gas permeability has increased significantly from sample D to sample E. This suggests that etching the membrane for 75 min exposed the CNT tips, allowing the gas to permeate in the SWNT pores. The permeabilities of all gases for this membrane were higher than Knudsen permeabilities by a factor of 8. It can also be observed that the gas permeabilities for this sample follow a linear

trend with molecular size $\sqrt{M}$ similar to Knudsen permeabilities. This is consistent with observations reported in literature[19].

Table 3-5. Selectivities of gases with respect to H_2 for various nanocomposite membranes.

Name of the Gas	**Selectivity of gas with respect to H_2**					
	Knudsen	*Sample A*	*Sample B*	*Sample C*	*Sample D*	*Sample E*
Helium	0.71	-	-	-	-	0.68
Oxygen	0.25	0.28	0.10	0.29	0.36	0.29
Nitrogen	0.27	0.08	-	0.09	0.18	0.31
Methane	0.36	0.17	0.07	0.16	0.25	0.46
Carbon-dioxide	0.21	1.58	0.42	1.56	1.41	0.31

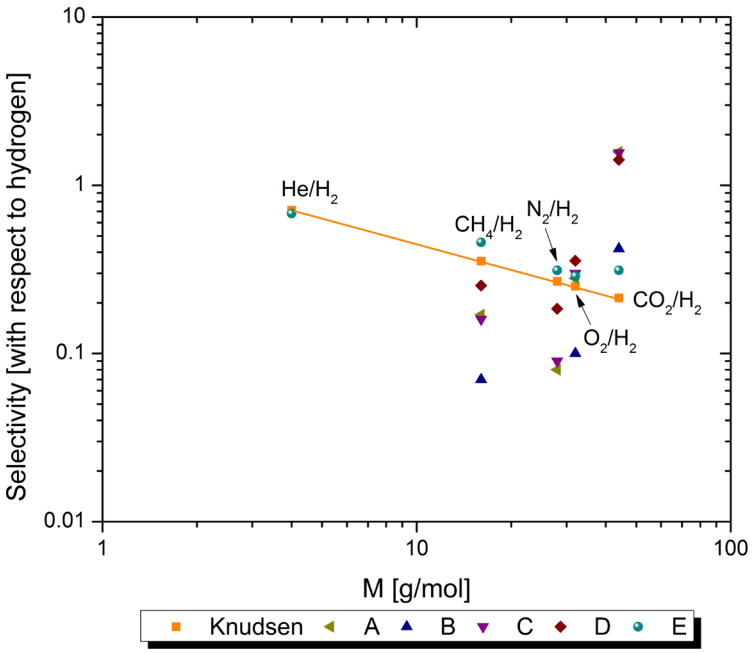

Figure 3-14. Selectivity of gases for different SWNTs/nanocomposite membranes. (Error bars are approximately the same size as the symbols)

The selectivity of gases with respect to hydrogen for all samples except sample E are scattered around Knudsen selectivities as shown in Figure 3-14. For sample E, the selectivities are similar to Knudsen selectivities, while for the other samples the selectivity is determined by

the polymer selectivity. These results also suggest that the carbon nanotube pores are much too large to separate gases by a size-exclusion mechanism.

3.4. Conclusions

The purification and cutting of SWNTs is an important first step in the fabrication of viable carbon nanotube membranes. SWNT/acrylic nanocomposite membranes made using cut (open) SWNTs showed higher gas permeabilities compared to membranes made with raw (closed) SWNTs. Etching the membrane removed the top excess polymer layer and exposed the tips of the SWNTs, which lead to an appreciable increase in the gas permeabilities. The gas permeabilities in etched membrane were higher than Knudsen permeabilities by a factor of 8 and selectivities were similar to Knudsen selectivities. The CO_2 sorption in carbon nanotubes functionalized with carboxylic acid groups was half that of non-functionalized SWNTs due to specific interactions between the functional group and the penetrant. Although we were not able to obtain highly selective membranes, these results set the stage for the use of SWNTs with pore size down to 4 Å and SWNTs modified with specific functional groups. These new approaches are described in detail in the next chapter.

3.5. References

1. Skoulidas, A.I., Ackerman, D.M., Johnson, J.K. & Sholl, D.S. Rapid Transport of Gases in Carbon Nanotubes. *Phys. Rev. Lett.* **89**, 185901 (2002).
2. Skoulidas, A.I., Sholl, D.S. & Johnson, J.K. Adsorption and diffusion of carbon dioxide and nitrogen through single-walled carbon nanotube membranes. *The Journal of Chemical Physics* **124**, 054708–054707 (2006).
3. Holt, J.K. Carbon Nanotubes and Nanofluidic Transport. *Adv. Mater.* **21**, 3542–3550 (2009).
4. Holt, J.K., Noy, A., Huser, T., Eaglesham, D. & Bakajin, O. Fabrication of a Carbon Nanotube-Embedded Silicon Nitride Membrane for Studies of Nanometer-Scale Mass Transport. *Nano Lett.* **4**, 2245–2250 (2004).
5. Holt, J.K. et al. Fast Mass Transport Through Sub-2-Nanometer Carbon Nanotubes. *Science* **312**, 1034–1037 (2006).
6. Hinds, B.J. et al. Aligned Multiwalled Carbon Nanotube Membranes. *Science* **303**, 62–65 (2004).
7. Spitalsky, Z., Tasis, D., Papagelis, K. & Galiotis, C. Carbon nanotube-polymer composites: Chemistry, processing, mechanical and electrical properties. *Progress in Polymer Science* **35**, 357–401 (2010).
8. Mi, W., Lin, Y.S. & Li, Y. Vertically aligned carbon nanotube membranes on macroporous alumina supports. *Journal of Membrane Science* **304**, 1–7 (2007).
9. Sun, L.F. et al. Materials: Creating the narrowest carbon nanotubes. *Nature* **403**, 384–384 (2000).
10. Deng, Z., Dalton, A., Terasaki, O. & Balkus, K.J., Jr Carbon nanotubes synthesized in zeolites UTD-1, UTD-18 and UTD-12. *Studies in Surface Science and Catalysis* **Volume**

154, Part 1, 903–910 (2004).
11. Wang, N., Tang, Z.K., Li, G.D. & Chen, J.S. Materials science: Single-walled 4 A carbon nanotube arrays. *Nature* **408**, 50–51 (2000).
12. Koshio, A., Yudasaka, M. & Iijima, S. Metal-free production of high-quality multi-wall carbon nanotubes, in which the innermost nanotubes have a diameter of 0.4 nm. *Chemical Physics Letters* **356**, 595–600 (2002).
13. Majumder, M., Chopra, N. & Hinds, B.J. Effect of Tip Functionalization on Transport through Vertically Oriented Carbon Nanotube Membranes. *J. Am. Chem. Soc.* **127**, 9062–9070 (2005).
14. Marand, E. & Sangil, K. Method for Making Oriented Single-Walled Carbon Nanotube/Polymer Nanocomposite Membranes. (2008).
15. Cinke, M. et al. Pore structure of raw and purified HiPco single-walled carbon nanotubes. *Chemical Physics Letters* **365**, 69–74 (2002).
16. Liu, J. et al. Fullerene Pipes. *Science* **280**, 1253–1256 (1998).
17. Bahr, J.L. & Tour, J.M. Covalent chemistry of single-wall carbon nanotubes. *J. Mater. Chem.* **12**, 1952–1958 (2002).
18. Marshall, M.W., Popa-Nita, S. & Shapter, J.G. Measurement of functionalised carbon nanotube carboxylic acid groups using a simple chemical process. *Carbon* **44**, 1137–1141 (2006).
19. Kim, S., Jinschek, J.R., Chen, H., Sholl, D.S. & Marand, E. Scalable Fabrication of Carbon Nanotube/Polymer Nanocomposite Membranes for High Flux Gas Transport. *Nano Lett.* **7**, 2806–2811 (2007).
20. Okpalugo, T.I.T., Papakonstantinou, P., Murphy, H., McLaughlin, J. & Brown, N.M.D. High resolution XPS characterization of chemical functionalised MWCNTs and SWCNTs. *Carbon* **43**, 153–161 (2005).
21. Graupner, R. Raman spectroscopy of covalently functionalized single-wall carbon nanotubes. *Journal of Raman Spectroscopy* **38**, 673–683 (2007).
22. Maultzsch, J. et al. Raman characterization of boron-doped multiwalled carbon nanotubes. *Appl. Phys. Lett.* **81**, 2647 (2002).
23. Kobayashi, Y., Takagi, D., Ueno, Y. & Homma, Y. Characterization of carbon nanotubes suspended between nanostructures using micro-Raman spectroscopy. *Physica E: Low-dimensional Systems and Nanostructures* **24**, 26–31 (2004).
24. Chen, H. & Sholl, D.S. Rapid Diffusion of CH_4/H_2 Mixtures in Single-Walled Carbon Nanotubes. *J. Am. Chem. Soc.* **126**, 7778–7779 (2004).
25. Chen, H. & Sholl, D.S. Predictions of selectivity and flux for CH_4/H_2 separations using single walled carbon nanotubes as membranes. *Journal of Membrane Science* **269**, 152–160 (2006).
26. Youxian, D., Griesser, H.J., Mau, A.W.H., Schmidt, R. & Liesegang, J. Surface modification of poly(tetrafluoroethylene) by gas plasma treatment. *Polymer* **32**, 1126–1130 (1991).
27. Kwon, O.-J., Tang, S., Myung, S.-W., Lu, N. & Choi, H.-S. Surface characteristics of polypropylene film treated by an atmospheric pressure plasma. *Surface and Coatings Technology* **192**, 1–10 (2005)

Chapter 4. Gas Sorption Properties of Zwitterion-Functionalized Carbon Nanotubes

4.1. Introduction

There has been a long-standing technical interest in carbon nanotubes (CNTs) driven by their exceptional electrical, thermal and mechanical properties[1]. Molecular simulations and experimental studies have uncovered unique transport properties of fluids within CNTs due to the unprecedented smoothness and regularity of the CNT pores[2,3]. For example, the transport of simple gases in both multi-walled and single-walled carbon nanotube membranes has been shown to be orders of magnitude larger than that predicted by Knudsen diffusion[4]. However, gas selectivities of single walled carbon nanotube (SWNT) membranes were found to generally follow the Knudsen model, being quite low in comparison to selectivities offered by neat polymer membranes[5-7]. This limitation can be attributed to the large pore size of the carbon nanotubes, typically on the order of 10 - 15 Å for SWNTs and 100 Å for multi-walled carbon nanotubes, in comparison to the kinetic diameters of small gas molecules, which range from about 2.7 Å to 6 Å, making molecular sieving difficult. We propose that one way to improve selectivity is to introduce functionalized moieties at the carbon nanotube entrance points (typically the tips, where the caps have been etched away). The functional groups could act in two ways: they reduce the effective diameter of the pore entrance through steric effects, thereby increasing size selective molecular sieving, and they could also be tailored to have specific molecular interactions with particular gases to facilitate molecular sieving through a chemical recognition or electrostatic repulsion mechanism[8].

Previous modeling work indicates that CNTs may be tailored or functionalized with different functional groups to serve as separation membranes for gases. Liu and Chen designed a hypothetical Y-Junction CNT and used molecular dynamics (MD) simulations to show that this junction acts as a molecular sieve for the separation of gases based on molecular size[9]. Arora and Sandler demonstrated that carbon nanotubes with a constriction can give a high transport resistance for N_2 while allowing O_2 to pass through the constriction[10]. Similarly, Zhang et al. showed that a kinked SWNT has the potential to separate N_2 and O_2 through transfer resistance to N_2 provided by the kink[11]. Corry predicted that charged functional groups bound to the entrance of SWNTs could provide resistance to ion flow in an aqueous salt solution that is otherwise missing in unfunctionalized nanotubes[12]. These simulations provide evidence that

steric or electrostatic modification of nanotubes is required in order to impart a high degree of selectivity to CNTs. However, the configurations studied are all hypothetical, especially for constricted and kinked CNTs, since there is no known way to easily produce CNTs with such specific geometries. However, nanotubes can indeed be functionalized, as demonstrated for example in our previous work where SWNTs were functionalized with long chain alkyl groups and incorporated into nanocomposite mixed matrix membranes[6]. Other simulation studies have examined how the functionalization of nanotubes influences equilibrium adsorption of fluids. Huang et al.[13] studied the influence of -CH_3 and -COOH functional groups at the entrance of very narrow nanotubes on the uptake of water. They found that -CH_3 groups have little effect on water uptake, but that -COOH groups could either increase or decrease the amount of water in the nanotubes, depending on the nanotube studied. Joseph et al.[14] examined the effect of putting functional groups of opposite charge on each end of a short nanotube on the transport of salt ions through the nanotube in an aqueous solution of KCl. They functionalized one end of the tube with $–COO^-$ groups and the other with $–NH_3^+$ groups. They used a static electric field to drive ions through the nanotube in a model membrane. They found that the Cl^- transport rate was much higher than the K^+ rate and attributed this asymmetry to the K^+ ions being "bound" to the $–COO^-$ groups at one end of the nanotube.

In addition to simulations, experimental work has demonstrated that the transport of fluids through CNTs can be altered through functionalizing the nanotube ends. Holt et al.[4,15,16] have constructed nanotube-Si_3N_4 composite membranes using chemical vapor deposition. Using an etching process, they exposed and selectively uncapped the CNTs to introduce hydroxyl, carbonyl and carboxylic functional groups at the nanotube entrance. Ionization of the carboxylic groups for example, created charged nanochannels that used both steric hindrance and electrostatic repulsion to achieve ion rejection[12]. Hinds and coworkers constructed CNT membranes by microtoming multiwalled CNT (7 nm inner diameter) and SWNT (1.5 nm inner diameter) epoxy composites[17-22]. They studied electro-osmotic flow by measuring the fluxes of both charged and neutral probe molecules through the membranes under external electric fields. An electrochemical diazonium grafting method was employed to enhance the surface anionic charge density of CNTs. The diazonium grafting increased carboxylate density on carbon nanotubes by about 5–6 times as compared to that of the as-produced (plasma-oxidized) CNT membranes. This led to an increase in ionic transport of a positively charged permeate along the

CNT core. The surface anionic charge was also further enhanced via a carbodiimide coupling reaction with the dye molecule containing four negatively charged SO_3 groups. This particular functionalization facilitated efficient pumping via electroosmosis of neutral caffeine molecules. Falconer et al. have recently shown that ion diffusion through dense CNT membranes can be gaited due to changes in water wettability[23].

In this study we demonstrate that SWNTs can be functionalized with both COOH and zwitterionic groups. We compare the gas sorption properties of SWNTs functionalized with these groups and present computer simulations to explain the differences observed experimentally in the sorption isotherms.

4.2. Methods

4.2.1. Materials

Carboxylic acid functionalized SWNTs, of outer diameter 1.5 nm and length 1 μm were purchased from Nano Lab Inc. (MA, USA). The SWNTs were produced by a CVD method, purified and functionalized with COOH groups by refluxing in sulfuric acid/nitric acid. Purity of the SWNTs was greater than 95% (by TGA). Concentration of COOH groups in the SWNTs was approximately 2-7 wt% (by titration). Reagents, thionyl chloride (99.5%) and 3-dimethylamino-1-propanol (99%), were purchased from Sigma Aldrich, USA and used as received. β-propiolactone (oxetan-2-one) was purchased from Biophoretics Inc., USA.

4.2.2. Synthesis of Zwitterionic Functionalized SWNTs

The COOH groups on the SWNTs served as precursors for the addition of zwitterion groups. The three-step chemical reactions required beginning from COOH functional groups to do this addition are shown in Figure 4-1.

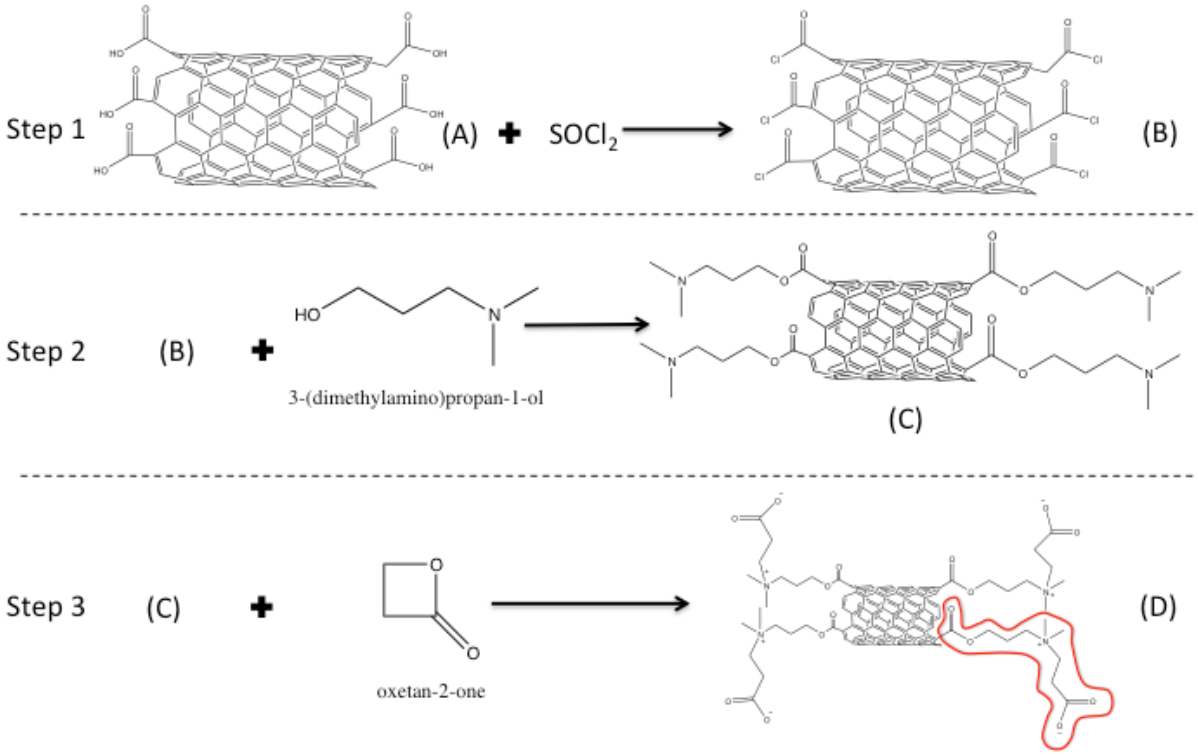

Figure 4-1. Schematic of the chemical reactions leading to the formation of zwitterion groups on the carbon nanotube tips.

In the first step, COOH functionalized SWNTs (A) were reacted with thionyl chloride to form SWNTs with COCl groups (B) as shown in Figure 4-1. The experimental procedure followed to make this conversion was reported by Jain et al.[24] The acyl chloride functionalized SWNTs (B) were reacted with 3-(dimethylamino)propan-1-ol to form product compound (C) as shown in step 2 of Figure 4-1. In brief, 100 mg of COCl SWNTs (0.1 mmol of COCl group) were added to a mixture of 1.2 ml 3-(dimethylamino)propan-1-ol (10 mmol) and 1.4 ml of triethyl amine (10 mmol) in a 100 ml flask. The reaction mixture was stirred for 6 days at 100 RPM and room temperature. The SWNTs were then washed with ethanol to remove ethylamine hydrochloride salt and dried under vacuum. In the third step, functionalized SWNTs (C) were reacted with β-propiolactone (oxetan-2-one) to form zwitterion functionalized SWNTs (D)[25]. 100 mg of functionalized SWNTs (C) from step 2 were added to 20 ml of dry tetrahydrofuran (THF) in a 50 ml flask. The reaction mixture was stirred under nitrogen protection at room temperature for 5 hours. SWNTs were washed with dry THF and separated by centrifuging. They were dried under vacuum to remove any washing solvent. The zwitterion functional group is outlined in red in Figure 4-1.

4.2.3. Characterization

Functionalized SWNTs were characterized by thermogravimetric analysis (TGA), x-ray photoelectron spectroscopy (XPS, PHI Quantera SXM) and gas sorption isotherms. Thermogravimetric analysis provides a plot of weight and weight derivative as a function of temperature. It tells the decomposition temperature and rate of the sample material. For TGA characterization, approximately 10 mg of sample was placed in a metal pan and heated from room temperature to 700 °C at 20 °C/minute.

Sorption properties of zwitterion and COOH functionalized SWNTs were studied using Intelligent Gravimetric analyzer (IGA 002), Hiden Analytical Inc., UK. Approximately 20 mg of SWNT powder was placed in a metal basket, placed inside a gas chamber, and degassed by applying a high vacuum ($P<10^{-7}$ bar). The sample was heated to 200 °C to remove any absorbed/adsorbed water in the sample when appropriate. All gas sorption data were recorded at 35 °C over a gas pressure ranging from 0 to 10 bar. More details about the procedure to perform a gas sorption run on IGA are provided in Appendix A. Wet gas sorption runs are performed by exposing the sample to an environment of a particular relative humidity inside the sample chamber. Relative humidity (RH) is obtained by mixing two feed gases, dry gas and gas saturated with water vapor. Dry gas is saturated with water vapor by passing it through a water bath maintained at the temperature of the isotherm. RH of the gas inside the sample chamber is the ratio of the flow rate of the wet gas to the dry gas. The change in the weight of the sample after being exposed to gas of particular RH compared to weight of sample exposed to dry gas is the amount of wet gas uptake in the sample. Additional details about the procedure to run a water sorption using IGA are provided in Appendix C.

4.2.4. Simulations

Atomistic simulations were performed by Prof. Karl Johnson and his research group at the University of Pittsburgh for model SWNT membranes. Four nanotubes were embedded in two graphene sheets, which act to prevent fluid molecules from entering the interstitial regions between the nanotubes, as shown in Figure 4-2. A region of bulk gas was located outside the nanotubes. The diameter of the SWNTs used in the simulation was about 1.6 nm, corresponding to a (20,0) SWNT, about the same as the experimentally measured diameters of the SWNTs used in this work. The length of each tube was about 40 Å and the length of the bulk region was about 300 Å. The dimensions of the simulation cell perpendicular to the tube axis (parallel to the plane

of the membrane) are 54.1 by 55.4 Å. Potentials for the nanotubes, graphene, functional groups and CO_2 molecules used in the simulation were obtained from the CHARMM27 force field[26]. All of the carbon atoms in SWNTs and graphene sheets were frozen during the simulation. Water molecules were simulated using the TIP3P water model[27]. The temperature of the system was controlled by a Nosé-Hoover thermostat, with a temperature damping parameter of 100 fs. Periodic boundary conditions were applied in all three dimensions. All of the calculations were performed using the LAMMPS package[28] with a time step of 1 fs.

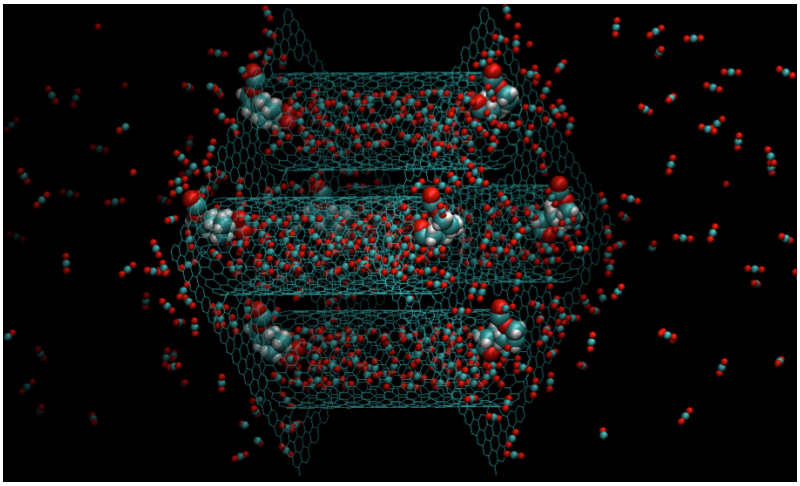

Figure 4-2. Section of the simulation cell showing the membrane, with four SWNTs embedded between two graphene sheets. Each end of each tube was functionalized with one zwitterionic group, shown by the space filling model. The CO_2 molcules are shown by the small red (oxygen) and cyan (carbon) atoms. The nanotubes and graphene sheets are shown as lines.

Potential of mean force (PMF) calculations for CO_2 entering the SWNTs were performed using the umbrella sampling method[29]. A harmonic baising potential along the tube center was applied to a CO_2 molecule with the force constant of 12 kcal/mol/Å^2. The test molecule was free to move along the other two dimensions. Simualtions were performed for 2 ns in each window with the last 1 ns of data used for analysis. The final unbiased PMF was analyzed by the weighted histogram analysis method[30,31], using Alan Grossfield's code.

4.3. Results and Discussion

4.3.1. Thermogravimetric Analysis

Thermogravimetric analysis (TGA) weight loss curves corresponding to COOH functionalized and zwitterion functionalized SWNTs are shown in Figure 4-3. The COOH-functionalized carbon nanotubes begin to lose weight around 450 °C, most likely associated with the pyrolysis of organic groups and reach 0% weight at 650 ^{o}C, when the remaining carbon

structures are pyrolyzed[32-34]. In the case of zwitterion-functionalized carbon nanotubes, the weight loss occurs in stages, starting at 150 °C and then again at 500 °C. This behavior of early weight loss of functionalized SWNTs (around 200 °C) was observed in the work by Dyke et al.[35,36] and others[37,38].

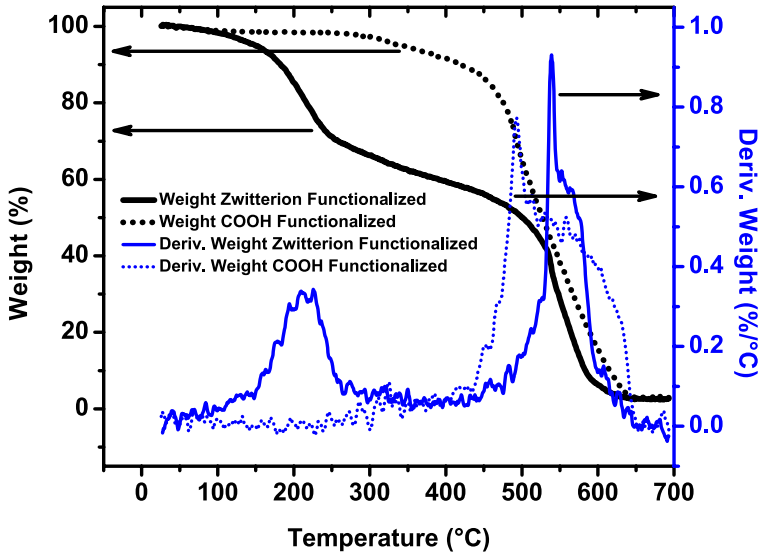

Figure 4-3. Thermogravimetric plot of COOH and zwitterion functionalized SWNTs.

To explain this behavior, we look at the weight derivative plot of zwitterion-functionalized SWNTs, which has a peak at 200 °C not observed in the COOH functionalized SWNTs. This early weight loss may be attributed to loosely bound water in the sample. Zwitterionic functional groups exhibit large affinity to absorb water via electrostatic interactions with water molecules[39]. This water, as we shall demonstrate later, can be removed by heating the sample above 200 °C. The weight derivative plot of the zwitterion functionalized SWNTs also demonstrates that they are more stable than the COOH functionalized nanotubes, as shown by the shift in the degradation peak to higher temperatures (550 °C) compared to the carboxylic acid groups (500 °C).

4.3.2. X-ray Photoelectron Spectroscopy

X-ray photoelectron spectroscopy was performed on the COOH and zwitterion functionalized SWNTs. XPS measures the elemental composition of the sample, and generates atomic percentage values of the elements. COOH functionalized SWNTs are predominantly composed of C and O, and zwitterion functionalized SWNTs have C, O and N. The results from XPS are shown in Table 4-1. The percentage of C decreased in zwitterion SWNTs compared to

COOH SWNTs, whereas the percentage of oxygen increased. This result is consistent with the atomic percentages based on chemical formula of the functional groups. Considering the zwitterion functional group in Figure 4-1 circled red, we see that it has more oxygen atoms compared to in COOH groups, and therefore it should have higher atomic percentage of O and lower of C atoms. In COOH functionalized SWNTs, theoretically the atomic percentage of N should be zero. However, it can be seen in Table 4-1 that COOH SWNTs has a very low percentage of N atoms. This small amount can originate from contamination of the sample by any catalyst particles in the sample or from the solvents and reactants used during the reactions of functionalization of the SWNTs with COOH groups. There is a significant increase in the atomic percentage of nitrogen in zwitterion SWNTs compared to in COOH SWNTs, as expected, since the zwitterion functional group contains a nitrogen atom in its chemical composition.

Table 4-1. Atomic percentages of C, O and N in COOH and zwitterion functionalized SWNTs measured by XPS.

SWNTs Functionalization	**C1s**	**N1s**	**O1s**
COOH	87.04	0.35	12.58
Zwitterion	76.9	1.82	19.01

The XPS and TGA results together confirmed the functionalization of SWNTs with zwitterion functional groups[40,41]. Effort was made to characterize zwitterion functionalized SWNTs using Fourier Transform Infrared Spectroscopy (FTIR). However, no reliable absorption spectrum could be obtained due to scattering of the laser light by the CNTs.

4.3.3. Gas Sorption Isotherms

The approximate sizes of zwitterion and COOH functional group are around 1.1-1.2 nm and 0.4 nm respectively. Thus, the presence of the groups may affect the effective pore diameter of the SWNTs. The effective pore diameter is defined as the diameter of the largest gas molecule that can enter inside of the tube through its opening. This dimension depends on the diameter of the SWNT, length of the functional group molecule as well as the molecular interactions between the gas molecule and the functional groups present at the entrance of the tube. The sorption isotherm represents the concentration of the gas sorbed in the SWNTs as a function of gas pressure inside the chamber at a given temperature. At each pressure, the equilibrium weight

of the sample is recorded and used for calculating the uptake or the concentration of the sorbed gas. The equilibration criterion for advancing to next isotherm point is satisfied when the uptake has changed by a 0.99 fraction of the difference between the initial reading (at the beginning of the isotherm point) and the predicted asymptote. IGA used the linear driving force model to fit the mass uptake data and predict the asymptotic uptake. The instrument software using the above model parameters predicts the total run time at a particular pressure point. For certain materials, this run time can be very long (on the order of days) depending on the characteristics of the gas diffusion in it. Extremely slow adsorption kinetics has been observed before for hindered diffusion[42].

Figure 4-4 shows the sorption isotherms for CO_2, N_2 and CH_4 in COOH functionalized SWNTs. As expected, the trends in the amounts of gas sorbed increased in the following order: $N_2 < CH_4 < CO_2$, which follows the trends in increasing critical temperature and polarizability for these molecules. Hence, COOH SWNTs are sorption selective to CO_2, given that the amounts of gas adsorbed at 10 bar are 6.21, 3.17, and 1.51 mmol/g for CO_2, CH_4, and N_2 respectively. For comparison, sorption isotherms for these same gases in zwitterion functionalized SWNTs that have been exposed to ambient humidity are shown in Figure 4-5.

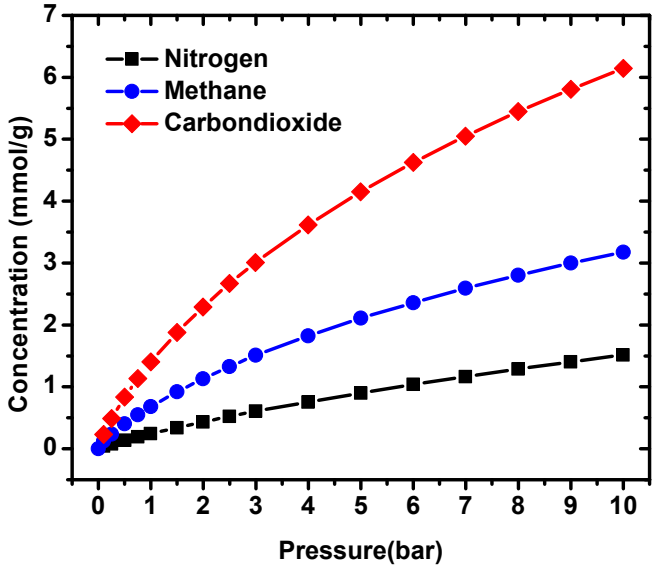

Figure 4-4. Sorption Isotherms of COOH functionalized SWNTs at 35 ^{o}C

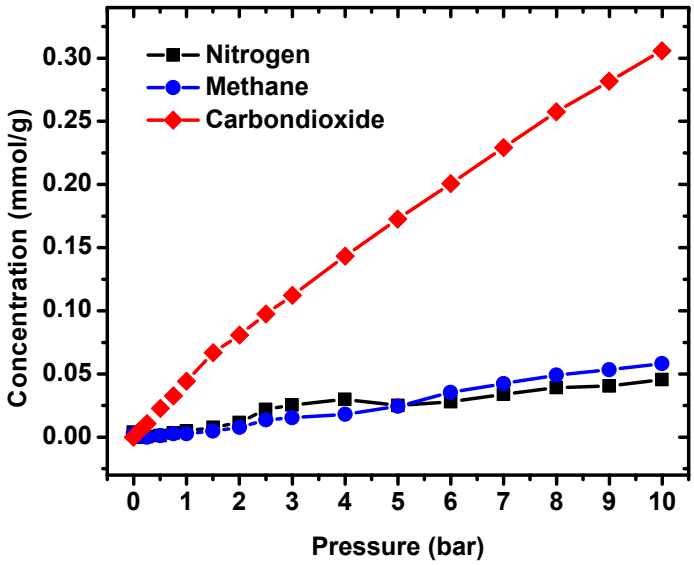

Figure 4-5. Sorption isotherms in zwitterion functionalized SWNTs at 35 ^{o}C

We see that the amount of gas adsorbed in the zwitterion functionalized SWNTs is dramatically reduced compared with the COOH functionalized nanotube by comparing the isotherms for N_2, CH_4 and CO_2 in Figure 4-4 and Figure 4-5. This very low sorption is most likely due to the hydrated zwitterion functional groups blocking gas molecules from entering the SWNTs. Zwitterionic functional groups have lengths of 1.1-1.4 nm. Their length is comparable to the diameter of the SWNTs used in this work (1.5 nm). Hence, their presence reduces the effective pore diameter by steric hindrance. The molecular simulations presented in the next section will be used to examine the blocking mechanism in detail. On the other hand, the size of the COOH groups (0.4 nm) is not large enough to completely block the opening of the carbon nanotubes. However, the presence of the COOH groups may affect the sorption of gases in SWNTs, as has been demonstrated in on our previous study on SWNTs having much smaller diameters (~9 Å)[43], where the sorption of CO_2 was lowered by half in COOH functionalized SWNTs compared to non-functionalized nanotubes. We note, however, that functionalization of the SWNTs in that work also resulted in significant changes to the length and morphology of the nanotubes that may also have had an impact on the adsorption capacity. The diameter of the nanotubes used in this work is large enough that one would not expect significant blocking effects due to COOH groups on the ends of the SWNTs. As seen in Figure 4-5, zwitterion functionalized SWNTs are also sorption selective for CO_2, with adsorption of 0.31, 0.05, and

0.04 mmol/g of CO_2, CH_4 and N_2 at P=10 bar, respectively. It is striking that the CH_4 and N_2 isotherms shown in Figure 4-5 are essentially identical. This will be discussed in the next section.

We have noted that the TGA graph of zwitterion functionalized SWNTs shown in Figure 4-3 indicates water loss upon heating to 200 °C. The zwitterion functionalized SWNTs used in the experiments reported in Figure 4-5 had not been heated, and therefore must contain water. We hypothesize that the water molecules complexing with the zwitterion-functionalized SWNTs further decrease gas sorption. To test this hypothesis, the zwitterion SWNTs were heated to 200 °C under vacuum and the gas sorption isotherms were measured again. As expected, a weight loss of around 26.25 mg (weight of the hydrated zwitterion sample was 45.52 mg and, dehydrated sample was 19.27 mg) was observed after heating and the concentration of CO_2 gas sorbed increased. These results are shown in Figure 4-6. The concentration of CO_2 gas increased from 0.31 mmol/g (at 10 bar) in hydrated zwitterion SWNTs to 1.7 mmol/g (at 10 bar) in non-hydrated (heated) zwitterion SWNTs. This is a significant increase, reflecting the removal of water molecules blocking the SWNTs pores.

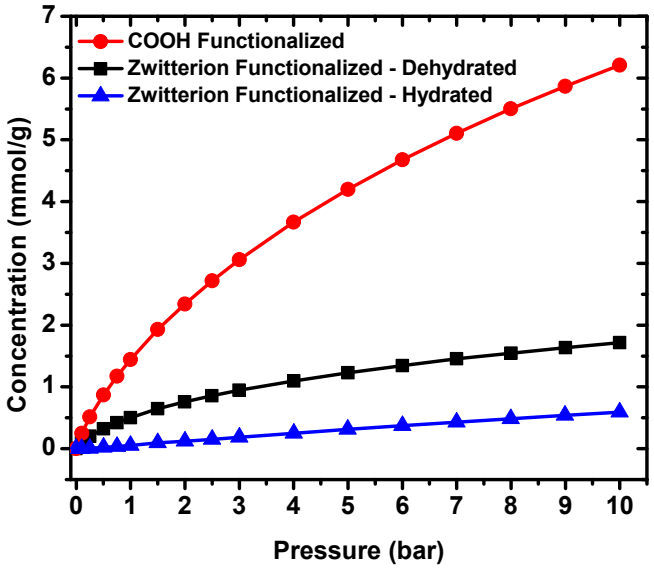

Figure 4-6. CO_2 gas sorption in COOH, zwitterion functionalized (heated to 200 ^oC) and zwitterion functionalized (not heated) SWNTs

4.3.4. Molecular Simulation Results

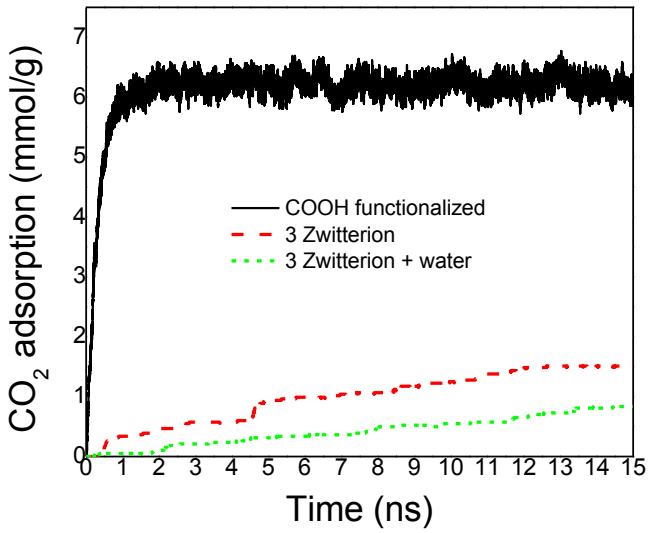

Figure 4-7. Adsorption of CO_2 molecule in the SWNT membrane as a function of time as computed from molecular simulation for an external CO_2 pressure of about 10 bar. The black line represents a system with five COOH groups at the ends of each nanotube. The red line is for three zwitterions at the pore entrances and the green line has three zwitterions per end, plus pre-exposure to 200 water molecules.

We have modeled the kinetics of the adsorption process for CO_2 in three different SWNT membranes: SWNTs functionalized with five COOH groups at the end of each tube, SWNTs functionalized with three zwitterion groups, and with three zwitterion groups exposed to 200 water molecules. The bulk gas phase was initially populated with CO_2 molecules at a density corresponding to about 10 bar. The CO_2 then adsorbed on the graphene sheets, on the ends of the tubes, and diffused inside the tubes as time progressed in the simulation and the size of the bulk region was compressed with time to keep the pressure at about 10 bar throughout the simulation. The amount of CO_2 adsorbed as a function of time for these three membranes is plotted in Figure 4-7. We see from Figure 4-7 that the COOH functionalized membrane quickly reached equilibrium and that the amount of CO_2 adsorbed is in remarkably good agreement with the experiments shown in Figure 4-4. No adjustable parameters were used in the simulations. We note that the uptake of CO_2 for the membrane functionalized with three zwitterion groups is dramatically slowed compared to the COOH membrane. The adsorption has not approached equilibrium at 15 ns and we expect the adsorption to continue and perhaps slow as time progresses. We have also simulated membranes with no functional groups and with one and two

zwitterions per tube end and these systems showed similar behavior to the COOH functionalized SWNTs. Thus, functionalization of the SWNTs with three zwitterions results in significant kinetic limitations compared with these other systems.

The effect of water on the zwitterion membranes can be modeled by placing water molecules in the bulk region of the simulation box and allowing the system to come to equilibrium. The final state of a simulation with 200 water molecules is shown in Figure 4-8, where it can be seen that all of the water molecules are adsorbed either on the zwitterions or are drawn into the SWNTs. Note also that the zwitterions are also drawn into the nanotubes due to increased van der Waals interactions with the walls of the SWNTs. The conformation of functional groups has previously been simulated by Halicioglu and Jaffe[44], who found that when the nanotube is solvated, polar groups (-COOH) are extended out into the water phase away from the nanotube end, but non-polar groups (-CH_3) are folded into the nanotube. However, the groups they studied are rather small and have limited flexibility. In this work we use longer and more flexible groups, and find that they generally prefer to be folded into the nanotube, even in the presence of water. The folded zwitterions inhibit diffusion of gas species into the nanotube, but at the conditions of our simulations do not fully block the entrances. The dynamic flexibility of the zwitterions allows CO_2 and water enter the tube. Water is more strongly attracted to the zwitterion groups because of the larger role of electrostatic interactions between water and the zwitterions. The presence of water leads to a further decrease in the kinetics of adsorption, as seen by the lower rate of adsorption for the system with three zwitterions per tube in the presence of water in Figure 4-7(green line). These trends from our simulations are in qualitative agreement with the experimental data shown in Figure 4-6. In addition to kinetic limitations, adsorption of water within the SWNTs will also decrease the equilibrium amount of gas that can be adsorbed due to competetive adsorption. Indeed, part of the trends seen in Figure 4-6 can be explained by the differences between the Henry's law constants of CO_2, CH_4, and N_2 in water; the value of the Henry's law constant for CO_2 is about a factor of 30 larger than CH_4.

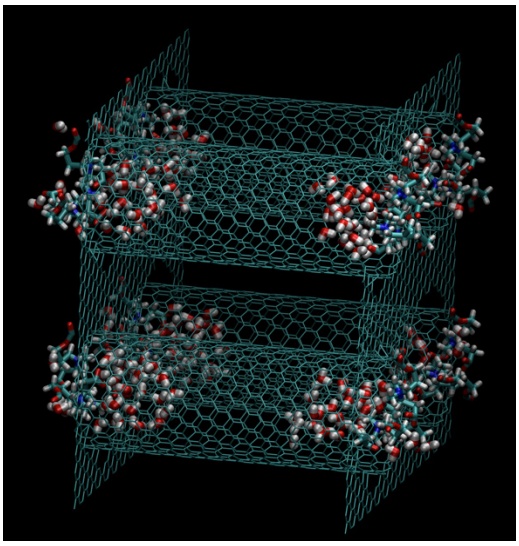

Figure 4-8. Water adsorbed in a SWNT membrane functionalized with three zwitterion groups on each end of each tube.

In addition to examining the kinetic limitations for CO_2 adsorption into functionalized SWNT membranes, we have also computed the potential of mean force (PMF) for CO_2 entering membranes functionalized with five COOH groups, with three zwitterions, with three zwitterions plus 200 water molecules, and with five zwitterions and 200 water molecules. The PMFs for these systems are plotted in Figure 4-9. We see that there is essentially no barrier for the COOH membrane. For the membrane with three zwitterions per tube end, the free energy barrier for entrance is about 2.4 kcal/mol. This barrier is the cause of the slow uptake of CO_2 in the zwitterion membrane noted in Figure 4-7. When 200 water molecules were pre-equilibrated with the three zwitterion membrane the barrier increases to about 2.9 kcal/mol, which is a slight increase in the barrier without water, and consistent with the slower uptake for hydrated zwitterions seen in Figure 4-7. We have also carried out a simulation with five zwitterion groups at the end of each tube along with 200 water molecules. The statistics for this system are very poor due to the high degree of variability as the zwitterions fluctuate at the tube ends. In some cases the tubes were essentially blocked as the zwitterions adopted configurations where three or more zwitterions were inside the tube. We also noted configurations where the blocking of the nanotubes was relatively small, with all five groups outside the tube, so that the barrier to CO_2 entry was small. This high degree of vairiability may be due to insufficient time for the functional groups to fully equilibrate. The average free energy barrier for CO_2 entering the nanotubes for this system is about 6 kcal/mol, as seen in Figure 4-9. This high barrier could

result in a very slow rate of adsorption. Thus, the simulations indicate that functionalization of the nanotubes will kinetically inhibit sorption of gases, but will not result in a dramatic decrease in equilibrium capacity unless water is present, since the zwitterions occupy only a small fraction of the nanotube when inside, even for nanotubes as short as 40 Å. If the barrier to gas entrance is high enough then the rate of adsorption could be negligably small, and this would be consistent with the experimental observations.

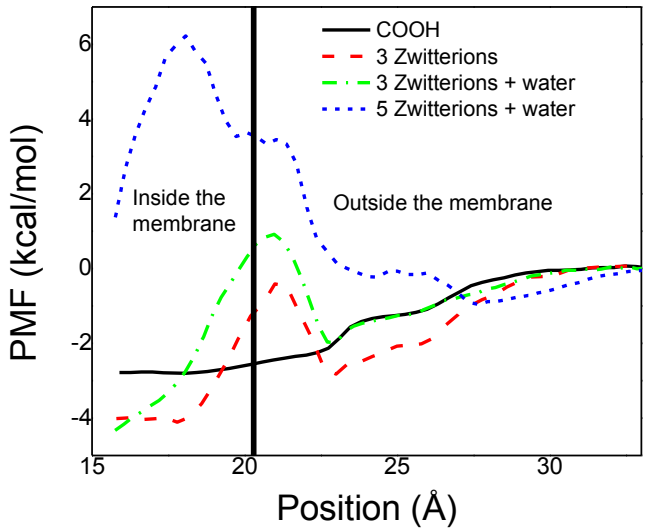

Figure 4-9. Potential of mean force for CO_2 entering tubes functionalized with five COOH groups (black), three zwitterion groups (red), three zwitterion groups with 200 water molecules around the entrance (green), and five zwitterions with 200 water molecules (blue). The nanotube entrance is located at 20.3 Å, as marked by the thick black vertical line.

4.3.5. Wet Gas Sorption Isotherms

Wet gas sorption isotherms are obtained for COOH and zwitterion functionalized SWNTs. At 35 ^{o}C, the change in the weight of the sample exposed to gas at particular RH, and weight of the sample exposed to dry nitrogen (inert gas) is measured. From the difference in the weight of the samples, the concentration of the wet N_2 gas absorbed is calculated and plotted as an isotherm with RH on the x-axis.

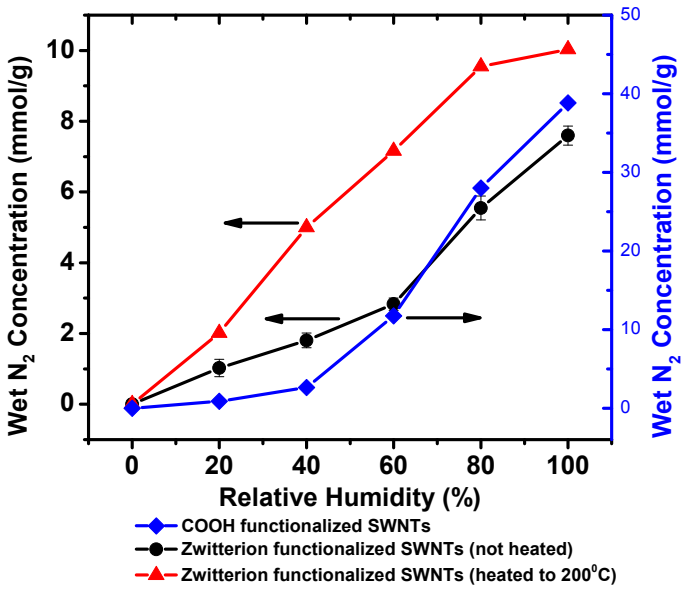

Figure 4-10. Wet nitrogen gas sorption isotherms at 35 ^{o}C in COOH and zwitterion functionalized SWNT samples.

Wet nitrogen gas sorption isotherms in three samples (i) COOH (ii) zwitterion (not heated) SWNTs and (iii) zwitterion (heated to 200 ^{0}C) are shown in Figure 4-10. Zwitterion SWNTs, when heated to 200 ^{0}C lost water molecules loosely bound to them, as evident in the significant weight loss of hydrated zwitterion SWNTs at around 150 ^{0}C observed in the TGA plot shown in Figure 4-3. Zwitterion SWNTs became dehydrated when heated to 200 ^{0}C under high vacuum. It can be observed in Figure 4-10 that the concentration of wet gas absorbed in COOH functionalized SWNTs is higher compared to hydrated zwitterion functionalized SWNTs. This result is consistent with the gas sorption isotherms in COOH and hydrated zwitterion functionalized SWNTs. As discussed earlier in gas sorption isotherms, COOH groups (0.4 nm) are shorter in length than the diameter of the SWNTs (1.5 nm) and hence do not block the wet gas from absorbing inside the pore of the CNT. Whereas, on the other hand, the length of the zwitterionic functional group (around 1.1-1.4 nm) is close to the diameter of the SWNT and hence the pore of the tube is blocked for the gas to enter. This resulted in lower absorption of wet gas in zwitterion functionalized SWNTs.

The sorption of wet gas is also studied in zwitterion SWNTs heated to 200 ^{0}C (dehydrated), and compared to non-heated (hydrated) zwitterion SWNTs. Non-heated zwitterion SWNTs, as discussed before, has water complexed with zwitterion functional groups in the tube.

This decreased the amount of wet gas absorbed in the sample compared to heated zwitterion SWNTs.

4.4. Conclusions

We have synthesized zwitterion functionalized carbon nanotubes and measured the performance of these nanotubes through gas sorption. Adsorption of gases in zwitterion functionalized SWNT is greatly reduced compared with SWNT functionalized with carboxylic acid groups. Water readily adsorbs on zwitterion functionalized nanotubes but can be removed by heating to 200 °C. Gas adsorption is increased in zwitterion functionalized SWNTs after water is removed, but is still considerably smaller than in COOH SWNTs. Molecular simulations indicate that there is essentially no kinetic inhibition to adsorption of gases in COOH SWNTs, or for SWNTs with one or two zwitterions per tube end. In contrast, the kinetics of adsorption are dramatically slowed when three or more zwitterions are attached to the entrances of the SWNTs. Water readily adsorbs at the entrances and within zwitterion SWNTs and further inhibits sorption of gases. Potential of mean force calculations indicate that the barrier to gas entry inside the SWNTs increases both as the number of zwitterions increase and also as water is added to the system. The simulations indicate that gas sorption in functionalized nanotubes could be kinetically limited, even at macroscopic time scales.

4.5. Acknowledgments

This work was supported by a grant from NSF-CBET 0755937. We thank the University of Pittsburgh's Center for Simulation and Modeling for computer time. We thank De-Li Chen and Xiao-hong Shao for helpful discussions.

4.6. References

1. Lieber, C. M., Odom, T. W., Huang, J.-L. & Kim, P. Atomic structure and electronic properties of single-walled carbon nanotubes : Abstract : Nature. *Nature* **391**, 62–64 (1998).
2. Whitby, M. & Quirke, N. Fluid flow in carbon nanotubes and nanopipes. *Nature* **2**, 87–94 (2007).
3. Hummer, G., Rasaiah, J. C. & Noworyta, J. P. Water conduction through the hydrophobic channel of a carbon nanotube. *Nature* **414**, 188–190 (2001).
4. Holt, J. K. Fast Mass Transport Through Sub-2-Nanometer Carbon Nanotubes. *Science* **312**, 1034–1037 (2006).
5. Mi, W., Lin, Y. S. & Li, Y. Vertically aligned carbon nanotube membranes on macroporous alumina supports. *Journal of Membrane Science* **304**, 1–7 (2007).
6. Kim, S., Chen, L., Johnson, J. K. & Marand, E. Polysulfone and functionalized carbon nanotube mixed matrix membranes for gas separation: Theory and experiment. *Journal of Membrane Science* **294**, 147–158 (2007).

7. Cong, H., Zhang, J., Radosz, M. & Shen, Y. Carbon nanotube composite membranes of brominated poly(2,6-diphenyl-1,4-phenylene oxide) for gas separation. *Journal of Membrane Science* **294**, 178–185 (2007).
8. Corry, B. Water and ion transport through functionalised carbon nanotubes: implications for desalination technology. *Energy Environ. Sci.* **4**, 751–759 (2011).
9. Liu, L. & Chen, X. Nanofluidic Transport in Branching Nanochannels: A Molecular Sieve Based on Y-Junction Nanotubes. *J. Phys. Chem. B* **113**, 6468–6472 (2009).
10. Arora, G. & Sandler, S. I. Molecular sieving using single wall carbon nanotubes. *Nano Lett.* **7**, 565–569 (2007).
11. Zhang, Z. Gas separation by kinked single-walled carbon nanotubes: Molecular dynamics simulations. *Phys. Rev. B* **78**, 035439–035444 (2008).
12. Fornasiero, F. *et al.* Ion exclusion by sub-2-nm carbon nanotube pores. *Proceedings of the National Academy of Sciences* **105**, 17250–17255 (2008).
13. Huang, L. L. *et al.* Molecular dynamics simulation study of the structural characteristics of water molecules confined in functionalized carbon nanotubes. *J. Phys. Chem. B* **110**, 25761–25768 (2006).
14. Joseph, S., Mashl, R. J., Jakobsson, E. & Aluru, N. R. Electrolytic transport in modified carbon nanotubes. *Nano Lett.* **3**, 1399–1403 (2003).
15. Holt, J. K. Carbon Nanotubes and Nanofluidic Transport. *Adv. Mater.* **21**, 3542–3550 (2009).
16. Holt, J. K., Noy, A., Huser, T., Eaglesham, D. & Bakajin, O. Fabrication of a Carbon Nanotube-Embedded Silicon Nitride Membrane for Studies of Nanometer-Scale Mass Transport. *Nano Lett.* **4**, 2245–2250 (2004).
17. Majumder, M. *et al.* Enhanced electrostatic modulation of ionic diffusion through carbon nanotube membranes by diazonium grafting chemistry. *Journal of Membrane Science* **316**, 89–96 (2008).
18. Wu, J., Gerstandt, K., Majumder, M., Zhan, X. & Hinds, B. J. Highly efficient electroosmotic flow through functionalized carbon nanotube membranes. *Nanoscale* **3**, 3321–3328 (2011).
19. Majumder, M., Chopra, N. & Hinds, B. . Mass Transport through Carbon Nanotube Membranes in Three Different Regimes: Ionic Diffusion and Gas and Liquid Flow. *ACS Nano* **5**, 3867–3877 (2011).
20. Hinds, B. J. *et al.* Aligned Multiwalled Carbon Nanotube Membranes. *Science* **303**, 62–65 (2004).
21. Majumder, M., Chopra, N. & Hinds, B. J. Effect of Tip Functionalization on Transport through Vertically Oriented Carbon Nanotube Membranes. *J. Am. Chem. Soc.* **127**, 9062–9070 (2005).
22. Majumder, M., Zhan, X., Andrews, R. & Hinds, B. J. Voltage Gated Carbon Nanotube Membranes. *J. Phys. Chem.* **23**, 8624–8631 (2007).
23. Yu, M., Funke, H. H., Falconer, J. L. & Noble, R. D. Gated Ion Transport through Dense Carbon Nanotube Membranes. *J. Am. Chem. Soc.* **132**, 8285–8290 (2010).
24. Jain, A. K. *et al.* Carbohydrate-conjugated multiwalled carbon nanotubes: development and characterization. *Nanomedicine: Nanotechnology, Biology and Medicine* **5**, 432–442 (2009).
25. Zhang, Z., Chen, S. & Jiang, S. Dual-Functional Biomimetic Materials: Nonfouling Poly(carboxybetaine) with Active Functional Groups for Protein Immobilization.

Biomacromolecules **7**, 3311–3315 (2006).
26. Feller, S. E. & MacKerell, A. D. An improved empirical potential energy function for molecular simulations of phospholipids. *Journal of Physical Chemistry B* **104**, 7510–7515 (2000).
27. Jorgensen, W. L., Chandrasekhar, J., Madura, J. D., Impey, R. W. & Klein, M. L. Comparison of simple potential functions for simulating liquid water. *J. Chem. Phys.* **79**, 926–935 (1983).
28. Plimpton, S. Fast parallel algorithms for short-range Molecular-dynamics. *Journal of Computational Physics* **117**, 1–19 (1995).
29. Torrie, G. M. & Valleau, J. P. Monte Carlo free energy estimates using non-Boltzmann sampling: Application to the sub-critical Lennard-Jones fluid. *Chemical Physics Letters* **28**, 578–581 (1974).
30. Kumar, S., Rosenberg, J. M., Bouzida, D., Swendsen, R. H. & Kollman, P. A. THE weighted histogram analysis method for free-energy calculations on biomolecules. I. The method. *J. Comput. Chem.* **13**, 1011–1021 (1992).
31. Roux, B. The calculation of the potential of mean force using computer simulations. *Computer Physics Communications* **91**, 275–282
32. Haggenmueller, R., Du, F., Fischer, J. E. & Winey, K. I. Interfacial in situ polymerization of single wall carbon nanotube/nylon 6,6 nanocomposites. *Polymer* **47**, 2381–2388 (2006).
33. Rinzler, A. G. *et al.* Large-scale purification of single-wall carbon nanotubes: process, product, and characterization. *Applied Physics A: Materials Science & Processing* **67**, 29–37 (1998).
34. Razdan, S. *et al.* Ionically Self-Assembled Polyelectrolyte-Based Carbon Nanotube Fibers. *J. Am. Chem. Soc.* **21**, 3062–3071 (2009).
35. Dyke, C. A. & Tour, J. M. Overcoming the Insolubility of Carbon Nanotubes Through High Degrees of Sidewall Functionalization. *Chem. Eur. J.* **10**, 812–817 (2004).
36. Dyke, C. A. & Tour, J. M. Unbundled and Highly Functionalized Carbon Nanotubes from Aqueous Reactions. *Nano Lett.* **3**, 1215–1218 (2003).
37. Zeng, L., Alemany, L. B., Edwards, C. L. & Barron, A. R. Demonstration of covalent sidewall functionalization of single wall carbon nanotubes by NMR spectroscopy: Side chain length dependence on the observation of the sidewall sp3 carbons. *Appl. Phys. A* **1**, 72–88 (2008).
38. Saini, R. K. *et al.* Covalent Sidewall Functionalization of Single Wall Carbon Nanotubes. *J. Am. Chem. Soc.* **125**, 3617–3621 (2003).
39. Chen, S., Zheng, J., Li, L. & Jiang, S. Strong Resistance of Phosphorylcholine Self-Assembled Monolayers to Protein Adsorption: Insights into Nonfouling Properties of Zwitterionic Materials. *J. Am. Chem. Soc.* **127**, 14473–14478 (2005).
40. Zhang, W. *et al.* Modular Functionalization of Carbon Nanotubes and Fullerenes. *J. Am. Chem. Soc.* **131**, 8446–8454 (2009).
41. Zhang, W. & Swager, T. M. Functionalization of Single-Walled Carbon Nanotubes and Fullerenes via a Dimethyl Acetylenedicarboxylate−4-Dimethylaminopyridine Zwitterion Approach. *J. Am. Chem. Soc.* **129**, 7714–7715 (2007).
42. Krungleviciute, V., Lask, K., Migone, A. D., Lee, J. Y. & Li, J. Kinetics and equilibrium of gas adsorption on RPM1-Co and Cu-BTC metal-organic frameworks: Potential for gas separation applications. *AIChE J.* **54**, 918–923 (2008).
43. Surapathi, A., Herrera-Alonso, J., Rabie, F., Martin, S. & Marand, E. Fabrication and gas

transport properties of SWNT/polyacrylic nanocomposite membranes. *Journal of Membrane Science* **375**, 150–156 (2011).
44. Halicioglu, T. & Jaffe, R. L. Solvent effect on functional groups attached to edges of carbon nanotubes. *Nano Lett.* **2**, 573–575 (2002).

Chapter 5. Gas Transport in Zwitterion-Functionalized Carbon Nanotube Nanocomposite Membranes

5.1. Introduction

Recent efforts to improve the performance of mixed matrix membranes have resorted to the incorporation of carbon nanotubes into polymeric materials[1-6]. This research is based on the hypothesis that carbon nanotubes facilitate unique transport properties of fluids within the CNTs due to the unprecedented smoothness and regularity of the CNT pores[4,6-14]. Thus, CNT incorporation into a polymer film or into an assembled membrane can potentially increase membrane performance. The unique transport properties of carbon nanotubes have been documented both by molecular simulations and experiments[4,6-14]. For example, the transport of simple gases in both multi-walled and single-walled carbon nanotube membranes has been shown to be orders of magnitude larger than that predicted by Knudsen diffusion[1,4,6]. However, gas selectivities of CNT membranes generally follow the Knudsen model as well, being quite low in comparison to selectivities offered by neat polymer membranes[4,6]. Since the pores of carbon nanotubes are typically on the order of 10 - 15 Å for SWNT and 100 Å for MWCNT, it is difficult to achieve molecular sieving of gases with kinetic diameters ranging from 2.7 Å to 6 Å. We hypothesize that one way to get around this problem is to introduce functionalized moieties at the carbon nanotube tips that can have specific molecular interactions with particular gases and/or whose presence partially blocks the access to the CNT pores, thereby decreasing the effective CNT pore size. Thus, one aim of this study is to compare the transport rates of CNT membranes made with single-walled carbon nanotubes functionalized with two different molecular moieties, namely carboxylic acid groups, COOH- (with molecular dimensions on the order of 0.4nm) and larger zwitterionic groups, $-COO-(CH_2)_3-N^+(CH_3)_2-(CH_2)_2COO-$ (with molecular dimensions between 1.1 -1.2nm).

Besides CNT functionalization, the structure of the carbon nanotube mixed matrix membrane can also be critical to performance. For example, carbon nanotubes have been mixed into polymer matrices and formed into membranes in order to take advantage of the high CNT transport rates. While several CNT mixed matrix membranes with improved gas selectivities and permeabilities[1-4,15] have been reported, it is doubtful that such improvements can be attributed to actual transport through the carbon nanotubes, whose composition in the mixed matrix membranes has been typically very low, i.e. 1-4 % by weight. More likely, the CNTs in the

mixed matrix membranes act as any other impermeable fillers, affecting the polymer morphology, chain stiffness and hence matrix permeability. To achieve viable transport through the carbon nanotubes, it would seem more desirable to create large-scale CNT membrane platforms with highly ordered vertical orientation of densely packed pores. A common way to do this is by chemical vapor deposition, a method that relies on precise catalyst patterning and special substrate materials[1,7]. For example, Holt et al., have constructed nanotube-Si_3N_4 composite membranes using chemical vapor deposition[7]. They used aligned double walled carbon nanotubes having a diameter of about 1.6 nm. Holt et al. confirmed that gas flow through narrow carbon nanotubes is orders of magnitude faster than would be expected for flow through a traditional nanoporous material based on Knudsen diffusion[1,7,16,17]. They also found that liquid water flow through their nanotube membranes was more than three orders of magnitude faster than expected from hydrodynamic flow. Moreover, their nanotube membranes exhibited extraordinarily high particle size exclusion selectivity[1,7,16,17]. However, no selectivity for gas mixtures was demonstrated. In related work, Hinds and coworkers[18] constructed polymer-nanotube composite membranes using multiwall carbon nanotubes having much larger diameters (6-7 nm) than those used by Holt et al. They have verified that transport of liquids (alkanes, water) is orders of magnitude faster than can be accounted for by conventional hydrodynamic flow[9].

More recently, Lin et al. have fabricated vertically aligned multi-walled carbon nanotubes supported by porous α-alumina by a multi-step method consisting of growing vertical CNTs by chemical vapor deposition, filling the inter-CNT gaps with polystyrene and removing the PS over-layer by polishing and acid treatment[1]. The average CNT pore dimensions were 6.3 nm. As expected the resulting CNT membranes exhibited gas diffusivity values about four times larger than the values predicted by the Knudsen diffusion model. However, the H_2/N_2 selectivity was 3.8, which is order of magnitude lower than what can be achieved by polymeric membranes. For example, polyimide membranes have H_2/N_2 selectivity of about 200[19].

The CVD method of CNT membrane fabrication is not practical for industrial-scale applications because the area of CVD-prepared CNT membranes is constrained by the size of the reactor and any scale up and cost are prohibitive. To overcome this challenge, we have developed a method of fabricating dense, semi-vertically oriented carbon nanotubes on a porous support using a high-pressure filtration method that relies on hydrodynamics to orient the carbon

nanotubes[4,14]. The advantage of this approach is that the carbon nanotubes can be obtained commercially or synthesized specifically for a given application with the desired pore size and functionality. Furthermore, the CNTs can be purified and their pore size and pore-size distribution can be characterized before they are assembled into a CNT membrane. In this study we employ a porous polymeric support and interfacial polymerization to fix the carbon nanotubes in a polymer matrix, an approach that should be easily adaptable in commercial membrane fabrication involving large surface areas.

5.2. Experiments

5.2.1. Materials

COOH functionalized SWNTs of outer diameter 1.5 nm and length 1μm were purchased from Nano Lab Inc. (MA, USA). The CNTs were produced by a CVD method, purified and functionalized with COOH groups by refluxing in sulfuric acid/nitric acid. Purity of the SWNTs was greater than 95% as determined by TGA. Concentration of COOH groups in the SWNTs was approximately 2-7 wt% as determined by titration. Polyethersulfone (PES) microporous supports were purchased from Trisep Corporation, CA. The two reagents, m-phenylenediamine (MPD, ≥99%) and trimesoyl chloride (TMC, 98%) were purchased from Sigma-Aldrich and used without any additional purification. Hexane, 99.9% purity was purchased from Fischer Scientific. Surfactant, sodium dodecylbenzene sulfonate was purchased from Sigma and has a purity of 80%.

The synthesis of the zwitterionic functionalized SWNTs, whose structure is shown in Figure 5-1, is reported elsewhere[20]. The zwitterion functional group is circled red in Figure 5-1.

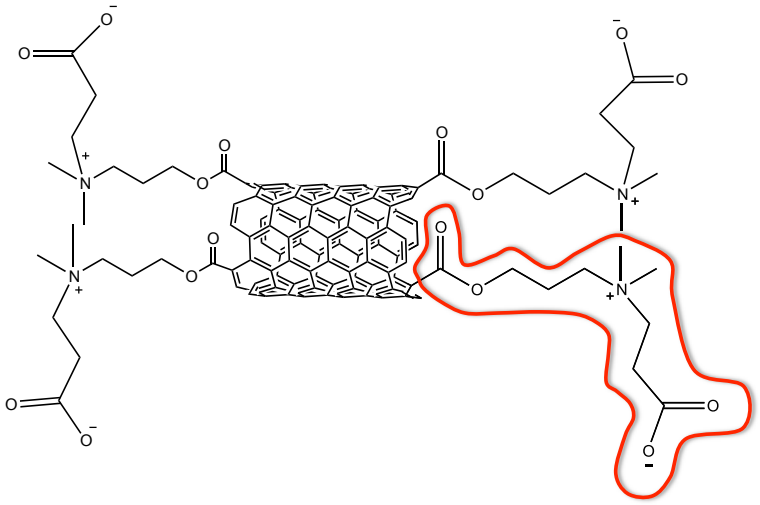

Figure 5-1. Structure of zwitterionic groups on the carbon nanotube tips.

5.2.2. Fabrication of Polyamide/SWNT Nanocomposite Membranes

5.2.2.1. Dispersion of SWNTs and Alignment by High Pressure Filtration

A predetermined amount of zwitterion functionalized SWNTs was sonicated in deionized water. The polyethersulfone membrane support was pretreated by soaking in a 0.5 % (w/v) surfactant solution of sodium dodecyl benzene sulfonate for 2 days. This pretreatment was necessary to make the membrane support more hydrophilic.

The aqueous SWNT suspension was then deposited on the membrane support using high-vacuum filtration method, in which the support acted as a filter paper and the CNTs were filtered out of the solution and aligned on the support. The filtration at high pressure was assumed to induce alignment of the SWNTs in the direction of the flowing solvent[21]. Filter disc, with a thin layer of SWNTs was dried under vacuum for 12 hours. The SWNT alignment was locked in a polyamide matrix polymer, formed by interfacial polymerization as discussed below. The concentration of the SWNTs in the polymer matrix ranged from zero to approximately 65% by weight. The various samples and their concentrations are summarized in Table 5-1.

5.2.2.2. Interfacial Polymerization (IP)

For interfacial polymerization, two solutions containing the monomers were prepared. The aqueous solution consisted of 2% (w/v) m-phenylene diamine (MPD) in water along with 0.2% (w/v) surfactant to improve the wetting of the support by the solution. The organic solution consisted of trimesoyl chloride (TMC) 0.5 % (w/v) in hexane.

The PES support with the deposited CNTs was placed between two circular PTFE frames, held together with a metal clamp. The polyester side of the PES support was soaked with MPD for 1 min. After that, the MPD solution was drained and the support dried for a minute, cleaning the excess MPD solution using a Kim wipe. Then, the TMC solution was introduced on the polysulfone side of the support, using a syringe. The TMC solution was drained very slowly after 2 minutes. The reaction time for the IP was 2 min. The TFN membrane prepared was cured in air-circulated oven at 68 ^{o}C for 5 min. The membrane was washed in deionized water to remove excess MPD, and then stored in water for at least one day before being tested.

5.2.3. Characterization

The cross-section morphology of the SWNT/polyamide membranes was analyzed by scanning electron microscopy (FESEM, LEO 1550). The gas transport properties of the membranes were measured using a constant-volume permeability apparatus[22]. Two types of

membranes were studied. The first type of membrane was made using carboxylic-acid functionalized single walled carbon nanotubes, COOH-SWNTs. The second membrane was made with zwitterion-functionalized SWNTs. All permeation tests were performed at room temperature with 2 atm feed pressure and vacuum on the permeate side. The gases used in the experiment were hydrogen (H_2), helium (He), oxygen (O_2), nitrogen (N_2), methane (CH_4), carbon dioxide (CO_2) and sulfur hexafluoride (SF_6).

5.3. Results and Discussion

5.3.1. Scanning Electron Microscopy (SEM)

Figure 5-2 shows the SEM image of the cross-section of the zwitterion functionalized SWNT TFN membranes. The porous region in the image represents polyethersulfone layer, which is present on top of the polyester support. Thin dense layer on top of the PES layer consists of the polyamide layer with zwitterion functionalized SWNTs. At this magnification, it is not possible to see the SWNTs embedded in the polyamide polymer. Because of the low magnification, it is very difficult to comment on the degree of alignment of the tubes within the matrix polymer simply by looking at the image. We only assume that SWNTs are aligned to some extent accepting that there is a lot of scope in improving the alignment of the SWNTs. Possible ways of improving the alignment of SWNTs are by employing electric field[23-25] and magnetic field[26-28].

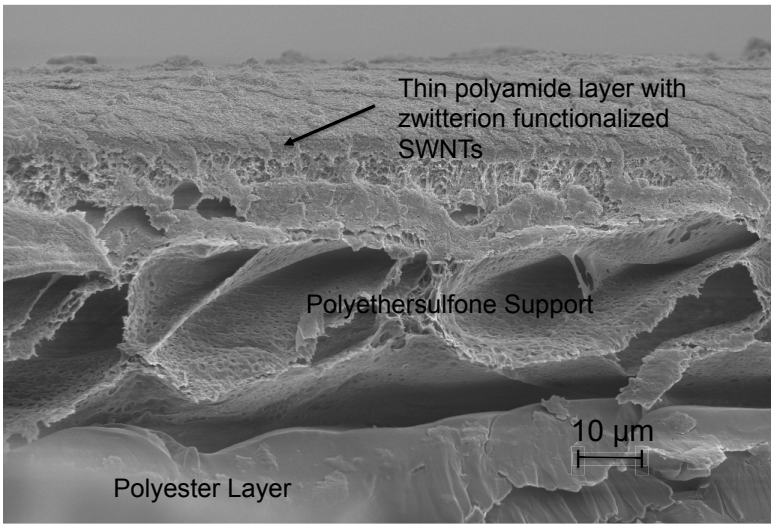

Figure 5-2. Cross-section SEM image of functionalized SWNT/polyamide membrane.

5.3.2. Gas Transport Properties of SWNT/Polyamide Nanocomposite Membranes

Thin film nanocomposite membranes having different SWNT concentrations in the polyamide separation layer were fabricated and tested for their gas transport properties. These concentrations are summarized in Table 5-1. Figure 5-3 shows the gas permeabilities of light gases (H_2, He, N_2, O_2, CH_4, CO_2 and SF_6) in the zwitterion functionalized SWNT thin film nanocomposite membrane in comparison to gas permeabilities in the neat polyamide (PA) membrane. Numerical data is presented in Table 5-2. As is evident in the plot, the permeabilities of all gases increased with increasing concentration of the CNTs in the separation layer. For example, the H_2 permeability increased by a factor of 25 from 325 Barrer in the pure PA to 8072 Barrer in the 65 wt% CNT PA membrane. Similar increases are observed for other gases (factor increase in parenthesis), He (19), N_2 (19), O_2 (33), CH_4 (21), CO_2 (37) and SF_6 (29). This tremendous increase in permeability is due to the transport through the CNT pores as well as through possible nano-channels formed around individual CNTs within CNT bundles. Although there is no way to prove this directly, the fact that the permeability of each gas increases with the concentration of CNTs in the matrix would be consistent with this explanation, since we would expect the number of nano-channels to increase with CNT content.

Table 5-1. Weight concentrations of functionalized SWNTs in matrix polymer.

Weight of Zwitterion –SWNTs (mg)	Weight % of Z-SWNTs in polyamide layer
0	0
1	26
1.5	32
2	38
5	65

Table 5-2. Gas permeabilities (in Barrer) of different gases in zwitterion functionalized SWNT polyamide nanocomposite membranes of various compositions (wt% of CNTs in membranes).

Gas	0 wt%	26 wt%	32 wt%	38 wt%	65 wt%
H_2	325	1912	2664	2760	8072
He	250	1407	1804	1963	4863
N_2	156	675	767	957	2902
O_2	77	570	776	805	2506
CH_4	203	957	1317	1306	4151
CO_2	71	575	763	770	2614
SF_6	65	391	510	507	1880

Figure 5-4 shows the selectivities of various gases with respect to He for TFN membranes with varying concentration of zwitterion functionalized SWNTs and presented in Table 5-3. As can be seen from the data, the selectivities of gases with respect to He remain nearly constant across all compositions. Unfortunately, this result does not support the idea that functionalization of the CNTs with these particular zwitterionic groups will improve selectivity. However, the membranes retained the intrinsic selectivity of the polyamide, while having tremendous enhancements in permeability.

Table 5-3. Selectivities of gases with respect to He in different nanocomposite membranes (wt% of CNTs in membranes).

Gas Pair	Knudsen	0 wt%	26 wt%	32 wt%	38 wt%	65 wt%
H_2/He	1.4	1.3	1.4	1.5	1.4	1.7
N_2/He	0.38	0.62	0.48	0.43	0.49	0.60
O_2/He	0.35	0.31	0.41	0.43	0.41	0.52
CH_4/He	0.5	0.81	0.68	0.73	0.67	0.85
CO_2/He	0.3	0.28	0.41	0.42	0.39	0.54
SF_6/He	0.17	0.26	0.28	0.28	0.26	0.39

There are two plausible explanations for the low selectivity obtained with functionalized SWNTs. Our corresponding gas sorption study of the same carbon nanotubes[20] suggests that the presence of zwitterion functional groups on the carbon nanotube tips, while retarding the sorption of gases inside the nanotubes, still allows the full passage of small molecules given

enough equilibrium time. The second possible explanation for the low gas selectivity is the presence of nano-channels depicted in Figure 5-5.

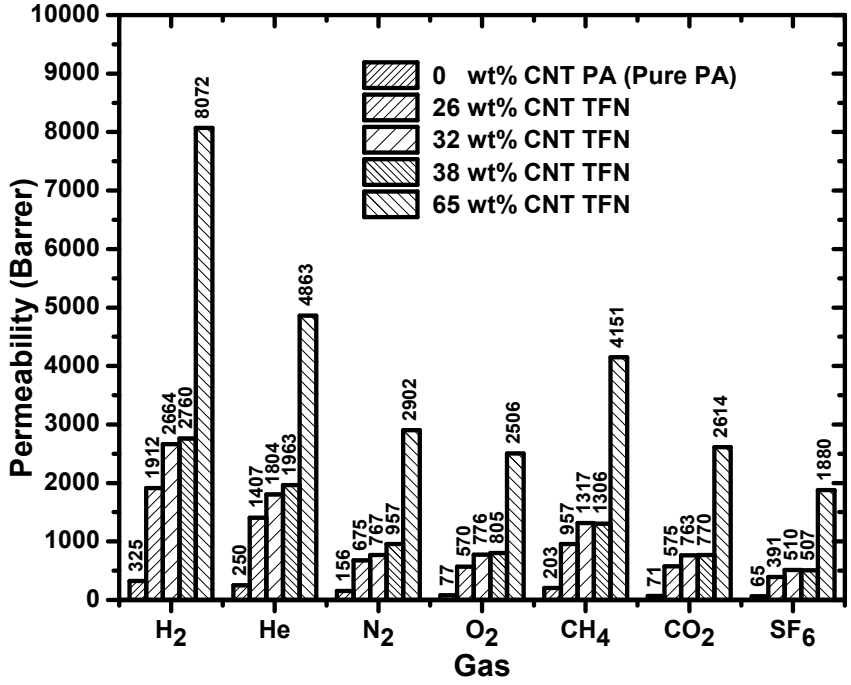

Figure 5-3. Gas permeabilities of different gases in zwitterion functionalized SWNT polyamide nanocomposite membrane.

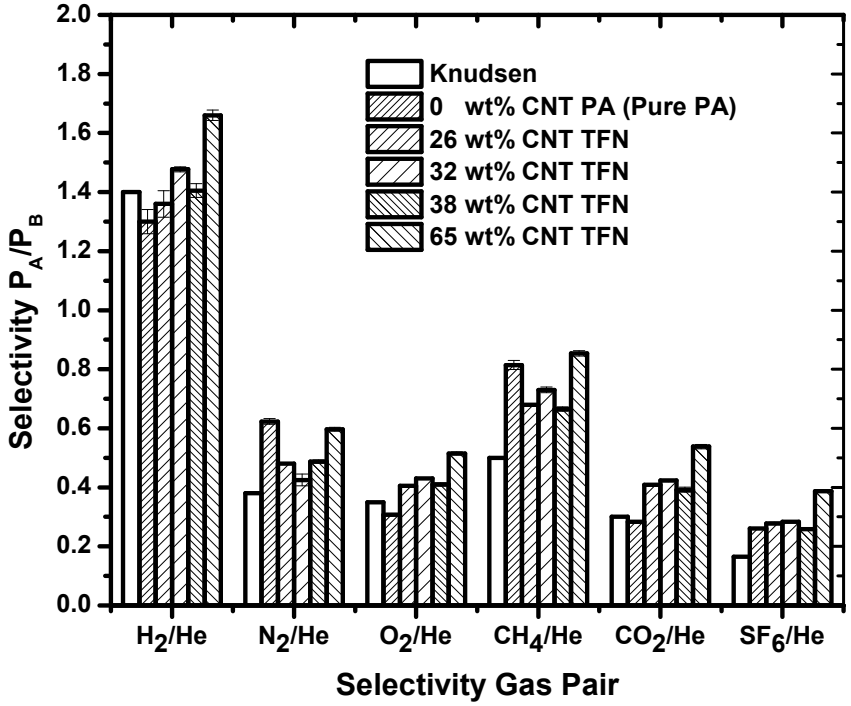

Figure 5-4. Selectivities of gases with respect to He in different nanocomposite membranes.

A gas molecule, while diffusing through the matrix polymer, encounters the opening of a zwitterion functionalized SWNT. This molecule has three paths of transport, path AB, AC and AD. The transport of gas molecule in the path AB is affected by two phenomenon namely (i) size exclusion and (ii) molecular interactions. For non-functionalized carbon nanotube, gas molecules experience resistance for entering inside the pore of the tube[29]. Once inside the tube, there is absolutely no resistance to transport of gas molecule due to the atomically smooth inner surface of the carbon nanotube. This factor dominates the entry/exit resistances, making the path AB (no functional group) as a favored path of motion for the gas molecule. However, if the kinetic diameter of the gas molecule is larger than the diameter of the CNT, it cannot enter the tube. This phenomenon is called size exclusion effect. Assuming in this case that the functional groups by their presence change the effective diameter of the CNT, the effective pore diameter would be defined as the diameter of the largest gas molecule that can enter inside of the tube through its opening. Hence, if the kinetic diameter of the gas molecule is smaller than the effective diameter of the CNT as shown in Figure 5-5(a), the gas molecule travels in the path AB. Secondly, if the functional group has a favorable interaction (like dipolar-dipolar interactions), then the path AB may be favored for transport by the gas molecule. This phenomenon is called molecular interactions effect. Our previous sorption studies[20] using the same CNTs of diameter 1.5 nm, have demonstrated that the concentration of gases adsorbed in the zwitterion functionalized CNTs is very low. This suggests that the entry of gas molecules inside the tube in the presence of zwitterion functional groups is not favored. These two phenomenon together define the gatekeeper mechanism, which affects the transport of the gas molecule through path AB.

On the other hand, path AC, where the molecule passes through the nano channel, which is mostly empty space, is a path of least resistance. These nano channels are formed since the glassy polymer is not flexible enough to conform to the sidewalls of the carbon nanotubes forming interfacial defect volumes. Hence, in zwitterion functionalized SWNTs of diameter 1.5 nm, path AC is favored more than path AB. Therefore, any kind of selectivity that may occur due to the interactions between the functional group and the incoming gas molecule is not realized because majority of the gas molecules diffusing through the membrane preferentially diffuse in the nanochannels rather than through the pore of the CNT. Path AD is the diffusion of the gas in the polymer, which has more resistance to transport compared to path AC. Hence, the gas molecules preferentially move through path AC than AD.

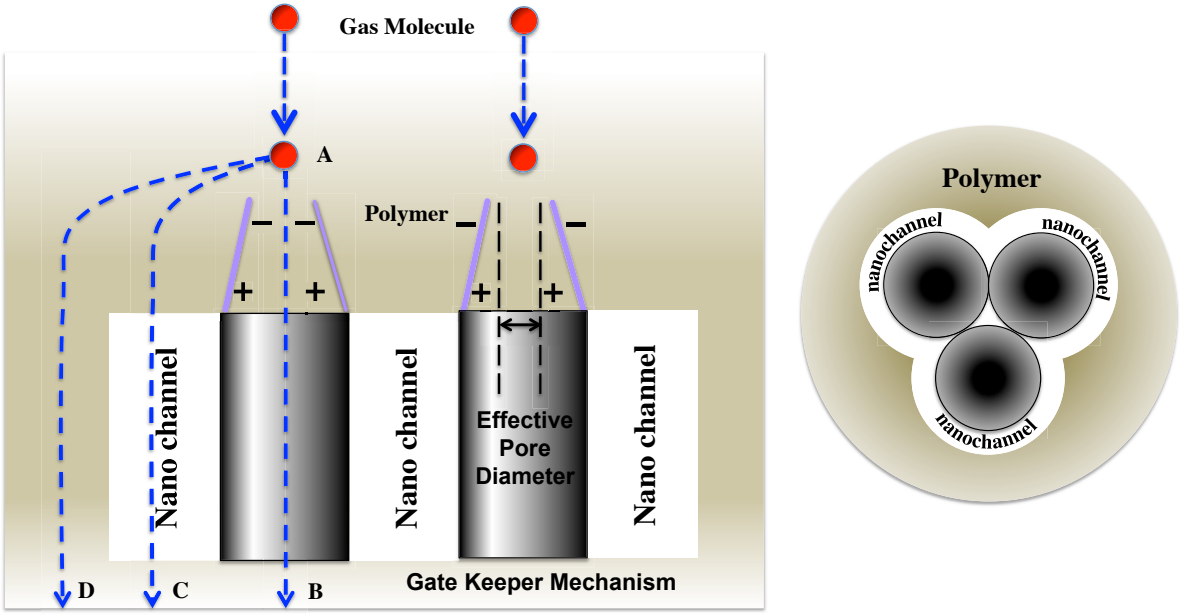

(A) (B)

Figure 5-5. Schematic of (A) the transport of a gas molecule near the opening of a SWNT embedded inside the matrix polymer (B) arrangement of SWNTs as bundles with nanochannels in between and around the tube inside the polymer.

Since a nanochannel is an empty volume, the diffusivity of the gas in it is much higher than the diffusivity of the gas in the polymer. As the concentration of CNTs increases, the density of the nanochannels within the membrane will also increase, thereby increasing the permeability of the gases by large factors.

We can probe the presence of nano-channels by comparing the permeation properties of zwitterion-functionalized CNT membranes with COOH-functionalized CNT membranes at the same CNT composition. If the transport through the membranes occurs only through the nano-channels, then the gas permeabilities of both types of membranes should be the same, regardless of the nature of functionalization. Clearly, this is not the case.

Figure 5-6 compares the permeabilities of the two types of membranes at the same CNT concentration. The data is also presented in Table 5-4. Although the gas permeabilities in both types of SWNT membranes are higher than the pure polyamide membrane, the gas permeabilities in the COOH functionalized SWNT membrane are significantly higher than in the zwitterion functionalized SWNT membrane. This result is consistent with our previous sorption studies, which demonstrated that gases adsorb more in COOH functionalized SWNTs than in

zwitterion functionalized SWNTs[20]. Based on the schematic in Figure 5-5, we can infer that in COOH functionalized SWNT membranes; path AB is also favorable along with the nanochannel (path AC) for gas diffusion. Since the transport of gas is very rapid through the inner core of the nanotube, the overall permeability of the COOH-SWNT membrane almost doubled compared to the zwitterion functionalized SWNT membrane.

Table 5-4. Permeability (in Barrer) of various light gases through 26 wt% SWNT TFN membranes with different functionalization, zwitterion and carboxylic acid groups.

Gas	0 wt% Pure PA	26 wt% Zwitterion-SWNTs	26 wt% COOH -SWNTs
H_2	325	1912	3625
He	250	1407	2479
N_2	156	675	1373
O_2	77	570	1021
CH_4	203	957	1765
CO_2	71	575	1167
SF_6	65	391	827

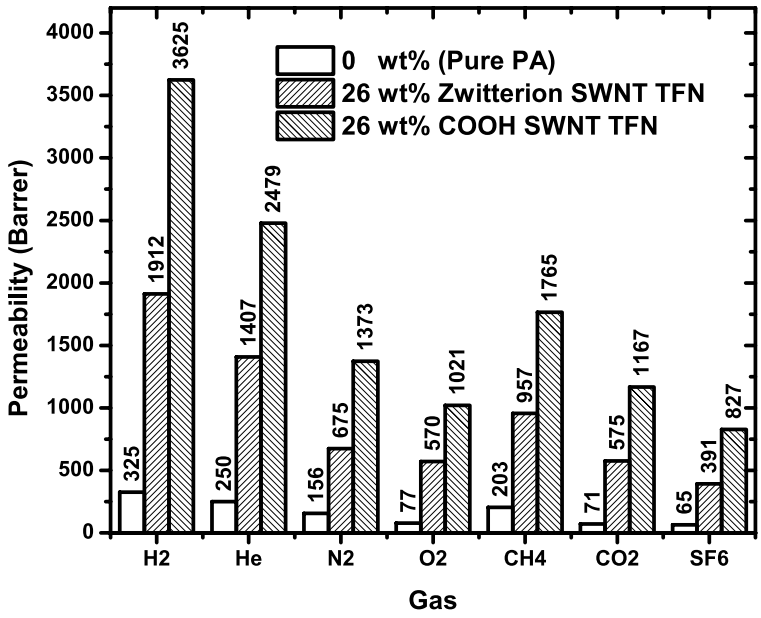

Figure 5-6. Permeability of various light gases through 26 wt% SWNT TFN membranes with different functionalization, zwitterion and carboxylic acid groups

Figure 5-7 compares the selectivities of gases with respect to helium in both types of functionalized SWNT membranes and the neat PA membrane of the same thickness. This data is also presented in Table 5-5. The selectivities change very little, suggesting that the separation is controlled by the inherent selectivity of the polyamide coating.

Table 5-5. Selectivities of various light gases through 26 wt% SWNT TFN membranes with different functionalization, zwitterion and carboxylic acid groups.

Gas Pair	0 wt% Pure PA	26 wt% Zwitterion-SWNTs	26 wt% COOH -SWNTs
H_2/He	1.3	1.4	1.5
N_2/He	0.62	0.48	0.55
O_2/He	0.31	0.41	0.41
CH_4/He	0.81	0.68	0.71
CO_2/He	0.28	0.41	0.47
SF_6/He	0.26	0.28	0.33

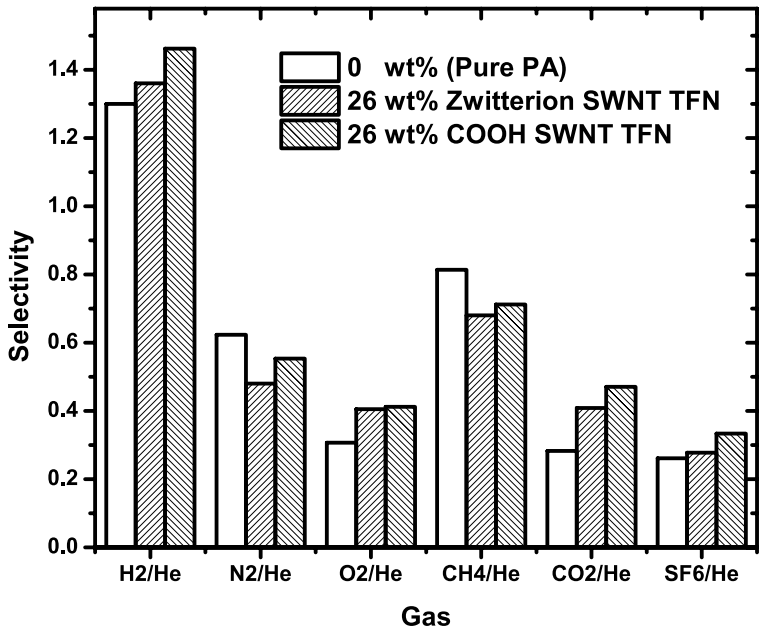

Figure 5-7. Selectivities of various light gases through 26 wt% SWNT TFN membranes with different functionalization, zwitterion and carboxylic acid groups.

The molecular diffusion in these nanostructured membranes clearly takes place through the inner CNT pores, partly through the nanochannels and eventually through the polymer matrix

according to the resistance offered by each mode. Hence, the overall selectivity of the membrane is affected by all three modes of transport. The gas selectivities in the nanostructured membranes as well as in the neat polyamide membrane are very similar and close in value to selectivities predicted by the Knudsen model.

Figure 5-8 represents the Robeson plots along with selected experimental data plotted on it. Two industrially important separations, CO_2 from CH_4, and O_2 from N_2, are chosen for comparing the gas separation performance of the current TFN membranes with the literature. The plots also include Knudsen permeability and selectivity data point for the respective gas pairs. Knudsen gas permeability was calculated based on the information reported in an earlier paper[4].

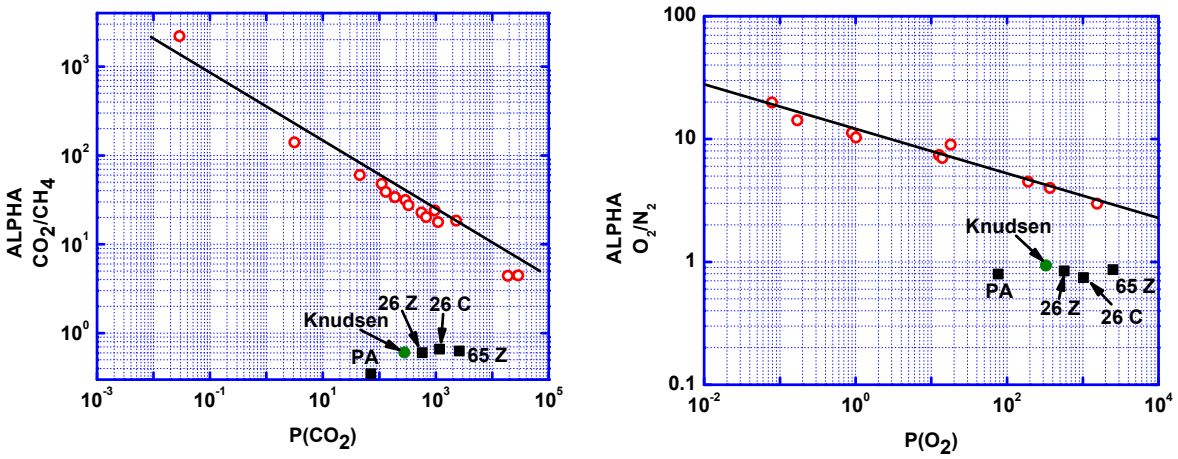

(A) (B)

Figure 5-8. Robeson plots of (A) CO_2 and CH_4 (B) O_2 and N_2, including the experimental data for the following membranes: **PA**-Polyamide, **26 Z**- 26 wt% zwitterion SWNT TFN, **65Z** - 65 wt% zwitterion SWNT TFN and **26 C** – 26 wt% COOH SWNT TFN membranes.

It can be seen from Figure 5-8(A) that permeability data points move horizontally with increase in the concentration of zwitterion SWNTs, without much loss in selectivity for CO_2/CH_4. It can also be observed that the gas permeabilities in TFN membranes are higher than Knudsen permeability while selectivities are very close to Knudsen selectivity. The selectivity/permeability data points of TFN membranes for different concentrations and functionalization of SWNTs were below the Robeson upper bound. Similar behavior is also observed in Figure 5-8(B), for O_2/N_2.

However, it is quite clear that with a proper choice of the matrix polymer (high selectivity but low permeability) and the functionalized SWNTs, it is possible to make TFN membranes,

which will exhibit high permeability and selectivity. This type of membrane is represented in a Robeson plot as shown in Figure 5-9.

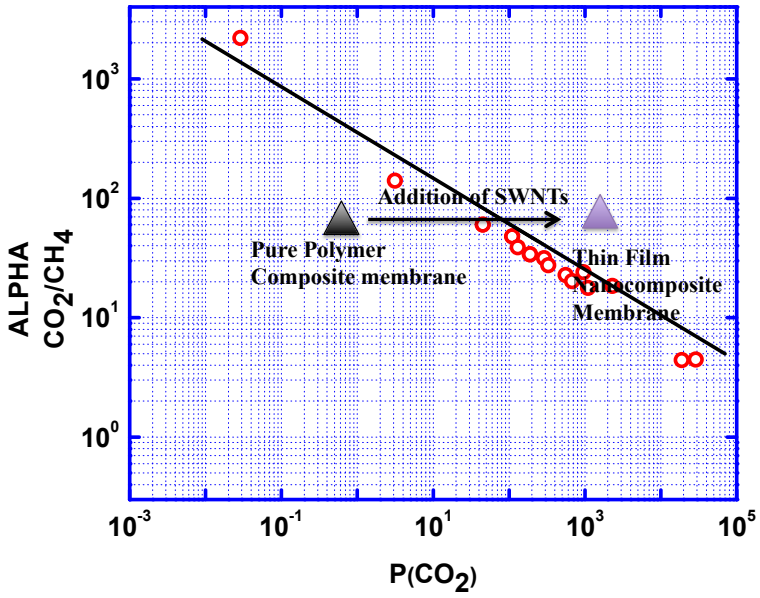

Figure 5-9. Robeson plot for CO_2/CH_4

5.4. Conclusions

The gas transport through nano-composite carbon nanotube membranes was orders of magnitude higher than that observed in neat polyamide membranes of the same thickness. The gas permeabilities increased in proportion to the concentration of single-walled carbon nanotubes in the membrane selective layer, while gas selectivities remained essentially constant when compared to the neat polyamide membrane. Functionalization of the carbon nanotubes also played a role in the overall transport. Zwitterion-functionalized carbon nanotube membranes demonstrated lower gas permeabilities than carboxylic acid functionalized carbon nanotube membranes, reflecting a gatekeeper type mechanism. The results also suggest that there may be at least three modes of transport through the nano-composite membrane, namely transport through the carbon nanotube pores, through nano-interstitial sites created by carbon nanotube bundles and through the polymer matrix. Hence, the overall permeability and selectivity of the carbon nanotube membrane is affected by all three modes of transport.

5.5. Acknowledgements

We like to thank the US Bureau of Reclamation for sponsoring this work via grant #R10AP81214.

5.6. References

1. Mi, W., Lin, Y. S. & Li, Y. Vertically aligned carbon nanotube membranes on macroporous alumina supports. *Journal of Membrane Science* **304**, 1–7 (2007).
2. Ismail, A. F., Goh, P. S., Sanip, S. M. & Aziz, M. Transport and separation properties of carbon nanotube-mixed matrix membrane. *Separation and Purification Technology* **70**, 12–26 (2009).
3. Majeed, S. *et al.* Multi-walled carbon nanotubes (MWCNTs) mixed polyacrylonitrile (PAN) ultrafiltration membranes. *Journal of Membrane Science* **403-404**, 101–109 (2012).
4. Surapathi, A., Herrera-Alonso, J., Rabie, F., Martin, S. & Marand, E. Fabrication and gas transport properties of SWNT/polyacrylic nanocomposite membranes. *Journal of Membrane Science* **375**, 150–156 (2011).
5. Kim, S., Pechar, T. W. & Marand, E. Poly(imide siloxane) and carbon nanotube mixed matrix membranes for gas separation. *Desalination* **192**, 330–339 (2006).
6. Marand, E., Surapathi, A., Johnson, J. K., Kumar, P. & Shankar, C. Nanofluidic and Gas Transport in Carbon Nanotube Membranes. *Advanced functional materials for membrane preparation* 51–63 (2011).
7. Holt, J. K., Noy, A., Huser, T., Eaglesham, D. & Bakajin, O. Fabrication of a Carbon Nanotube-Embedded Silicon Nitride Membrane for Studies of Nanometer-Scale Mass Transport. *Nano Lett.* **4**, 2245–2250 (2004).
8. Holt, J. K. Fast Mass Transport Through Sub-2-Nanometer Carbon Nanotubes. *Science* **312**, 1034–1037 (2006).
9. Majumder, M., Chopra, N., Andrews, R. & Hinds, B. J. Nanoscale hydrodynamics: Enhanced flow in carbon nanotubes. *Nature* **438**, 44–44 (2005).
10. Majumder, M., Chopra, N. & Hinds, B. J. Effect of Tip Functionalization on Transport through Vertically Oriented Carbon Nanotube Membranes. *J. Am. Chem. Soc.* **127**, 9062–9070 (2005).
11. Chen, H. & Sholl, D. S. Predictions of selectivity and flux for CH_4/H_2 separations using single walled carbon nanotubes as membranes. *Journal of Membrane Science* **269**, 152–160 (2006).
12. Chen, H. & Sholl, D. S. Rapid Diffusion of CH_4/H_2 Mixtures in Single-Walled Carbon Nanotubes. *J. Am. Chem. Soc.* **126**, 7778–7779 (2004).
13. Ackerman, D., Skoulidas, A., Sholl, D. & Johnson, J. K. Diffusivities of Ar and Ne in Carbon Nanotubes. *Mol. Simulation* **29**, 677–684 (2003).
14. Kim, S., Jinschek, J. R., Chen, H., Sholl, D. S. & Marand, E. Scalable Fabrication of Carbon Nanotube/Polymer Nanocomposite Membranes for High Flux Gas Transport. *Nano Lett.* **7**, 2806–2811 (2007).
15. Choi, J.-H., Jegal, J., Kim, W.-N. & Choi, H.-S. Incorporation of multiwalled carbon nanotubes into poly(vinyl alcohol) membranes for use in the pervaporation of water/ethanol mixtures. *J. Appl. Polym. Sci.* **111**, 2186–2193 (2009).
16. Holt, J. K. Carbon Nanotubes and Nanofluidic Transport. *Adv. Mater.* **21**, 3542–3550 (2009).
17. Noy, A. *et al.* Nanofluidics in carbon nanotubes. *Nano Today* **2**, 22–29 (2007).
18. Hinds, B. J. *et al.* Aligned Multiwalled Carbon Nanotube Membranes. *Science* **303**, 62–65 (2004).
19. Pinnau, I. & Koros, W. J. Gas-permeation properties of asymmetric polycarbonate, polyestercarbonate, and fluorinated polyimide membranes prepared by the generalized

dry–wet phase inversion process. *J. Appl. Polym. Sci.* **46**, 1195–1204 (1992).
20. Surapathi, A., Chen, H.-Y., Marand, E. & Johnson, J. K. Gas Sorption Properties of Zwitterion-Functionalized Carbon Nanotubes. *Journal of Membrane Science*
21. deHeer, W. A. *et al.* Aligned Carbon Nanotube Films: Production and Optical and Electronic Properties. *Science* **268**, 845–847 (1995).
22. Dhingra, S. S. & Marand, E. Mixed gas transport study through polymeric membranes. *Journal of Membrane Science* **141**, 45–63 (1998).
23. Chen, X. Q., Saito, T., Yamada, H. & Matsushige, K. Aligning single-wall carbon nanotubes with an alternating-current electric field. *Appl. Phys. Lett.* **78**, 3714–3716 (2001).
24. Martin, C. A. *et al.* Electric field-induced aligned multi-wall carbon nanotube networks in epoxy composites. *Polymer* **46**, 877–886 (2005).
25. Park, C. *et al.* Aligned single-wall carbon nanotube polymer composites using an electric field. *J. Polym. Sci. B Polym. Phys.* **44**, 1751–1762 (2006).
26. Fischer, J. E. *et al.* Magnetically aligned single wall carbon nanotube films: Preferred orientation and anisotropic transport properties. *J. Appl. Phys.* **93**, 2157 (2003).
27. Mauter, M. S., Elimelech, M. & Osuji, C. O. Nanocomposites of Vertically Aligned Single-Walled Carbon Nanotubes by Magnetic Alignment and Polymerization of a Lyotropic Precursor. *ACS Nano* **4**, 6651–6658 (2010).
28. Smith, B. W. *et al.* Structural anisotropy of magnetically aligned single wall carbon nanotube films. *Appl. Phys. Lett.* **77**, 663 (2000).
29. Chen, H., Johnson, J. K. & Sholl, D. S. Transport Diffusion of Gases Is Rapid in Flexible Carbon Nanotubes. *J. Phys. Chem. B* **110**, 1971–1975 (2006).

Chapter 6. The Role of Solubility Partition Coefficient at the Mixed Matrix Interface in the Performance of Mixed Matrix Membranes

6.1. Introduction

Mixed matrix membranes have the potential to achieve significant improvement in membrane performance in gas separations by combining a continuous polymer bulk phase with a highly selective and/or permeable dispersed inorganic phase[1-18]. It has been shown that the matching of the permeabilities of the matrix and the filler is an important factor in the design of mixed matrix membranes[13]. For example if the matrix permeability is either too high or too low in comparison to the filler, the selectivity of the mixed matrix system will not improve in comparison to the neat polymer. In this paper we propose that an additional property that needs to be matched in the two-component system is that of the solubility partition coefficient at the mixed matrix interface. Strathmann et al. have demonstrated the importance of the partition coefficient by using numerical simulations to predict the penetrant concentrations in a polymeric matrix filled with permeable particles[3]. Their results showed that the apparent permeability of the dispersed phase is actually lower than the intrinsic permeability of the dispersed phase when the flux through the filler particles is restricted by the polymer phase. This is true because the driving force over the heterogeneous membrane, expressed as the concentration gradient, is not the same as the driving force over the particles and the polymer phase when measured separately. In fact, a discontinuity in concentration exists at the interface between the matrix and the particle. This phenomenon has a direct implication on the effective permeability of the mixed matrix membrane.

Aside from numerical simulations, numerous analytical models have been utilized in an attempt to predict the membrane performance of mixed matrix membranes as a function of the intrinsic transport properties of the components and the volume fraction of the dispersed phase[2,14,17,19,20]. These models, such as Maxwell, Bruggeman, Pal and Feske provide a simple quantitative framework for estimating the effective permeability of a mixed matrix system. Because of their simplicity, though, application of these models to variety of mixed matrix systems can lead to inconsistent results[21]. Most of these discrepancies can be attributed to poor interfacial contact between the molecular sieve and glassy polymers, high loading conditions and large filler aspect ratios, which don't meet the assumptions associated with the simple predictive models. However, even effective permeabilities of mixed matrix systems with idealized

interfacial conditions may not conform to the various theoretical models[21]. For example, both the Bruggeman and the Maxwell Models gave poor predictions for Matrimid®/carbon molecular sieve mixed matrix membranes, overestimating the gas permeabilities of CO_2 and O_2 gases[20]. The lower-than-predicted permeabilities have been attributed to an inhibition of polymer chain mobility at the polymer-sieve interface. Koros et al. was able to account for this phenomenon by introducing an additional interfacial "rigidified" region at the matrix/filler interface with separate intrinsic properties in the Maxwell model[14,15,20]. Shimekit et al.[19] have modified the Pal model with the "rigidified interface" as well, to obtain an improved agreement with experimental data for several mixed matrix systems. Although the fit of such modified models with the experimental data is better, the additional parameters, such as the volume fraction of the rigidified interfacial layer and its intrinsic permeability are additional adjustable parameters that cannot be determined independently with high degree of accuracy.

Finally, with the exception of Vu et al.[20], who have employed the Dual Mode/Partial Immobilization Model to model the gas permeabilities of an Ultem® continuous phase in a CMS/Ultem® matrix, most applications of the various mixed matrix models do not account for the gas solubility differences of the two components making up the mixed matrix system. In fact, most transport models for composite media, such as the Maxwell model effectively predict diffusion coefficients (the equivalent of conductivity in the flux equation)[22], not permeabilities, which have a thermodynamic component. Yet, when these transport models are applied to real systems, it is the permeability that is used in the fitting process. This approach implicitly assumes that the solubility partition coefficient is essentially equal to one, thus implying that there is no thermodynamic resistance at the interface. However, this condition may not be necessarily met, even when the permeabilities of the two components are comparable. Indirect experimental evidence for this can be inferred from the work of Tantenkin-Ersolmaz et al.,[23] who have examined the role of zeolite particle size on the performance of polymer-zeolite mixed matrix membranes. Their work has clearly demonstrated that the permeability of the mixed matrix system decreases with decreasing particle size of the dispersed component while keeping the overall particle volume fraction constant. This result suggests that the larger interfacial area present in dispersions with smaller particles actually magnifies the mass-transfer resistance arising from the penetrant having to desorb from the matrix phase and resorb in the dispersed phase.

In this paper we utilize the effective medium theory according to Davis[24] to demonstrate the role of the solubility partition coefficient at the phase-boundary on the effective transport properties of mixed matrix membranes. The reason why we have chosen the effective medium theory is that it allows us to predict diffusion coefficients for components experiencing different concentration gradients.

6.2. Background

6.2.1. Theory

The effective medium theory (EMT) was originally developed by Landauer[25] to describe conduction in nonhomogeneous, random, binary metallic mixtures. It was assumed that the binary system is a random, isotropic medium. Later, Davis[24,26] modified this theory to account for the concentration gradients present in the two phases making up the mixed system. In his application of the EMT theory to the diffusion in composite media, Davis considers isothermal diffusion in which the diffusive flux is expressed in the form

$$J = -L\Delta\mu \qquad \text{Equation 6-1}$$

Where L is the Onsager coefficient and μ is the chemical potential of the diffusing species. Noting the connection between the Onsager coefficient and the diffusion coefficient in region i,

$$D_i = L_i\left(\frac{\partial\mu}{\partial C}\right)_{\text{T, phase i}} \qquad \text{Equation 6-2}$$

The diffusive flux through the binary composite system as given by Fick's Law is

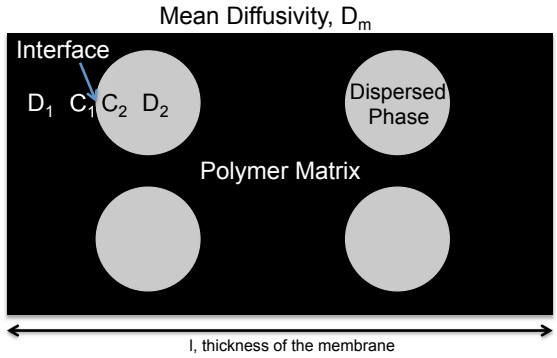

Figure 6-1. Schematic of a mixed matrix membrane with thickness, l, and D_1, diffusivity of the gas in the polymer matrix, D_2, diffusivity of the gas in the dispersed phase, C_1, concentration of the gas in the polymer near the interface, and C_2, in the dispersed phase.

$$J = -D_m\frac{\Delta\overline{C}}{l} \qquad \text{Equation 6-3}$$

Where D_m is the mean diffusion coefficient in the composite system of thickness l and $\Delta\overline{C} = \overline{C}(z = l) - \overline{C}(z = 0)$. Combining Equation 6-1 and Equation 6-3 in the EMT expression for the overall conductivity (or in this case, the diffusion coefficient), Davis obtained the following equation for the mean diffusion coefficient, D_m, in terms of the intrinsic diffusion coefficients of the binary components, D_1 (matrix) and D_2 (dispersed phase), the partition coefficient, K, and the volume fraction of the dispersed phase, ε as shown in Figure 6-1. K also represents the thermodynamic resistance at the interface to the transport of gas in the mixed matrix membrane.

$$\frac{D_m}{D_2} = \frac{1}{K}\left(\frac{\Delta C_1}{\Delta\overline{C}}\right)\left[a + \left(a^2 + \frac{1}{2}Kx\right)^{1/2}\right] \qquad \text{Equation 6-4}$$

Where

$$x = \frac{D_1}{D_2}, K = \frac{C_1}{C_2} \text{ and } a = \frac{1}{4}\left[3\varepsilon - 1 + Kx(2 - 3\varepsilon)\right] \qquad \text{Equation 6-5}$$

For sufficiently small Δμ,

$$\frac{\Delta\overline{C}}{\Delta C_1} = 1 + \varepsilon\frac{(1-K)}{K} \qquad \text{Equation 6-6}$$

It is important to note that in the limit as C_2 approaches 0, $K \to \infty$ Equation 6-4 reverts to an expression describing the effective diffusion of a mixed matrix system with impermeable particles,

$$\lim_{K\to\infty} D_m = \frac{1}{2}\left(\frac{2 - 3\varepsilon}{1 - \varepsilon}\right)D_1 \qquad \text{Equation 6-7}$$

Which in the limit as ε approaches 0, reduces to D_m=D_1, as it should. Although Equation 6-7 correctly predicts a decrease in the effective diffusion coefficient with increasing volume fraction of the impermeable particles, it is valid only at low volume fractions (<0.67), consistent with the assumptions of the EMT theory. Furthermore, when K =1, Equation 6-4 reverts to the EMT shown in Equation 6-8, which predicts an increase in membrane selectivity with filler volume fraction similar to the Maxwell model. In that case, though, the diffusion coefficients are replaced with permeabilities.

$$\frac{D_m}{D_2} = a + \left(a^2 + \frac{1}{2}x\right)^{1/2} \qquad \text{Equation 6-8}$$

6.3. Results and Discussion

In this section, we examine the effect of (i) partition coefficient, K (ii) volume fraction, ε and (iii) $x=D_1/D_2$ on the effective diffusivity of MMM, D_m, as predicted by the EMT theory. For the purpose of the study in (i) and (ii), we assumed a mixed matrix system consisting of a dispersed phase in a polymer matrix, such that the diffusion through the dispersed phase is ten times faster than that through the polymer, i.e. x=0.1. For (iii), the volume fraction of the dispersed phase in the MMM is fixed at 40%. Later, in the section, the selectivity of oxygen to nitrogen in the MMM is predicted based on the experimental diffusivity values of the gases (rather than an assumed value of x) in the polymer matrix for different partition coefficients, K. The results are plotted in Robeson type plot. Furthermore, we predict the selectivities of O_2/N_2 and CO_2/CH_4 in MMM for different filler loadings using the EMT theory. These predictions are based on real diffusivities and K values of the gases in the polymer matrix and the dispersed phase and are compared to the experimental values.

6.3.1. Effect of Partition Coefficient, K, on D_m

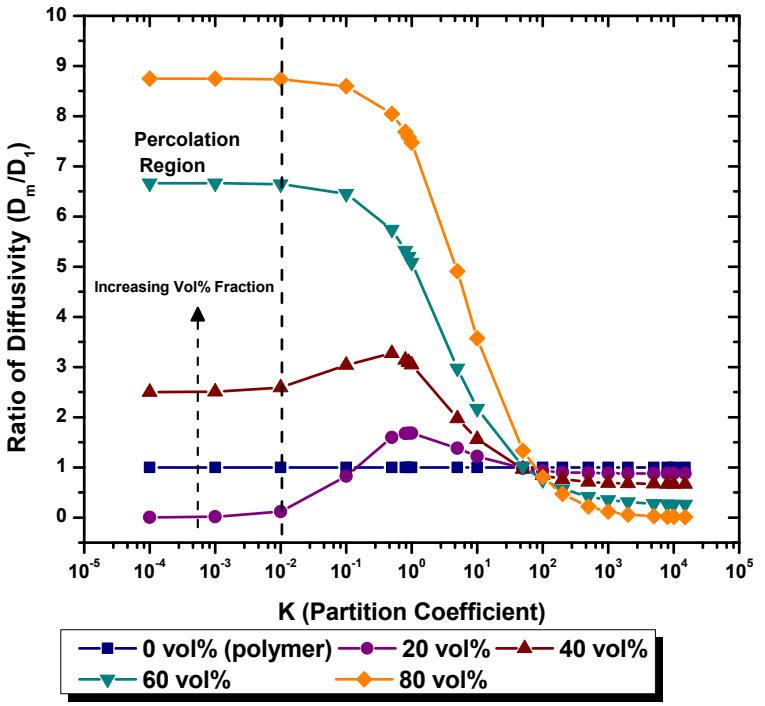

Figure 6-2. Ratio of the diffusivity of the mixed matrix membrane to diffusivity of the pure polymer (D_m/D_1) vs the partition coefficient (K) for different volume fractions of the filler material, $D_1/D_2=0.1$.

Using the EMT expression in Equation 6-4 and $D_1/D_2=0.1$, we can calculate the mean diffusion coefficient of an arbitrary penetrant in the mixed matrix membrane as a function of the

partition coefficient, K, and the volume fraction of the dispersed phase. This behavior is shown in Figure 6-2, normalized by the diffusion coefficient of the neat matrix, D_1. It is interesting to note that with the addition of the dispersed phase, the mean diffusion coefficient can either increase or decrease depending on the value of K. For example, in the case of MMM with 20 vol% filler, the D_m/D_1 ratio is less than 1 for $K < 0.1$ and greater than 1 for $0.1< K<100$. As the volume fraction of the dispersed phase increases, the effect of K is magnified. At volume fractions greater than 60 vol%, the D_m/D_1 ratio is greater than 1 for $K <100$, however, for K values above 1, the D_m/D_1 ratio decreases precipitously. What this means, is that even if we have a mixed matrix system, whose dispersed phase is highly porous and thus accommodates faster diffusion than the polymer matrix, if the partitioning of the gas molecules into the dispersed phase is too low, there will be no enhancement in gas transport properties.

6.3.2. Effect of Volume Fraction, ε, on D_m

Likewise, we can examine the role of the volume fraction on the effective diffusion through the mixed matrix membrane at low K values. This behavior is shown in Figure 6-3. Assuming again that $D_1/D_2 = 0.1$, i.e. that we have a highly porous dispersed phase compared to the polymer matrix, we see that major enhancements in the effective diffusion coefficient of the mixed matrix membrane are realized only above a certain concentration threshold.

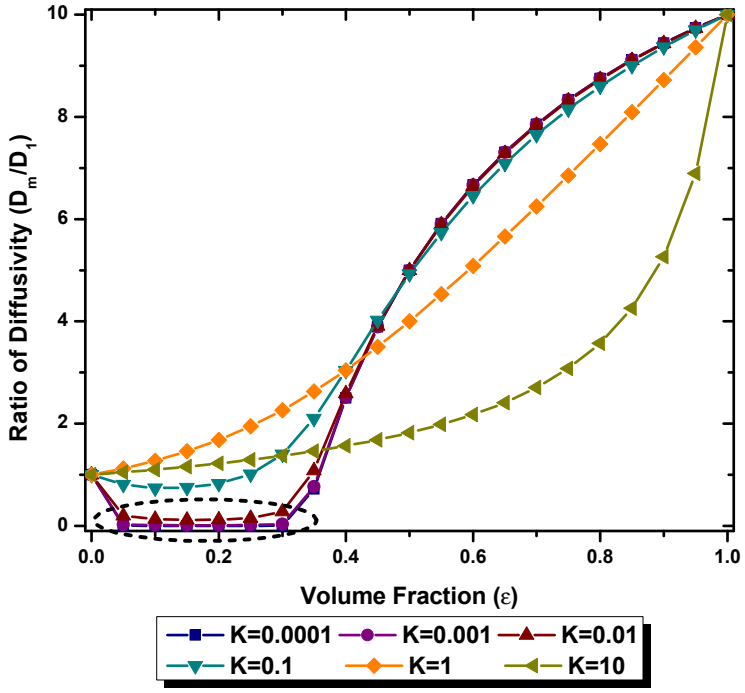

Figure 6-3. Ratio of diffusivity (D_m/D_1) vs volume fraction (ε) of the filler in MMM for different K values and D_1/D_2=0.1.

According to the percolation theory, a low diffusing material will transform dramatically into a high diffusing material when the volume fraction of the filler is above a critical value, ε_c[24]. Both, Figure 6-2 and Figure 6-3 demonstrate that for very low K values (K < 0.01), there exists a critical volume fraction, $\varepsilon_c = 0.3$, below which the gas diffusivity in the mixed matrix membrane is very low (see area circled in black). In fact, the mixed matrix diffusivity appears lower than the diffusivity in the polymer. This particular trend arises from the limitation of the EMT theory in predicting the effective diffusivity of a MMM at very low K values below the percolation threshold as suggested in the work by Davis et al[24]. Hence, according to EMT theory, a particular choice of polymer and filler system will not show a significant increase in diffusivity with the addition of the filler until the volume fraction is above the critical value.

6.3.3. Effect of x=(D_1/D_2) on D_m

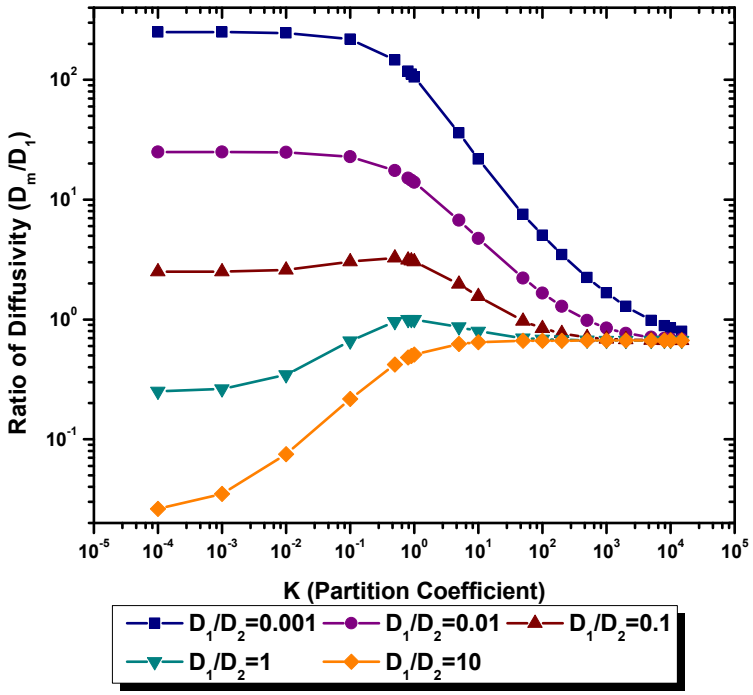

Figure 6-4. Ratio of the diffusivity of the mixed matrix membrane to diffusivity of the pure polymer (D_m/D_1) vs the partition coefficient (K) for different x (=D_1/D_2) values at a fixed 40 vol% dispersed phase.

So far we have looked at transport behavior assuming that the mixed matrix consists of a highly porous filler in a polymer matrix, such that D_1/D_2 =0.1. We can also examine the behavior of the mean diffusion in the mixed matrix membrane as a function of the ratio D_1/D_2 at a fixed volume fraction of the dispersed phase. For example, high values of D_1/D_2 imply that the diffusion in the continuous matrix dominates the transport process, with the dispersed phase acting more or less as impermeable filler. Low values of D_1/D_2 reflect greater diffusion in the dispersed phase than in the matrix. The impact of this ratio on the effective diffusivity is shown in Figure 6-4. Interestingly, the plots in Figure 6-4 demonstrate that the effective diffusivity in the mixed matrix systems will be higher in comparison to the neat matrix when x = D_1/D_2 is less than 0.1 at any given K value. The small x value implies that the penetrant needs to travel faster in the filler material compared to the matrix to achieve improvements in the overall diffusion, D_m. Furthermore, whether the diffusivity increases or decreases with the K value depends on the value of x=D_1/D_2. For values of x=1 and 10, the diffusivity ratio increases with increasing K values. For x values of 0.1, 0.01 and 0.001, the diffusivity ratio decreases with increasing K values. This implies that when the solubility in the continuous matrix is high, the effective

diffusion coefficient in the mixed matrix membrane is dictated by the diffusion in the matrix. However, for all the cases of x, the D_m/D_1 ratio reaches a constant value at high K. This limiting value of D_m/D_1 is a function of the filler loading in the material as given by Equation 6-7.

6.3.4. Discussion: Effect of K, ε and x on D_m

When the value of $x = (D_1/D_2)$ is set to 0.1, the penetrant will diffuse 10 times faster in dispersed phase than in the polymer matrix. For low K values ($K<10^{-2}$), the penetrant is more soluble in the dispersed phase than in the polymer. Since penetrant travels faster in the dispersed phase than in the matrix and if the penetrant is more soluble in dispersed phase, the cumulative effect will show a tremendous increase in the effective diffusivity of the MMM. However, to observe this particular effect on diffusivity of the MMM, the volume fraction of the dispersed phase needs to be above a threshold volume fraction as seen in Figure 6-3. This threshold volume fraction exists only for low K values. Once the volume fraction is above this particular value, adding more dispersed phase will create more regions within the MMM, where the diffusivity and solubility are higher than in the matrix polymer, thereby increasing the effective diffusivity of the membrane. When K>1, the penetrant is more soluble in the polymer matrix than in the dispersed phase. The concentration of the penetrant in the matrix, C_1, is higher than the concentration of the penetrant in the filler, C_2. Yet, even though the diffusivity of the penetrant is higher in dispersed phase than the polymer matrix, since there are not enough molecules of the penetrant (smaller C_2) in the dispersed phase, the filler cannot be very effective in enhancing the diffusivity. So, a decrease in effective diffusivity when K>1 can be seen in Figure 6-2. In fact, for high K values, the dispersed phase can completely behave as an impermeable region. At this point, addition of more dispersed phase (higher volume fractions) will form more impermeable regions in the membrane and consequently will decrease the effective diffusivity, as seen in Figure 6-2.

The enhancement in diffusivity of the membrane by the dispersed phase also depends on the relative values of diffusivity in the matrix polymer and in the dispersed phase. The greater the diffusivity of the penetrant in the dispersed phase, the greater is the increase in the effective diffusivity of the MMM. However, to observe this effect, the partition coefficient value, K, needs to be small as seen in Figure 6-4. Penetrant molecules should easily sorb into the dispersed phase allowing faster diffusion than inside the matrix, thereby increasing the effective diffusivity. If the K values are high, as discussed previously, the concentration of penetrant molecules in the

dispersed phase will be small. Hence, the dispersed phase will not be effective in enhancing the diffusivity of the MMM, making its value fall back to the impermeable dispersed phase MMM given by Equation 6-7. This value is independent of the ratio of the diffusivities in the dispersed phase and in the matrix polymer. Thus, even using a dispersed phase with very high diffusivity in the fabrication of the MMM, when the partition coefficient value for the polymer and dispersed phase system is high, we may not see the desired increase in the effective diffusivity of the mixed matrix membrane.

In the next section, the effect of K on the selectivity of O_2 and N_2 will be examined and discussed.

6.3.5. Effect of Partition Coefficient, K on the Selectivity of O_2 to N_2

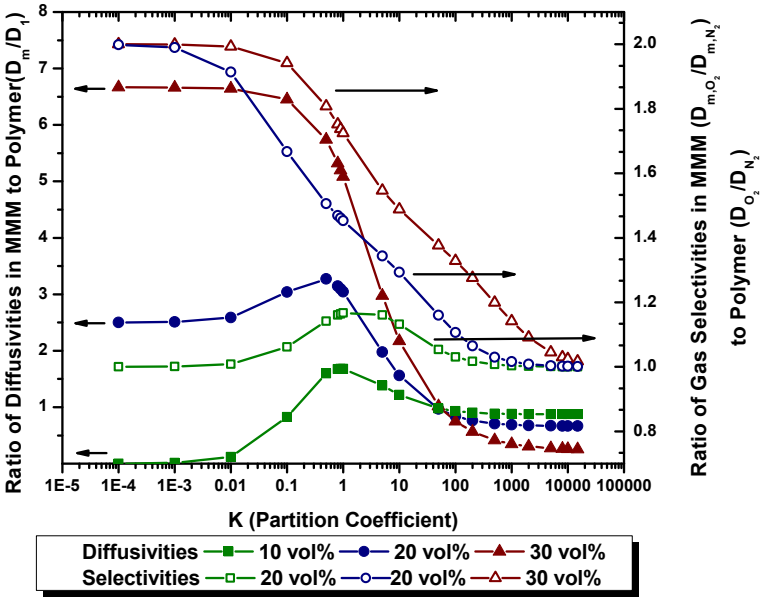

Figure 6-5. Ratio of the O_2 diffusivity of the mixed matrix membrane to O_2 diffusivity of the pure polymer (D_m/D_1), Ratio of the O_2/N_2 selectivity of the MMM to the pure polymer vs the partition coefficient (K) for different weight loadings of the filler. $(D_1/D_2)_{O2}$=0.1; $(D_1/D_2)_{N2}$=0.2.

Figure 6-5 examines the O_2/N_2 selectivity and O_2 diffusivity as a function of the K partition coefficient at different volume fractions, assuming that $(D_1/D_2)_{O2}$=0.1; $(D_1/D_2)_{N2}$=0.2. The chosen D_1/D_2 ratios are typical for a polymer – carbon molecular sieve system[20]. As shown in Figure 6-5, the values of D_m/D_1 increase with increasing filler loading in the MMM for K values below 100. For K above 100, the diffusivity decreases with increasing filler loadings. Enhancements in the O_2/N_2 selectivity with the addition of the filler particles were only observed at K values less than 0.1. These results suggest that in order to obtain enhanced membrane

performance in mixed matrix membranes, the partition of the penetrant in the dispersed phase has to be favored over that in the matrix. This result is summarized in the typical trade-off curve shown in Figure 6-6, which shows the O_2/N_2 selectivity as a function of O_2 diffusivity for different values of K. Here we have assumed that O_2 and N_2 have the same partition coefficient, K, but different rates of diffusion, i.e. $(D_1/D_2)_{O2}=0.1$; $(D_1/D_2)_{N2}=0.2$. This probably would not be a good assumption if the penetrants were highly condensable gases, but in the case of O_2 and N_2 this assumption is reasonable since their critical temperatures are very low. Furthermore, we have assumed O_2 diffusivity of $9x10^{-9}$ cm^2/s in the pure polymer and O_2/N_2 selectivity of 10 in the pure polymer, which are typical for a polyimide[27].

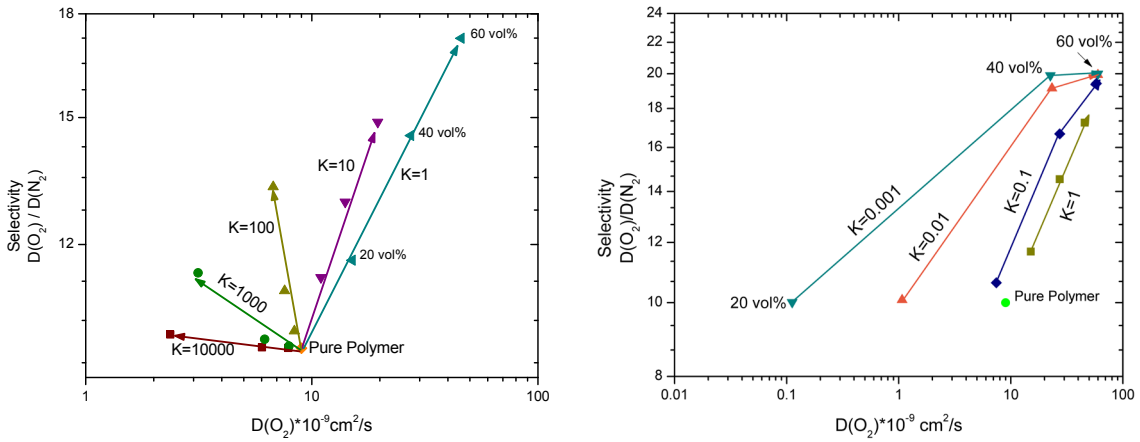

(A) (B)

Figure 6-6. Selectivity of oxygen to nitrogen versus diffusivity of oxygen gas in a membrane. Pure polymer diffusivity = $9*10^{-9}$ cm^2/s and selectivity O_2/N_2 = 10 are assumed. Results are shown for values of K >1 (A) and K<1 (B).

Thus, the EMT theory predicts that both, the diffusivity and the selectivity of the MMM should increase when K< 10 by adding a more permeable filler to the matrix. For K > 10, addition of a filler can still increase the selectivity of the MMM compared to that of the polymer but it will decrease the effective O_2 diffusion. This result is typical of some of the experimental trends reported in literature[15] suggesting that in those mixed matrix systems the diffusing species was more soluble in the matrix than in the filler. When K<1, the penetrant is more soluble in the dispersed phase than it is in the matrix. Since the penetrant also diffuses faster in the dispersed phase than in the matrix, an overall increase in diffusivity can be observed at high volume fractions of the dispersed phase. Thus, the value of the partition coefficient plays a critical role in the enhancement of performance of the mixed matrix membrane.

6.3.6. Comparison with Experimental Data

The comparison of membrane performance predicted by the EMT model with experimentally measured trade-off behavior of the mixed matrix membranes requires not only the intrinsic solubility coefficients of pertinent gases in the polymer matrix and the filler material, but also the individual diffusion coefficients in the two components. Such data is typically unavailable, since many published mixed matrix studies only report the permeability values. Furthermore, there appears to be much discrepancy in diffusion coefficients associated with gas diffusion in zeolites and porous materials published in the literature. Fortunately, some of our earlier work with mixed matrix membranes containing mesoporous MCM-41 nanoparticles was highly comprehensive, including most of the needed transport data[28]. Because mesoporous silica, MCM-41, is highly porous, the diffusion coefficients in the polymer compared to those in MCM-41 are significantly lower. Hence, the EMT Equation 6-4 reduces to the following relationships when x<<<1.

$$D_m = \left[\left(\frac{3}{2}\varepsilon - \frac{1}{2}\right)\frac{D_2}{K} + \frac{D_1}{3\varepsilon - 1}\right]\left(\frac{\Delta C_1}{\Delta \overline{C}}\right) \qquad \varepsilon>1/3 \qquad \text{Equation 6-9}$$

$$= \frac{D_1}{1-3\varepsilon}\left(\frac{\Delta C_1}{\Delta \overline{C}}\right) \qquad \varepsilon<1/3 \qquad \text{Equation 6-10}$$

Assuming

$$\frac{\Delta \overline{C}}{\Delta C_1} = 1 + \varepsilon\frac{(1-K)}{K} \qquad \text{Equation 6-11}$$

$$\text{and } K = \frac{C_1}{C_2} \qquad \text{Equation 6-12}$$

In the discussion below, we consider the separation of two gas pairs, O_2/N_2, and CH_4/CO_2. From separate gas sorption isotherms found in the reference[28], we can isolate the solubility coefficient of the various gases in MCM-41(C_2) at 308 K and 4 atm, which are the same conditions used in the transport studies of the mixed matrix membranes. This sorption data, along with the diffusion coefficients are summarized in Table 6-2 through Table 6-3. While the gas diffusion coefficients (D_1) in the neat polymer membrane were obtained from time-lag measurements, the diffusion coefficients in MCM-41 (D_2) were calculated from time-dependent sorption (non-equilibrium) data at 4 bar using the gas diffusion Equation 6-13 in a spherical particle[29].

$$\frac{M_t}{M_\infty} = 1 - \frac{6}{\pi^2}\sum_{n=1}^{\infty}\frac{1}{n^2}\exp\left(-\frac{Dn^2\pi^2 t}{a^2}\right) \qquad \text{Equation 6-13}$$

The solubility co-efficients, C_1 in the polymer were calculated from the permeability (P) and diffusivity (D_1) from the reference[28] using the equation $C_1 = P/D$. The values for C_2 were calculated from the gas sorption isotherms, using the concentration at 4bar. Table 6-2 shows these values for nitrogen gas along with the reference section in the article[28]. Table 6-3 shows these values for gases oxygen, carbon dioxide and methane.

Table 6-1 shows the volume fractions calculated from the weight fraction reported in reference[28], assuming that the density of porous silicon is 0.7 g/cc and that of the polymer is 1 g/cc.

Table 6-1. Conversion of weight fractions to volume fraction using the density values of constituent materials, MCM-41 and PSF

Weight fraction %	**Volume fraction (ε) %**
10	14
20	26
40	49

Table 6-2 summarizes the experimental data used in the EMT predictions[28].

Table 6-2. Parametric N_2 transport data[28].

Parameter	**Value**	**Reference in the article**
Solubility of N_2 in PSF (C_1)	1.714×10^{-3} cm^3 (STP) / cm^3. cm Hg	From N_2 permeability in Table 1 in[28], 0.18 Barrer and diffusivity from Table 3 in[28], 1.05×10^{-8} cm^2/s
Solubility of N_2 in MCM-41 (C_2)	6×10^{-3} cm^3 (STP) / cm^3. cm Hg	From Figure 7(a) in[28], concentration of gas sorbed is 1.8 cm^3 (STP) / cm^3 at 4 bar
Diffusivity of N_2 in PSF (D_1)	1.05×10^{-8} cm^2/s	From Table 3 in[28]
Diffusivity of N_2 in MCM-41 (D_2)	1.25×10^{-3} [1.08×10^{-7}]* cm^2/s	From the kinetic sorption data of N_2 isotherm in Figure 7(a) in[28] and fitting this data to Equation 6-13

*The diffusivity value (D_2) in the parenthesis was calculated using the gas permeance in MCM-41 from[30] and gas solubility from sorption isotherms[28].

Similarly, the remaining data was collected for other gases, O_2, CO_2 and CH_4.

Table 6-3. Parametric values of gases, O_2, CO_2 and CH_4 for measuring overall diffusivity for the respective gases from reference[28].

Gas	O_2	CO_2	CH_4
Solubility of gas in PSF (C_1)	2.94×10^{-3} cm^3 (STP) / cm^3. cm Hg	40.9×10^{-3} cm^3 (STP) / cm^3. cm Hg	6.54×10^{-3} cm^3 (STP) / cm^3. cm Hg
Solubility of gas in MCM-41 (C_2)	6.48×10^{-3} cm^3 (STP) / cm^3. cm Hg	25×10^{-3} cm^3 (STP) / cm^3. cm Hg	8.69×10^{-3} cm^3 (STP) / cm^3. cm Hg
K, partition coefficient	0.454	1.636	0.751
Diffusivity of gas in PSF (D_1)	3.33×10^{-8} cm^2/s	1.1×10^{-8} cm^2/s	0.26×10^{-8} cm^2/s
Diffusivity of gas in MCM-41 (D_2)	1.25×10^{-3} cm^2/s	$1.10\times10^{-4}[2.04\times10^{-5}]$* cm^2/s	5.02×10^{-4} $[8.69\times10^{-3}]$* cm^2/s

*The diffusivity value (D_2) in the parenthesis was calculated using the gas permeance for MCM-41 from[30] and gas solubility from sorption isotherms [28].

6.3.7. Prediction of Nitrogen Diffusivity

From Table 6-2 of this article, $K=C_1/C_2 = 0.286$. Using this value and Equation 6-9, Equation 6-10 and Equation 6-11, the diffusivity values were calculated for different volume fractions shown in Table 6-1.

Table 6-4. Calculated overall diffusivity values of N_2 compared with experimental data[28].

Volume fraction %	Equation used	Parametric result in D_1 and D_2	Calculated values	Experimental Values
14	10	1.28 D_1	1.33×10^{-8} cm^2/s	1.77×10^{-8} cm^2/s
26	10	2.75 D_1	2.89×10^{-8} cm^2/s	1.76×10^{-8} cm^2/s
49	9	0.37 D_2+0.32 D_1	4.63×10^{-4} $[4.32\times10^{-8}]$* cm^2/s	2.30×10^{-8} cm^2/s

*The overall diffusivity (D_m) in the parenthesis was calculated using the intrinsic data from the reference[30].

6.3.8. Prediction of Oxygen Diffusivity

From Table 6-3 of this article, K= 0.454, and Equation 6-9, Equation 6-10 and Equation 6-11, the following values in Table 6-5 were calculated.

Table 6-5. Calculated overall diffusivity values of O_2 compared with experimental data[28]

Volume fraction%	**Equation used**	**Parametric result in D_1 and D_2**	**Calculated values**	**Experimental Values**
14	2	1.48 D_1	4.93×10^{-8} cm^2/s	5.50×10^{-8} cm^2/s
26	2	3.46 D_1	11.5×10^{-8} cm^2/s	5.95×10^{-8} cm^2/s
49	1	0.33 D_2+1.34 D_1	4.13×10^{-4} cm^2 /s	7.16×10^{-8} cm^2/s

The diffusivity of O_2 at volume fraction 49% is much higher than the experimental value because of the high D_2 value, the estimated diffusivity of the gas in MCM-41.

6.3.9. Prediction of Carbon-Dioxide Diffusivity

Table 6-6. Calculated overall diffusivity values of CO_2 compared with experimental data at K = C_1/C_2 =1.636 (from Table 6-3 of this article).

Volume fraction	**Equation used**	**Parametric result in D_1 and D_2**	**Calculated values**	**Experimental Values**
14	2	1.82 D_1	2.0×10^{-8} cm^2/s	1.8×10^{-8} cm^2/s
26	2	5.05 D_1	5.56×10^{-8} cm^2/s	2.5×10^{-8} cm^2/s
49	1	0.177 D_2+2.63 D_1	1.95×10^{-5} [3.64×10^{-6}]*cm^2/s	3.2×10^{-8} cm^2/s

*The overall diffusivity (D_m) in the parenthesis was calculated using the data from the reference[30].

6.3.10. Prediction of Methane Diffusivity

Table 6-7. Calculated overall diffusivity values of CH_4 compared with experimental data for K = C_1/C_2 = 0.751 (from Table 6-3 of this article)

Volume fraction	Equation used	Parametric result in D_1 and D_2	Calculated values	Experimental Values
14	2	1.65 D_1	0.45×10^{-8} cm^2/s	0.39×10^{-8} cm^2/s
26	2	4.18 D_1	1.09×10^{-8} cm^2/s	0.46×10^{-8} cm^2/s
49	1	0.27 D_2+1.83 D_1	1.36×10^{-4} [2.34×10^{-3}]* cm^2/s	0.93×10^{-8} cm^2/s

*The overall diffusivity (D_m) in the parenthesis was calculated using the data from the reference[30].

6.4. Prediction of Selectivities of O_2/N_2 and CO_2/CH_4

The corresponding single gas selectivities calculated from the predicted and experimental values of diffusivity are presented in Table 6-8. As can be seen, there are discrepancies between the predicted and experimental values particularly at the largest volume fraction of 49% of the filler. This discrepancy is a direct consequence of the extremely high gas diffusion coefficients in MCM-41, which were estimated from separate studies and which can vary greatly depending on the measurement method. It's also most likely that the apparent diffusivity in the dispersed phase restricted by the polymer matrix is actually lower than the intrinsic diffusivity in the dispersed phase alone.

Table 6-8. Selectivities of gas pairs, O_2/N_2 and CO_2/CH_4

Volume Fraction	O_2/N_2		CO_2/CH_4	
	Predicted Value	*Experimental Value*	*Predicted Value*	*Experimental Value*
0	-	3.2	-	4.2
14	3.7	3.1	4.4	4.6
26	4.0	3.4	5.1	5.4
49	0.9	3.1	0.1	3.4

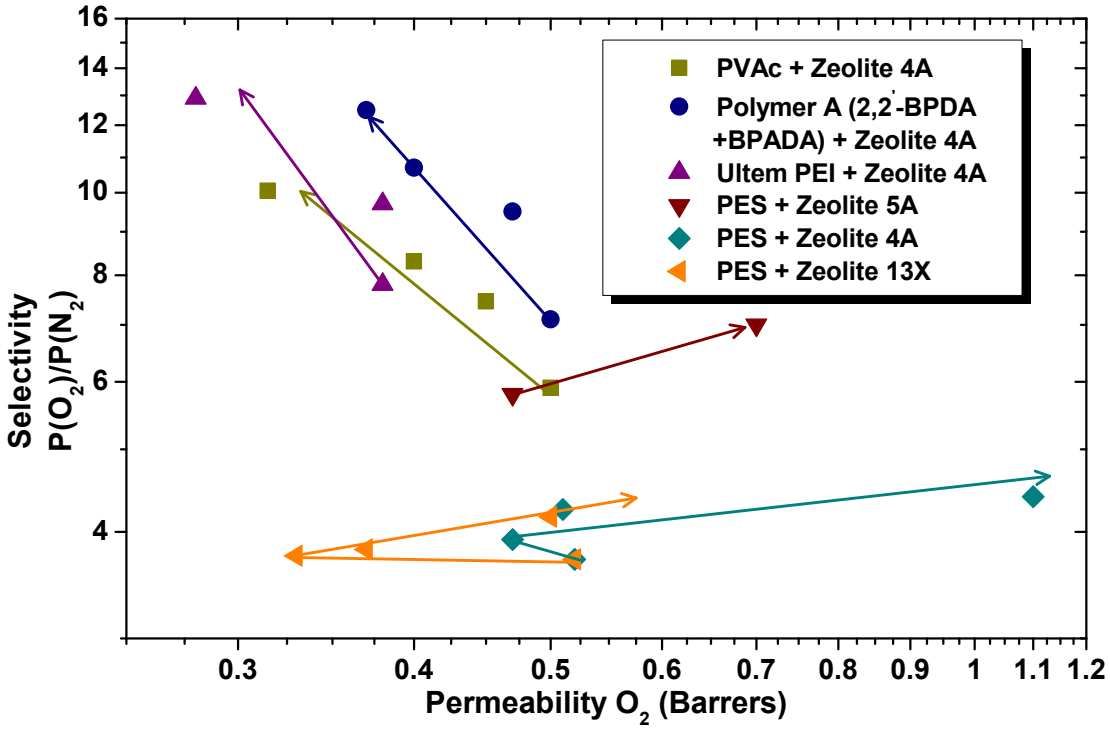

Figure 6-7. Selectivity of oxygen to nitrogen vs. permeability of oxygen for various mixed matrix systems as a function of zeolite volume fraction. (The arrows point in the direction of increasing zeolite loading).

Finally, Figure 6-7 shows a summary of experimental data from the literature, in which the dispersed phase consists of porous zeolite particles. This data was plotted on a Robeson-type plot for comparison with selectivity-diffusion behavior shown in Figure 6-6. For example, the polymer and zeolite systems, poly(vinylacetate) – zeolite 4A, polymer A – zeolite 4A, and poly(ether imide) – zeolite 4A[15], show an increase in O_2/N_2 selectivities, while oxygen permeabilities decrease with increasing zeolite A loading. This behavior, which cannot be explained by the simple Maxwell model, now can be explained by the K-EMT theory. For example, as seen in Figure 6-5, when K values are above 100, the selectivity of MMM increases with loading of the dispersed phase, accompanied by a decrease in diffusivity. Hence, it may be possible that the partition coefficient, K for these polymer-filler systems is above 100, which exhibits this particular trend in permeability and selectivity. For polyethersufone (PES)-zeolite 5A system[31], both, the permeability and selectivity increased with zeolite volume fraction. Mixed matrix systems show this type of behavior when the partition coefficient is below 10. For the PES-zeolite 4A and zeolite 13X systems[32], a very particular behavior is observed. Compared to the pure polymer, adding a low volume fraction of the zeolite to the mixed matrix system caused

the permeability to decrease and selectivity to increase. However, adding more zeolite (higher volume fraction) induced an increase in both permeability and selectivity. This behavior can be partly explained by the percolation concept, which identifies a threshold volume fraction, below which no increase in diffusivity is observed. Instead, adding low volume fractions of the zeolite to the matrix induces a decrease in overall permeability because the zeolite acts as non-permeable filler. Once the dispersed phase loading crosses the percolation threshold volume fraction, appreciable increase in permeability can be observed. Another explanation for the experimental behavior is that solvent trapped during the fabrication process is blocking access to the zeolite pore structure.

Thus, in order to maximize the performance of mixed matrix membranes, the solubility partition coefficient of the matrix – filler system has to be matched, ideally when K =1. We expect that the value of the partition coefficient can be influenced by several physical parameters; including poor interfacial contact between the polymer matrix and the filler, molecular chain rigidification at the interface, as well as the intrinsic solubilities of the mixed matrix components. Both, poor interfacial contact and molecular chain rigidification would be expected to increase the value of K, i.e. favoring penetrant partitioning in the polymer matrix.

6.5. Conclusions

We have shown that the value of the sorption partition coefficient plays a critical role in the enhancement of performance of mixed matrix membranes. Ideally, this value should be close to 1 when trying to separate non-condensable gases. Systems with K values greater than one will exhibit a decrease in diffusivity with increasing volume fraction of the dispersed phase. On the other hand, mixed matrix systems with K values less than one, will gain improvement in selectivity and diffusivity only at concentrations of the dispersed phase above the percolation threshold. Employing this approach will help guide the design of viable mixed matrix systems, whose performance should pass the Robeson upper bound.

6.6. Acknowledgments

We would like to thank Dr. Sangil Kim (Laurence Livermore labs) for his kind help in re-analyzing his sorption data. A. Surapathi acknowledges financial support from the Department of Chemical Engineering at Virginia Tech.

6.7. References

1. Adams, R. T. *et al.* CO_2–CH_4 permeation in high zeolite 4A loading mixed matrix membranes. *Journal of Membrane Science* **367**, 197–203 (2011).

2. Aroon, M. A., Ismail, A. F., Matsuura, T. & Montazer-Rahmati, M. M. Performance studies of mixed matrix membranes for gas separation: A review. *Separation and Purification Technology* **75**, 229–242 (2010).
3. Boom, J. Transport through zeolite filled polymeric membranes. *Journal of Membrane Science* **138**, 237–258 (1998).
4. Chung, T.-S., Jiang, L. Y., Li, Y. & Kulprathipanja, S. Mixed matrix membranes (MMMs) comprising organic polymers with dispersed inorganic fillers for gas separation. *Progress in Polymer Science* **32**, 483–507 (2007).
5. Duval, J. M. *et al.* Preparation of zeolite filled glassy polymer membranes. *J. Appl. Polym. Sci.* **54**, 409–418 (1994).
6. Galve, A. *et al.* Copolyimide mixed matrix membranes with oriented microporous titanosilicate JDF-L1 sheet particles. *Journal of Membrane Science* **370**, 131–140 (2011).
7. Hennepe, te, H. J. C., Boswerger, W. B. F., Bargeman, D., Mulder, M. H. V. & Smolders, C. A. Zeolite-filled silicone rubber membranes Experimental determination of concentration profiles. *Journal of Membrane Science* **89**, 185–196 (1994).
8. Hudiono, Y. C., Carlisle, T. K., LaFrate, A. L., Gin, D. L. & Noble, R. D. Novel mixed matrix membranes based on polymerizable room-temperature ionic liquids and SAPO-34 particles to improve CO_2 separation. *Journal of Membrane Science* **370**, 141–148 (2011).
9. Jia, M., Peinemann, K.-V. & Behling, R.-D. Molecular sieving effect of the zeolite-filled silicone rubber membranes in gas permeation. *Journal of Membrane Science* **57**, 289–292 (1991).
10. Jia, M.-D., Pleinemann, K.-V. & Behling, R.-D. Preparation and characterization of thin-film zeolite–PDMS composite membranes. *Journal of Membrane Science* **73**, 119–128 (1992).
11. Kim, S., Marand, E., Ida, J. & Guliants, V. V. Polysulfone and Mesoporous Molecular Sieve MCM-48 Mixed Matrix Membranes for Gas Separation. *Chem. Mater.* **18**, 1149–1155 (2006).
12. Kulprathipanja, S., Neuzil, R. W. & Li, N. N. Separation of fluids by means of mixed matrix membranes. **95/51**, (1988).
13. Mahajan, R. & Koros, W. J. Factors Controlling Successful Formation of Mixed-Matrix Gas Separation Materials. *Ind. Eng. Chem. Res.* **39**, 2692–2696 (2000).
14. Mahajan, R. & Koros, W. J. Mixed matrix membrane materials with glassy polymers. Part 1. *Polym. Eng. Sci.* **42**, 1420–1431 (2004).
15. Mahajan, R. & Koros, W. J. Mixed matrix membrane materials with glassy polymers. Part 2. *Polym. Eng. Sci.* **42**, 1432–1441 (2004).
16. Pechar, T. W. *et al.* Fabrication and characterization of polyimide-zeolite L mixed matrix membranes for gas separations. *Journal of Membrane Science* **277**, 195–202 (2006).
17. Zimmerman, C., Singh, A. & Koros, W. J. Tailoring mixed matrix composite membranes for gas separations. *Journal of Membrane Science* **137**, 145–154 (1997).
18. Zornoza, B., Esekhile, O., Koros, W. J., Téllez, C. & Coronas, J. Hollow silicalite-1 sphere-polymer mixed matrix membranes for gas separation. *Separation and Purification Technology* **77**, 137–145 (2011).
19. Shimekit, B., Mukhtar, H. & Murugesan, T. Prediction of the relative permeability of gases in mixed matrix membranes. *Journal of Membrane Science* **373**, 152–159 (2011).
20. Vu, D. Q., Koros, W. J. & Miller, S. J. Mixed matrix membranes using carbon molecular sieves: II. Modeling permeation behavior. *Journal of Membrane Science* **211**, 335–348

(2003).
21. Erdem-Senatalar, A., Tatlier, M. & Tantekin-Ersolmaz, S. Questioning the validity of present models for estimating the performances of zeolite-polymer mixed matrix membranes. *Chem Eng Commun* **190**, 677–692 (2003).
22. Maxwell, J. C. *A treatise on electricity and magnetism*. **1**, (Clarendon Press: Oxford, 1873).
23. Tantekin-Ersolmaz, S. Effect of zeolite particle size on the performance of polymer–zeolite mixed matrix membranes. *Journal of Membrane Science* **175**, 285–288 (2000).
24. Davis, H. T., Valencourt, L. R. & Johnson, C. E. Transport Processes in Composite Media. *J American Ceramic Society* **58**, 446–452 (1975).
25. Landauer, R. The Electrical Resistance of Binary Metallic Mixtures. *J. Appl. Phys.* **23**, 779 (1952).
26. Davis, H. T. The Effective Medium Theory of Diffusion in Composite Media. *J American Ceramic Society* **60**, 499–501 (1977).
27. Bernardo, P., Drioli, E. & Golemme, G. Membrane Gas Separation: A Review/State of the Art. *Ind. Eng. Chem. Res.* **48**, 4638–4663 (2009).
28. Kim, S. & Marand, E. High permeability nano-composite membranes based on mesoporous MCM-41 nanoparticles in a polysulfone matrix. *Microporous and Mesoporous Materials* **114**, 129–136 (2008).
29. Crank, J. *The mathematics of diffusion*. (Clarendon Press: Oxford, [Eng], 1979).
30. Sakamoto, Y., Nagata, K., Yogo, K. & Yamada, K. Preparation and CO_2 separation properties of amine-modified mesoporous silica membranes. *Microporous and Mesoporous Materials* **101**, 303–311 (2007).
31. Li, Y., Chung, T.-S., Cao, C. & Kulprathipanja, S. The effects of polymer chain rigidification, zeolite pore size and pore blockage on polyethersulfone (PES)-zeolite A mixed matrix membranes. *Journal of Membrane Science* **260**, 45–55 (2005).
32. Süer, M. G., Baç, N. & Yilmaz, L. Gas permeation characteristics of polymer-zeolite mixed matrix membranes. *Journal of Membrane Science* **91**, 77–86 (1994).

Chapter 7. Zwitterion-Functionalized Carbon Nanotube/Polymer Composite Membranes for Desalination

7.1. Introduction

As population grows and agriculture and industry expands, fresh water – especially clean fresh water is getting scarcer. Out of the total water on earth, 97.5% is salt water and only 2.5% is fresh water. Among that small percentage of fresh water, 2/3 is frozen. Clearly, finding a way to desalinate sea water, clean up brackish water, and remove harmful ions from contaminated water at low cost in a sustainable way would be a major step towards solving much of the world's water problems.

Current methods for desalination include distillation and reverse osmosis. The first method is unavoidably energy intensive, because of the thermodynamics involved. Water has a very high heat of vaporization, making distillation unattractive on an energy consumption basis. Reverse osmosis requires high-pressure drop across the membranes, which can be both costly and difficult to scale up to meet high production demands. This problem could be solved by constructing RO membranes that have high ionic selectivity and support fast water flow rates. In particular, membranes constructed with carbon nanotubes (CNTs) have been shown, both from experiments and simulations, to have remarkably high flux while maintaining high size selectivity[1-9].

There has been a long-standing technical interest in carbon nanotubes (CNTs) driven by their exceptional electrical, thermal and mechanical properties[10]. Molecular simulations and experimental studies have discovered unique transport properties of fluids within CNTs due to the unprecedented smoothness and regularity of the CNT pores[1,2,5,6,8,11]. These studies suggest that the transport of water through sub-nanometer CNTs occurs via a cooperative, pulse-like movement of hydrogen-bonded molecules within the channel, similar to what has been observed in aquaporin biological channels[12]. This transport mechanism has been shown to lead to flow rates that are faster than predicted by classical hydrodynamics[13,14]. The observed enhanced water transport together with CNT pore diameters on the order of nanometers opens the possibility of employing CNTs to filter ions from water. To date, there have been very few fundamental studies of transport of small ions through single-walled CNTs. Recent molecular dynamics (MD) simulation studies[15,16] have examined the ability of CNTs with diameters ranging from 6 to 11 Å to filter ions from water. These results indicated that ions can be almost completely excluded

from pores up to 9 Å in diameter due to ion desolvation energy barriers. By contrast, water faces relatively low energy barriers and is able to pass through these small nanotubes, but at rates that are much lower than in larger nanotubes. The work did not address the effects of charged functionalities in the CNT open tips on ion transport. Also using molecular simulation, Joseph et al.[17] explored the occupancy of ions in CNT channels when partial charges were placed on the rim atoms of the nanotubes and an external field was applied along their axis. The simulation results showed that the ion occupancy in a carbon nanotube solvated in an electrolyte was very low for neutral nanotubes and increased significantly in the presence of charged functionalities. Experimental work on ionic flux through functionalized CNTs has been performed by Hinds et al.[18] Their work has focused on studying transport of two different sized but equally charged molecules, ruthenium bipyridine [Ru-$(bipy)_3^{+2}$] and methyl viologen [MV^{2+}], through multiwalled CNTs with 7 nm nominal core diameters. The effective pore size of the CNT was adjusted by introducing functional groups at the ends of the nanotubes. They examined molecules such as straight chain alkanes, anionically charged dye molecules, and aliphatic amines elongated by polypeptide spacers at the CNT tips. In general, functionalization of the membrane with anionically charged dye molecules led to increased flux of the positively charged species. This effect was reduced at higher solution ionic strength consistent with shorter Debye screening length.

In a recent work, Bakajin et al. have studied ion exclusion in carbon nanotubes with sub-2-nm pores as a function of solution ionic strength, pH, and ion valence[19,20]. Their results suggest a Donnan-type rejection mechanism, dominated by electrostatic interactions between fixed charges on the CNTs and mobile ions. However, this also means that the rejection rates decreased significantly at higher electrolyte concentrations. Because the hydrated radii of the ions species are on the order of 0.3 to 0.6 nm, compared to the 1.6—2 nm CNT pore radius, separation of ions by size exclusion was not possible.

Hence carbon nanotubes with much smaller inner pore diameters are necessary to achieve rejection at all solution concentrations. While carbon nanotubes with pore diameters down to 0.4 nm have been reported[21], it may be more efficient and cheaper to take larger diameter carbon nanotubes (15 to 20 Å) and reduce the pore size by introducing specific functional groups at the CNT pore entrance, which can block pore access because of their bulk. In addition, functional groups with charged moieties can participate in electrostatic interactions. To the best of our

knowledge, there is no systematic study of the effect of functionalization of nanotubes on the transport of ions and water through CNTs. Won et al.[22] have shown from simulations that charge distributions on free standing CNTs affect the free energy of ions and water inside the CNT. This report indicates the possibility of significant thermodynamic effects due to the functionalization of nanotubes. We note here that the reported charge distributions by Won et al. may not be physical, since in reality the tips of CNTs are functionalized with various groups such as COOH, OH etc., which arise from the oxidation of the caps routinely used to open the CNTs. Suk and Aluru[23] have shown that the application of electric fields to nanotubes affects the flux of water under applied pressure for (6,6) CNTs. Therefore, different charged or zwitterion functional groups on the entrance of CNTs can be an important design tool. Studies on (10,10) boron nitride nanotubes versus (10,10) CNTs[22] show reversed selectivity of K^+ and Cl^- ions due to different entrance effects that result from the difference in charges at the entrance of the nanotubes. All these results point to tip entrance and charge effects being key to the design of high-efficiency functionalized nanotube membranes.

Our hypothesis is that highly efficient ion filtration can be achieved by employing functionalized CNT/ultra-thin polyamide composite membranes that reject ionic species through a combination of size exclusion and electrostatic (Donnan) interactions. These membranes have two main design parameters that can be tuned to achieve the desired permeance and selectivity: (1) the diameters of the nanotubes and (2) the functional groups attached to the ends of the nanotubes that act as gatekeepers and reject hydrated ionic species. The overall goal of this work is to investigate the fundamental properties of functionalized carbon nanotube nanocomposite membranes for the removal of ionic species and harmful chemicals from water. The basic hypothesis of the proposed work is that functionalization of the carbon nanotube tips with functional groups such as hydrated zwitterions will lead to the rejection of ionic species via a charged-gatekeeper mechanism, involving both steric effects and Donnan exclusion, while allowing rapid permeation of water via H_2O displacement of the hydrated shell through the hydrophilic carbon nanotube pore entrance. The zwitterions also have the distinct advantage of providing protection against biological threats since zwitterions have been shown to be resistant to cell adhesion and biofouling[24-26]. Here we fabricate carbon nanotube membranes that are used in the direct evaluation of the water transport properties.

7.1.1. Fabrication

The fabrication procedure of zwitterion functionalized thin film nanocomposite (TFN) membranes is similar to the procedure described in Section 5.2.2.

7.1.2. Water Permeation Setup

The water transport properties of the TFN membranes will be studied using the setup build in the lab. The schematic of the setup is shown in Figure 7-1. This test unit is comprised of a membrane cell (GE Sepa^{TM} CF Cell shown in Figure 7-2), high pressure pump (Hydra-cell pump, Warner Engineering), back-pressure regulator (US Paraplate), bypass valve (Swagelock), feed water reservoir (Nalgene), a closed loop mode with both permeate and retentate being circulated into the feed water reservoir. A small area of the TFN membrane is masked using aluminum masking tape as shown in Figure 7-3. Masked membrane is placed inside the membrane cell for testing. The concentration of the sodium cation present in the permeate was measured by a sodium ion-selective electrode (Thermo Scientific; 8611BNWP,MA).

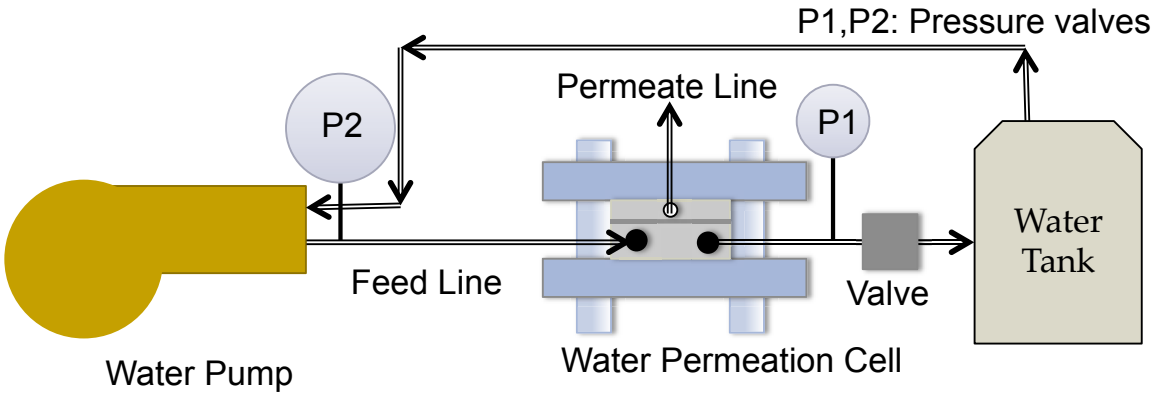

Figure 7-1. Water permeation setup for testing SWNT thin film nanocomposite membranes.

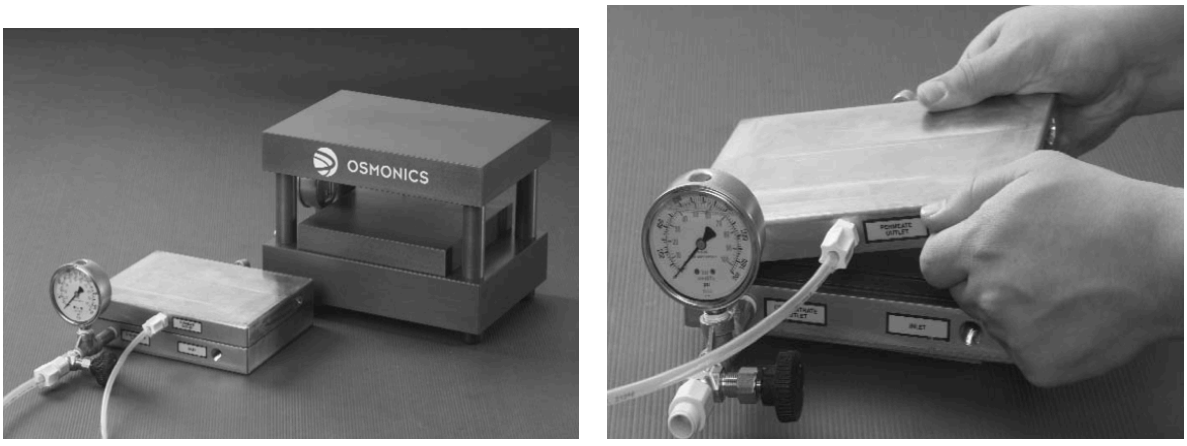

Figure 7-2. Pictures showing the GE Sepa^{TM} CF Cell used for testing water transport properties of SWNT TFN membranes.

Figure 7-3. Picture of a CNT membrane masked with aluminum tape for testing inside the water permeation setup.

7.1.3. Characterization Methods

TFN membranes are tested for water transport and salt rejection of Na^+ ion, which is derived from sodium chloride salt. The water flux and salt rejection performance of the CNT nanocomposite membranes with varying concentration of zwitterion functionalized SWNTs are compared with that of a pure polyamide membrane. The operating feed pressure is 530 psi. All the membranes are tested for three consecutive days to examine their stabilities. The feed solution was 1000 ppm NaCl in concentration and the membrane area covered with CNTs is 9.6 cm^2.

7.2. Results and Discussion

7.2.1. Water Transport Properties of SWNT/Polymer Nanocomposite Membranes

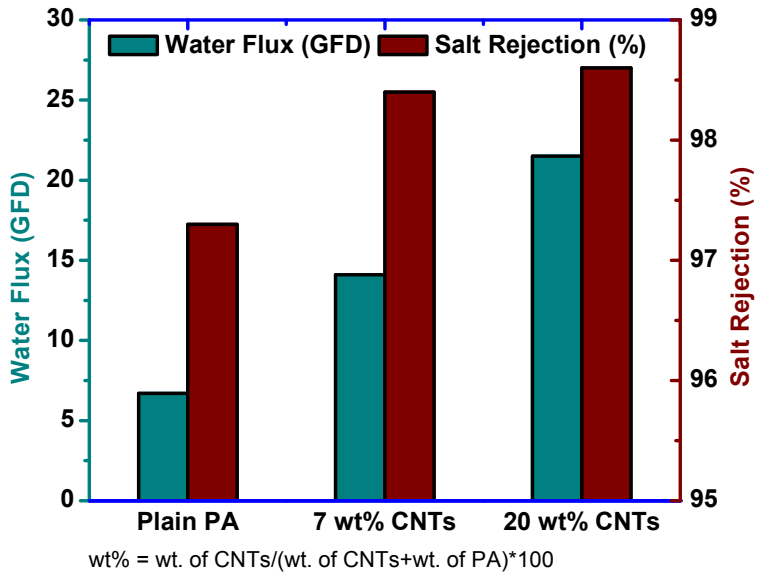

Figure 7-4. Water flux and salt rejection in three varying concentration of TFN membranes (i) neat polyamide (ii) 7 wt% CNT TFN membrane and (iii) 20 wt% CNT TFN membrane.

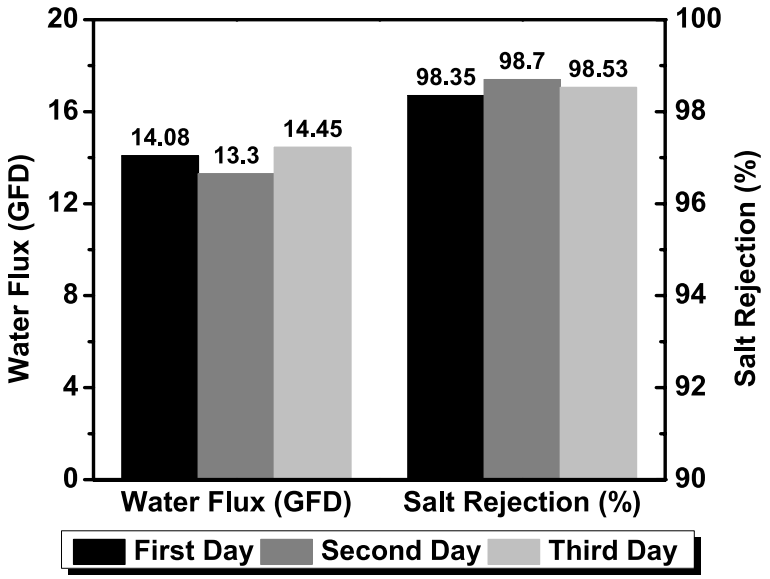

Figure 7-5. Performance stability of 7 wt% zwitterion functionalized SWNT nanocomposite membrane.

It can be observed from Figure 7-4 that the water flux and salt rejection increased with increasing concentration of CNTs in the membrane. For example, the water flux increased 3 times from 6.7 GFD in neat polyamide membrane to 21.5 GFD in 20 wt% CNT TFN membrane. CNTs imparted a new transport mechanism to the membrane, since increasing the flux through a polymer membrane would be expected to result in a decrease of the salt rejection rate[27]. We have previously shown that adding closed CNTs to a polymer membrane actually decreases the flux, whereas using open nanotubes increases the flux[9]. This clearly demonstrates that flow of the fluid takes place primarily through the opened CNTs. Membranes are tested for their water flux and salt rejection over three consecutive days to study their performance stability. Figure 7-5 shows the performance stability graph of 7 wt% TFN membrane. Over a period of three days, the standard deviation in water flux is 0.58 GFD and salt rejection is 0.18%. Since the deviations are very small, it can be concluded that SWNT TFN membranes demonstrated stability in their desalination performance within the experimental time.

Similarly, the salt rejection increased from 97.3% in neat polyamide membrane to 98.6% in 20 wt% CNT TFN membrane. The zwitterionic functional groups in the CNT serve as gatekeepers that control the exclusion of ionic species from the carbon nanotube pores. Figure 7-6 shows the proposed mechanism of salt rejection. The extremely high dipole moment of the zwitterionic groups (10–20 Debye) gives rise to strong interactions with water only at the

entrance port. In fact hydration preferentially stabilizes the zwitterionic structure and the resulting hydration layer increases excluded-volume effects, thus effectively blocking access to the CNT pore to moieties other than water. The zwitterion complex remains unperturbed by the solvated Na^+ and Cl^- ions and effectively blocks ions from entering the CNT pore due to size constraints, while allowing the passage of water. The size of the hydrated sodium ion is about 0.74 nm and therefore it cannot pass through the functionalized zwitterionic groups at the CNT entrance. Considering that the lifetime of water in a hydrated cluster is about 10^{-11} seconds, water molecules are transported via exchange through the hydration spheres.

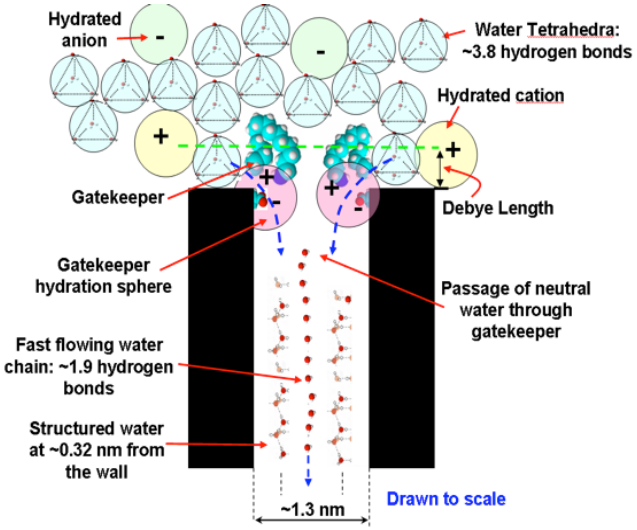

Figure 7-6. Proposed ion rejection mechanism by functionalized carbon nanotubes.

7.2.2. Molecular Dynamic Simulations

Atomistic simulations were performed to test the hypothesis of the operation of functionalized nanotube membranes. The simulation work was carried out by Prof. Karl Johnson and his research group at University of Pittsburgh. The simulation setup is shown in Figure 7-7, where a model membrane composed of four carbon nanotubes embedded in graphene sheets (to force the fluid flow through the nanotubes). Each nanotube has a single zwitterion group attached to each end. A section of bulk salt water is placed on the outside of the nanotube membrane and periodic boundary conditions are applied. We have calculated the flux of water and ions through CNTs functionalized with COOH and zwitterion groups using molecular dynamics simulations. Flow of water and ions was induced in the simulation by imposing a pressure drop across the membrane and carrying out simulations for several ns. The flux of water, sodium ions (Na^+) and chloride ions (Cl^-) through the model membrane was measured during the

course of the simulation. Results for COOH and zwitterion functionalized nanotubes are plotted in Figure 7-8. The results of the simulations provide a proof-of-concept that zwitterions can function as gatekeeper molecules to effectively inhibit the flow of salt ions (Na^+ and Cl^-) through the nanotube membrane. Simulations under identical conditions for the COOH functionalized CNTs show that the conductance of salt ions through the membrane increases linearly with time, and hence the membrane is ineffective at blocking salt transport and would therefore not be effective for use in a desalination membrane. On the other hand, the simulations clearly demonstrate that functionalizing the ends of each of the nanotubes with two zwitterion functional groups makes the ion flux drop to zero over the length of the simulation. Hence, the simulations show that the zwitterions are effective gatekeeper moieties that turn an unselective membrane into a highly selective membrane suitable for desalination. These simulations provided the motivation for carrying out experiments on functionalized nanotubes in membranes.

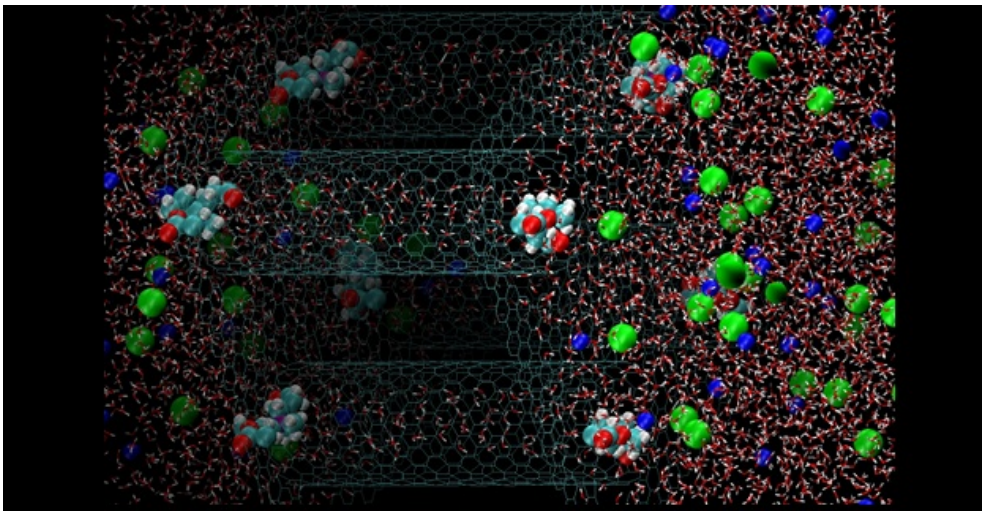

Figure 7-7. Simulation system containing a model carbon nanotube membrane (light blue frame) immersed in a mixture of water (red and white sticks) and salt (Cl^-, green, Na^+, blue). Each nanotube has one zwitterion group (space filling model) bound to each end.

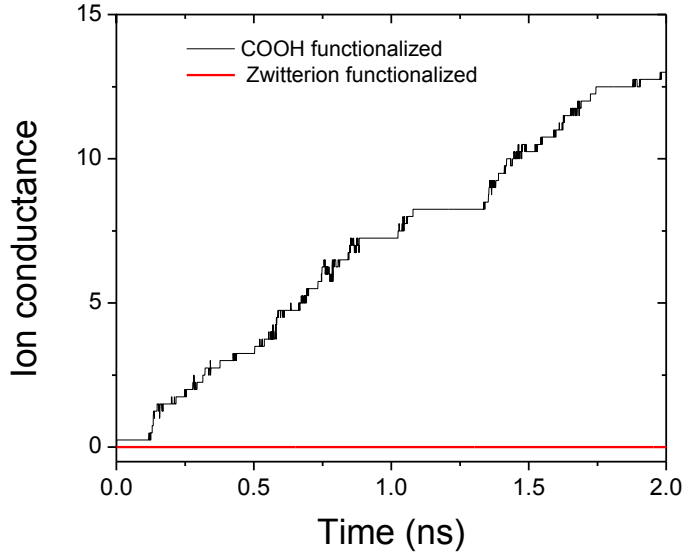

Figure 7-8. Computer simulations of the conductance of salt ions (in total ions per tube) through CNT membranes functionalized with COOH groups (black line) functionalized with two zwitterions on the end of each nanotube (red line). The zwitterions effectively block the salt flux under identical conditions of operation.

7.3. Conclusions

Thin film nanocomposite membranes were fabricated using zwitterion functionalized SWNTs employing interfacial polymerization. TFN membranes were tested for their water transport and salt rejection properties. Water flux increased by three times in 20 wt% SWNT TFN membrane compared to in neat polyamide membrane. Salt rejection also increased in the zwitterion SWNT TFN membranes. The water permeation result is a proof-of-concept that water flux can be increased in a polyamide membrane by adding zwitterion functionalized SWNTs without losing any salt rejection. Introducing functionalized carbon nanotubes into the membrane polymer layer under optimized conditions will increase the water flux of the commercially-available materials several fold with similar if not better salt rejection.

7.4. References

1. Holt, J. K., Noy, A., Huser, T., Eaglesham, D. & Bakajin, O. Fabrication of a Carbon Nanotube-Embedded Silicon Nitride Membrane for Studies of Nanometer-Scale Mass Transport. *Nano Lett.* **4**, 2245–2250 (2004).
2. Holt, J. K. Fast Mass Transport Through Sub-2-Nanometer Carbon Nanotubes. *Science* **312**, 1034–1037 (2006).
3. Kim, S., Chen, L., Johnson, J. K. & Marand, E. Polysulfone and functionalized carbon nanotube mixed matrix membranes for gas separation: Theory and experiment. *Journal of Membrane Science* **294**, 147–158 (2007).

4. Kim, S., Jinschek, J. R., Chen, H., Sholl, D. S. & Marand, E. Scalable Fabrication of Carbon Nanotube/Polymer Nanocomposite Membranes for High Flux Gas Transport. *Nano Lett.* **7**, 2806–2811 (2007).
5. Majumder, M., Chopra, N., Andrews, R. & Hinds, B. J. Nanoscale hydrodynamics: Enhanced flow in carbon nanotubes. *Nature* **438**, 44–44 (2005).
6. Majumder, M., Chopra, N. & Hinds, B. J. Effect of Tip Functionalization on Transport through Vertically Oriented Carbon Nanotube Membranes. *J. Am. Chem. Soc.* **127**, 9062–9070 (2005).
7. Skoulidas, A. I., Ackerman, D. M., Johnson, J. K. & Sholl, D. S. Rapid Transport of Gases in Carbon Nanotubes. *Phys. Rev. Lett.* **89**, 185901 (2002).
8. Skoulidas, A. I., Sholl, D. S. & Johnson, J. K. Adsorption and diffusion of carbon dioxide and nitrogen through single-walled carbon nanotube membranes. *J. Chem. Phys.* **124**, 054708–054707 (2006).
9. Surapathi, A., Herrera-Alonso, J., Rabie, F., Martin, S. & Marand, E. Fabrication and gas transport properties of SWNT/polyacrylic nanocomposite membranes. *Journal of Membrane Science* **375**, 150–156 (2011).
10. Jorio, A., Dresselhaus, G. & Dresselhaus, M. S. *Carbon nanotubes : advanced topics in the synthesis, structure, properties, and applications*. (Springer: Berlin; New York, 2008).
11. Holt, J. K. Carbon Nanotubes and Nanofluidic Transport. *Adv. Mater.* **21**, 3542–3550 (2009).
12. Fangqiang Zhu, E. T. K. S. Theory and Simulation of Water Permeation in Aquaporin-1. *Biophysical Journal* **86**, 50 (2004).
13. Thomas, J. A. & McGaughey, A. J. H. Reassessing Fast Water Transport Through Carbon Nanotubes. *Nano Lett.* **8**, 2788–2793 (2008).
14. Thomas, J. & McGaughey, A. Water Flow in Carbon Nanotubes: Transition to Subcontinuum Transport. *Phys. Rev. Lett.* **102**, (2009).
15. Corry, B. Designing Carbon Nanotube Membranes for Efficient Water Desalination. *J. Phys. Chem. B* **112**, 1427–1434 (2008).
16. Song, C. & Corry, B. Intrinsic Ion Selectivity of Narrow Hydrophobic Pores. *J. Phys. Chem. B* **113**, 7642–7649 (2012).
17. Joseph, S. & Aluru, N. R. Why Are Carbon Nanotubes Fast Transporters of Water? *Nano Lett.* **8**, 452–458 (2008).
18. Hinds, B. J. *et al.* Aligned Multiwalled Carbon Nanotube Membranes. *Science* **303**, 62–65 (2004).
19. Fornasiero, F. *et al.* pH-Tunable Ion Selectivity in Carbon Nanotube Pores. *Langmuir* **26**, 14848–14853 (2012).
20. Fornasiero, F. *et al.* Ion exclusion by sub-2-nm carbon nanotube pores. *Proceedings of the National Academy of Sciences* **105**, 17250–17255 (2008).
21. Sun, L. F. *et al.* Materials: Creating the narrowest carbon nanotubes. *Nature* **403**, 384–384 (2000).
22. Won, C. Y. & Aluru, N. R. A chloride ion-selective boron nitride nanotube. *Chemical Physics Letters* **478**, 185–190 (2009).
23. Suk, M. E. & Aluru, N. R. Effect of induced electric field on single-file reverse osmosis. *Phys. Chem. Chem. Phys.* **11**, 8614–8619 (2009).
24. Cheng, G. *et al.* Zwitterionic carboxybetaine polymer surfaces and their resistance to long-term biofilm formation. *Biomaterials* **30**, 5234–5240 (2009).

25. Ladd, J., Zhang, Z., Chen, S., Hower, J. C. & Jiang, S. Zwitterionic Polymers Exhibiting High Resistance to Nonspecific Protein Adsorption from Human Serum and Plasma. *Biomacromolecules* **9**, 1357–1361 (2008).
26. Li, G. *et al.* Ultra low fouling zwitterionic polymers with a biomimetic adhesive group. *Biomaterials* **29**, 4592–4597 (2008).
27. Geise, G. M., Park, H. B., Sagle, A. C., Freeman, B. D. & McGrath, J. E. Water permeability and water/salt selectivity tradeoff in polymers for desalination. *Journal of Membrane Science* **369**, 130–138 (2011).

Chapter 8. Conclusions

Membranes are widely used for gas separation applications in chemical industry. For example, membranes are used to separate oxygen from nitrogen, separation of hydrogen from hydrocarbons in refinery hydrogen recovery and many other industrially important gas separations. For gas separations using membranes to be economically competitive to other separation methods like cryogenics and pressure swing absorption, membranes have to separate large volumes of gas mixtures producing high purity product at low energy consumption. Hence efforts were made by researchers to fabricate membranes demonstrating high permeability and selectivity of gases. Atomistic simulations predicted that the diffusion of gases inside single walled carbon nanotubes was orders of magnitude faster than in other nanoporous materials[1-5]. This fast transport of gases is due to the atomically smooth inner surface of the nanotubes[5]. The objective of the current research was to fabricate thin nanocomposite membranes using single walled carbon nanotubes exhibiting high permeability and selectivity of gases. The thickness of the separation layer should be below 1μm in order to get high fluxes of gas through the membrane. These membranes should also be defect free without any voids so that there is no loss of gas selectivity. As reported in earlier work by Kim et. al.[6], the selectivities of gases in CNT membranes were very low. Since the diameter of the SWNT was larger than the kinetic diameter of all light gases and also, the mean free path of the gas molecules was larger than the diameter of the pore, the gas selectivities were very close to Knudsen selectivities, which are not useful for industrial gas separation applications[7]. Functionalization of tip of the CNTs with specific chemical groups[8,9] can enhance the gas selectivities. Functional groups can affect the absorption of gases inside the nanotubes via specific molecular interactions and steric hindrance.

SWNT nanocomposite membranes were fabricated using COOH functionalized SWNTs and in-situ polymerization of a polymer matrix. The role of the polymer matrix was to support the carbon nanotubes in an aligned arrangement. In-situ polymerization allowed better dispersion of CNTs in the matrix polymer avoiding any interfacial defects/voids. Initially, raw carbon nanotubes were purified by a two-step purification[10] method to remove any amorphous carbon and Fe catalyst particles. Purified CNTs were long (length around 1000μm), entangled and bundled. The ends were also closed, and so the inner pore was not accessible for gas transport. Also, these CNTs were non-functionalized. To make thin membranes, long CNTs were cut into short tubes by sonicating in an oxidizing acid mixture (3:1, v/v) of sulfuric and nitric acid. The

CNTs were cut into small open tubes of length around 200nm, and also functionalized with COOH groups on the sidewall and terminal ends of the tubes. The carboxylic acid functional groups acted as the anchor points for any conversion of COOH groups into the desired functional groups such as zwitterion functional groups. In this work, COOH groups in CNTs were converted into a chemical group with a terminal double bond. It was believed that these terminal bonds participated in the UV polymerization, thereby forming a good interfacial contact between the surface of the CNTs and the matrix polymer.

Sorption studies were performed on functionalized SWNTs to understand their effectiveness in enhancing the gas selectivities in SWNT nanocomposite membranes. They were performed on raw and purified SWNTs. The concentration of the light gases sorbed in purified SWNTs was much higher than in raw SWNTs. This indicated that purified SWNTs were de-bundled, and consequently larger surface area was available for higher absorption of gas. Sorption studies were also performed on cut CNTs functionalized with COOH groups. It was observed from the gas sorption isotherms that COOH groups did not affect the sorption of hydrogen gas inside the tube, but blocked substantially the sorption of CO_2 gas. The concentration of CO_2 gas in purified-cut SWNTs was almost half of its concentration in purified SWNTs. This result indicated that the presence of the COOH functional groups in the ends of the CNTs affected the entry of the CO_2 gas inside the pore and subsequently its selectivity in the membrane. This effect is called the 'gatekeeper' mechanism of the functional groups[11].

Initially, nanocomposite membranes were fabricated using two monomers, butyl methacrylate and butyl acrylate for the matrix polymer by UV polymerization. They were mixed in the ratio 90:10 (w/w) together with a UV initiator. A suspension of COOH functionalized SWNTs was filtered through a porous filter support by high-pressure vacuum filtration depositing partially aligned CNTs on top of it. The porous support with CNTs was placed in a Teflon plate pre-filled with the monomer mixture, and UV polymerized for 4 hours. Excess polymer on top of the membrane was removed by oxygen plasma etching, allowing the tip of the CNTs to be exposed on the feed side of the membrane for gas diffusion. Plasma etching was a very important step in fabricating these membranes since it makes the inner pore of the CNT accessible for gas transport. The thickness of the SWNT/matrix polymer was around 20μm. The gas permeabilities had increased in the etched membrane compared to the permeabilities calculated by Knudsen model. However, the gas selectivities were still very close to the Knudsen

selectivities. This may be due to the ineffectiveness of COOH functional groups on SWNTs affecting the gas transport in the membrane unlike the gas sorption in SWNTs. Hence membranes were fabricated with improved gas permeabilities but not the selectivities. Furthermore, the thickness of the separation layer could not be decreased to below 1μm and functionalization of the tip of CNTs with COOH groups failed in enhancing the gas selectivities. Hence the investigation was focused on functionalizing SWNTs with a more effective functional group and simultaneously making thin membranes exhibiting both high permeability and selectivity of gases.

The new objective of the research was to functionalize SWNTs with short zwitterionic functional groups and make membranes with ultra thin separation layer. Zwitterionic functional groups have a strong dipole moment (20 Debye for sulfobetaine-type zwitterions). It was hypothesized that these groups would have strong dipole-dipole interactions with polar gas molecules (e.g. CO_2) and no interaction with non-polar gas molecules (e.g. CH_4) affecting the gas selectivity (e.g. CO_2/CH_4) significantly. Similar to the earlier study, sorption studies were performed on zwitterion and COOH functionalized SWNTs. It was observed from the gas sorption isotherms that the concentration of the gases sorbed in the zwitterion functionalized SWNTs was much lower compared to in COOH SWNTs. This may be due to the blocking of the pore of the CNT by the zwitterion functional group, whose length (1.1-1.2 nm) is close to the diameter of the CNT (1.5 nm).

Subsequently, zwitterion functionalized SWNTs were used in making thin film nanocomposite membranes. Dispersion of zwitterion SWNTs in water was filtered through a polyethersulfone support allowing the CNTs to deposit on top of the support. A very thin layer of polyamide embedding the CNTs was formed on top of the support by interfacial polymerization. The monomers used in interfacial polymerization were trimesoyl chloride and m-phenylenediamine. The thickness of the polyamide layer was around 500 nm. Membranes were fabricated with different weight percentages of the SWNTs and two different functional groups, COOH and zwitterion groups. The gas permeabilities increased for all gases with weight percentage of the SWNTs in the membrane. For example, the permeability of hydrogen increased by a factor of 25 in 65 wt% SWNT nanocomposite membrane compared to neat polyamide membrane and by a factor of 29 for sulfur hexafluoride (SF_6), the largest kinetic diameter gas molecule. The rate of increase in permeability with weight percentage was highest

for hydrogen having the smallest kinetic diameter. The rate of increase in permeability decreased with increase in the kinetic diameter of the gas molecules. The gas permeabilities in COOH functionalized TFN membranes were almost twice compared to in zwitterion SWNT TFN membranes. This result is in consistence with the gas sorption isotherms, which showed that the concentration of gases sorbed in the zwitterion functionalized SWNTs was much lower than in the COOH functionalized SWNTs. However, the selectivities did not change either with the functionalization on the SWNT or the concentration of the zwitterion functionalized SWNTs in the membrane. Indeed, the selectivities were very close to the intrinsic selectivities of the pure polyamide membrane. The permeation results in SWNT/polyamide nanocomposite membranes were explained with the help of a three-path gas diffusion model. According to this model, inside a membrane gas transported in three possible paths (i) diffusion of gas inside the pore of the CNT controlled by the gatekeeper mechanism of the functional groups on the tips of the tube (ii) gas diffusion around the nanotube through the nanochannels, which are the interfacial defects formed between the nanotube and the matrix polymer, and (iii) in the matrix polymer itself. The preference for any of the above three paths by the gas molecule for diffusion strongly depended on the functional group in the SWNTs. For example, the concentration of the gases sorbed in COOH SWNTs and the gas permeabilities in COOH TFN membranes were higher than in zwitterion SWNTs and zwitterion SWNT TFN membranes respectively. These results indicated that majority of the gases diffused through the inner pore of the COOH SWNTs in the COOH SWNT TFN membrane compared to inside the zwitterion SWNTs in zwitterion SWNT TFN membrane. However, the overall permeability is still a combined effect of the diffusion of gases through all the three paths discussed in the model.

More controlled studies and experiments discussed in detail in the next chapter are necessary to understand the gas transport in SWNT/polymer nanocomposite membranes and the role of SWNT. This would eventually help in improving the gas selectivities in the membrane without lowering the gas permeabilities, moving above the Robeson upper bound in gas separation performance.

8.1. References

1. Sholl, D. S. & Johnson, J. K. Making High-Flux Membranes with Carbon Nanotubes. *Science* **312**, 1003–1004 (2006).
2. Skoulidas, A. I., Sholl, D. S. & Johnson, J. K. Adsorption and diffusion of carbon dioxide and nitrogen through single-walled carbon nanotube membranes. *J. Chem. Phys.* **124**, 054708–054707 (2006).

3. Chen, H. & Sholl, D. S. Rapid Diffusion of CH_4/H_2 Mixtures in Single-Walled Carbon Nanotubes. *J. Am. Chem. Soc.* **126**, 7778–7779 (2004).
4. Ackerman, D., Skoulidas, A., Sholl, D. & Johnson, J. K. Diffusivities of Ar and Ne in Carbon Nanotubes. *Mol. Simulation* **29**, 677–684 (2003).
5. Skoulidas, A. I., Ackerman, D. M., Johnson, J. K. & Sholl, D. S. Rapid Transport of Gases in Carbon Nanotubes. *Phys. Rev. Lett.* **89**, 185901 (2002).
6. Kim, S., Jinschek, J. R., Chen, H., Sholl, D. S. & Marand, E. Scalable Fabrication of Carbon Nanotube/Polymer Nanocomposite Membranes for High Flux Gas Transport. *Nano Lett.* **7**, 2806–2811 (2007).
7. Kesting, R. E. & Fritzsche, A. K. *Polymeric gas separation membranes*. (Wiley: New York, 1993).
8. Majumder, M., Chopra, N. & Hinds, B. J. Effect of Tip Functionalization on Transport through Vertically Oriented Carbon Nanotube Membranes. *J. Am. Chem. Soc.* **127**, 9062–9070 (2005).
9. Majumder, M., Chopra, N. & Hinds, B. . Mass Transport through Carbon Nanotube Membranes in Three Different Regimes: Ionic Diffusion and Gas and Liquid Flow. *ACS Nano* **5**, 3867–3877 (2011).
10. Cinke, M. *et al.* Pore structure of raw and purified HiPco single-walled carbon nanotubes. *Chemical Physics Letters* **365**, 69–74 (2002).
11. Hinds, B. J. *et al.* Aligned Multiwalled Carbon Nanotube Membranes. *Science* **303**, 62–65 (2004).

Chapter 9. Future Work

The thin film nanocomposite membranes fabricated using zwitterion functionalized SWNTs and interfacial polymerization demonstrated high gas permeabilities compared to in neat polyamide membrane but no improvement in selectivities. In fact, the gas selectivities are close to Knudsen selectivities. There are two possible ways of improving gas selectivities in an effort to make high gas permeability and selectivity membranes. One way is to use a polyamide matrix with higher intrinsic gas selectivity and functionalization of CNT. The other approach is to align the carbon nanotubes in the membrane by using an electric field. These ideas are discussed in detail in Section 9.1 and 9.2 of this chapter. Sections 9.3 and 9.4 discuss about improving the alignment of SWNTs in membrane and their quantitative characterization. Section 9.5 discuss the experiments necessary to better understand and improve the desalination properties of CNT membranes.

9.1. Higher Functionality Monomers

The observed low gas selectivity in the neat polyamide membrane may be due to the loose polyamide structure in the separation layer of the membrane[1], also making the gas selectivities to fall close to the Knudsen selectivities. The monomers used in interfacial polymerization forming polyamide layer of the membrane are trimesoyl chloride (TMC) and m-phenylenediamine (MPD). The chemical structure of these monomers is shown in Figure 9-1.

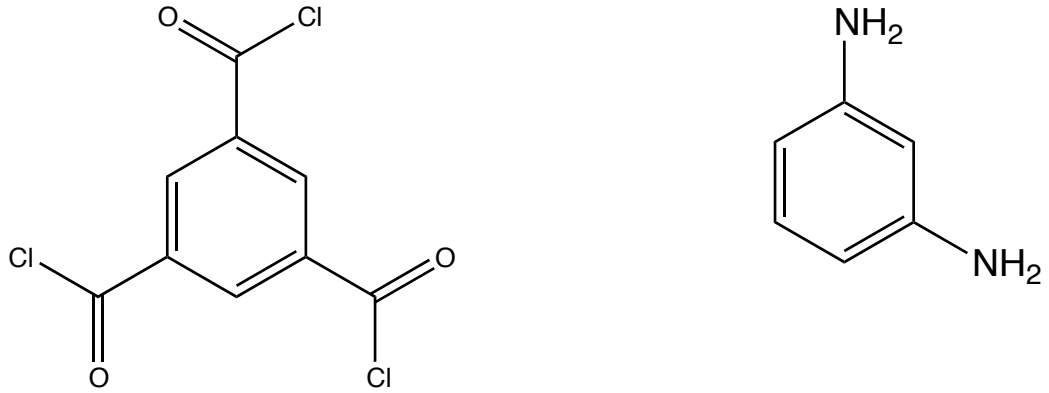

(A) (B)

Figure 9-1. Monomers used in the interfacial polymerization reaction (A) trimesoyl chloride and (B) m-phenyldiamine.

The functionalities of TMC and MPD are 3 and 2 respectively. Since the functionality of monomers is greater than 2, the polyamide formed between the two monomers is cross-linked. The selectivities of the gases in the pure polyamide (PA) composite membrane suggest that the

polyamide formed from these two monomers is not highly cross-linked. In the future, tetraethylene tetramine (TETA) with a functionality of 4 as shown in Figure 9-2 will be used as amine monomer for interfacial polymerization. The polyamide formed from these monomers should be more densely cross-linked giving higher gas selectivities.

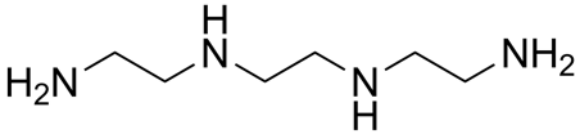

Figure 9-2. Structure of tetraethylene tetramine.

Zhao et. al.[2] fabricated composite polyamide membranes using TETA and TMC as monomers by interfacial polymerization. They reported CO_2 permeability of 2.66 Barrer and CO_2/CH_4 selectivity of 94.1. These values plotted on a Robeson plot for CO_2 and CH_4 gas pair is shown in Figure 9-3.

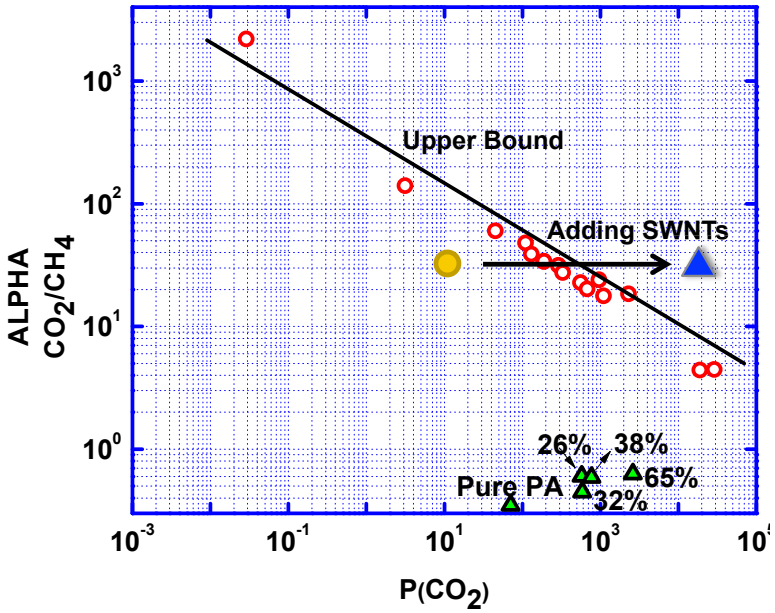

Figure 9-3. Robeson plot for CO_2/CH_4. The permeability and selectivity of TFN membranes with different concentrations of zwitterion SWNTs were plotted. The data point (yellow) represents the membrane made by Zhao et. al[2].

From our experiments, we have observed that the CO_2 permeability increased significantly with the concentration of zwitterion functionalized SWNTs in the membrane. Hence the hypothesis for future work is that using TETA and TMC as monomers (higher intrinsic polyamide selectivity) for interfacial polymerization, and adding zwitterion functionalized SWNTs to the

separation layer of membrane, it should be possible to fabricate high permeability and selectivity membranes as shown in Figure 9-3.

9.2. Functionalization of SWNTs: Gatekeeper Mechanism

Gatekeeper mechanism[3-8] of the functional group depends on the length of the functional group (size exclusion) and charge of the group (molecular interactions). When the kinetic diameter of the gas molecule is larger than the diameter of the SWNT, it cannot enter the tube for gas transport. This effect is called 'size exclusion' (or) 'molecular sieving' of gas molecules. The effective pore diameter is defined as the diameter of the largest gas molecule that can enter inside of the tube through its opening. Functional groups by their presence change the effective pore diameter of the CNT thereby providing more control in design of CNT membrane separating gas molecules very close in kinetic diameters such as oxygen (3.5 Å)[9] and nitrogen (3.6 Å)[9]. Simulations by Karl Johnson[10] and his group from University of Pittsburgh showed that long functional groups such as zwitterionic groups which are flexible can adopt different configurations. For example, zwitterionic functional groups adopted two configurations (i) extended configuration from the tube ends into the solution phase and (ii) folded inside the nanotube. Thermodynamically, the folded configuration is more stable than extended zwitterionic group. The folded zwitterion group inside the nanotube changed the effective pore diameter. Hence the folded configuration of flexible, long functional groups can also change the effective pore diameter. The gas molecules may also experience favorable interactions such as dipolar-dipolar interactions with the functional group in the SWNT. This effect is called the 'molecular interactions' effect. These two phenomenon together define the gatekeeper mechanism of functional groups. To understand this mechanism, CNTs functionalized with the functional groups shown in Table 9-1 need to be studied for their gas sorption properties.

Table 9-1. Functional groups to be introduced at the core.

Functional Group	**Approximate Size (nm)**	**Charge**
$-COO^-$ (high pH)	<0.4	-1
-COOH (low pH)	<0.4	neutral
$-CONH-(CH_2)_2-NH_2$ (high pH)	0.58	neutral
$-CONH-(CH_2)_2-NH_2^+$ (low pH)	0.58	neutral
$-COO-(CH_2)_2-N^+(CH_2)_2-(CH_2)_2COO^-$	1.1-1.2	Zwitterion (+1,-1)
$-CONH-(CH_2)_4-CH_3$	0.69	neutral
$-CONH-(CH_2)_8-CH_3$	1.14	neutral

(A) Length of the functional group: To study the effect of the length of the functional group, CNTs need to be functionalized with $-CONH-(CH_2)_4-CH_3$ and $-CONH-(CH_2)_8-CH_3$, whose lengths are 0.69 nm and 1.14 nm respectively. Both functional groups are neutral. Hence the effective pore diameter in the SWNTs functionalized with the above two groups will be different. For example, assuming the diameter of the CNT is 1.5 nm the effective pore diameter of SWNT with $-CONH-(CH_2)_4-CH_3$ is 0.81 nm and $-CONH-(CH_2)_8-CH_3$ is 0.36 nm. SWNTs with $-CONH-(CH_2)_4-CH_3$ functional group should block any gas molecule larger than 0.8 nm and allow other smaller gases (He, H_2, CO_2, O_2, N_2, CH_4, SF_6) to absorb inside the pore of the nanotube. SWNTs with $-CONH-(CH_2)_8-CH_3$ functional group should block gas molecules larger than 0.36 nm (N_2, CH_4, SF_6) and allow smaller gas molecules (He, H_2, CO_2, O_2) to absorb inside the nanotube. CNT with the above functional group based on size exclusion can theoretically separate O_2 from N_2, and CO_2 from CH_4, which are industrially important gas mixtures for separation.

(B) Charge on the functional group: To study the effect of the charge in the functional group, gas sorption properties of CNTs functionalized with $-COO^-$ (negative) and -COOH (neutral) will be studied. Both groups have very similar molecular length below 0.4 nm. Gas molecules such as CH_4 have dipole moment along the individual bond -C-H- and CO_2 along the -C-O- bond. In

CH_4 molecule, the positive partial charge on $C^{\delta+}$ experiences an electrostatic attraction force from the negative charged -COO^- group in the SWNT. Similarly CO_2 molecule also experiences an attraction force from the -COO^- group in the SWNTs. On the other hand, the above gas molecules does not experience any kind of interaction from the –COOH molecule since it is neutral. Hence CO_2 and CH_4 absorbs more preferentially than other gas molecules in SWNTs functionalized with -COO^- group, whereas no such preferential absorption predicted in SWNTs with COOH groups.

(C) Dipole moment of functional group: To study the effect of the dipole, CNTs functionalized with short zwitterionic groups -COO-$(CH_2)_2$-$N^+(CH_2)_2$-$(CH_2)_2COO^-$ and neutral group -CONH-$(CH_2)_8$-CH_3 having the same molecular length around 1.4 nm, but earlier group having a dipole will be studied. The zwitterion functional group with its strong dipole moment (20 Debye for sulfobetaine-type zwitterions) experiences strong dipole-quadrupole interactions with polar gas molecules[11]. CO_2 gas molecule has a very strong quadrupole moment whereas CH_4 molecule has weaker quadrupole moment. Hence CO_2 gas molecule experiences stronger dipole-quadrupole attraction force than CH_4 predicting preferential absorption of CO_2 than CH_4 in zwitterion functionalized SWNTs. Since the functional group -CONH-$(CH_2)_8$-CH_3 does not have any dipole moment, it is predicted that the group is ineffective in affecting the absorption of any gas inside the SWNT.

The terminal COOH acid groups in chemically cut single walled carbon nanotubes are the anchor points for functionalizing CNTs with the desired functional groups presented in Table 9-1. The COOH groups can be converted into COO^- by changing the pH of the COOH SWNT solution. COOH-SWNTs can be reacted with ethylene diamine (NH_2-$(CH_2)_2$-NH_2) to form functional group -CONH-$(CH_2)_2$-NH_2 in low pH solution. Functional group -CONH-$(CH_2)_2$-NH_2^+ can be obtained by changing the pH of the solution to low acidic conditions. The synthesis of zwitterion functional group is already explained in Section 4.2.2. To obtain -CONH-$(CH_2)_4$-CH_3 and -CONH-$(CH_2)_8$-CH_3 functional groups, COOH SWNTs are reacted with n-pentanamine (CH_3-$(CH_2)_4$-NH_2) and n-nonanamine (CH_3-$(CH_2)_8$-NH_2) respectively.

(D) Diameter of the SWNT: The diameter of the SWNT is also a variable, which can be varied to study the gatekeeper mechanism. Commercial suppliers produce SWNTs with diameters in the range of 0.8-1.5nm. Smaller diameter SWNTs are more expensive because the growth conditions by CVD need to be controlled very precisely. Due to the cost reasons, it is more economical to

use large diameter CNTs in making the membranes. Although large diameter CNTs cannot separate gases by size exclusion, they can be functionalized with chemical groups thus reducing the effective pore diameter and thereby molecular sieving of the gas molecules. Hence CNTs of various diameters ranging from 1 nm to 2 nm, having the same functional group (may be positive, negative, neutral or dipole) will be studied for their gas sorption properties. The results from all these studies together should help in understanding the effect of (i) length and (ii) charge (iii) dipole moment of the functional group and (iv) the diameter of the CNT on the gatekeeper mechanism of functional groups in CNTs.

9.3. Alignment of SWNTs by Electric Field

SWNTs in the polymer CNT nanocomposite membranes can be aligned by electric field[12-14] and magnetic field[15-17]. However, high strength of magnetic fields is required for SWNT alignment in nanocomposites. Fischer et. al.[15] and Smith et.al.[16] used magnetic field strengths of 7 T and 25 T respectively for SWNT alignment, which is achievable only in certain specially equipped laboratories. Hence, electric field for SWNT alignment will be studied in detail in the future. Also, alignment by electric field is highly employed for making aligned electrospun fibers[18,19]. The theory behind the alignment of CNTs by an external electric field is described in the following paragraph.

Single walled carbon nanotubes (SWNTs) are sonicated in the monomers to form a suspension. SWNTs in a suspension are polarized under the external electric field[20]. Due to the interactions between the resulting CNT dipoles within the solution, the nanotubes get aligned in the direction of the electric field. For the purpose of discussion, assume CNT is a particle of radius a. Assuming nanotube as a rigid cylinder, the radius of gyration is given by[14],

$$a = R_g = \left(\left(\frac{R^2}{2}\right) + \left(\frac{L^2}{12}\right)\right)^{\frac{1}{2}} \approx \left(\frac{L^2}{12}\right)^{\frac{1}{2}} \qquad \text{Equation 9-1}$$

Consider a single particle of radius 'a' and dielectric constant ε_p, suspended in a solvent of dielectric constant ε_s. Gauss's law for this system with no free charges is written in terms of Laplace equation,

$$\nabla^2\psi = 0 \qquad \text{Equation 9-2}$$

where Ψ is the electric potential. If a uniform electric field is applied in the z-direction for a co-ordinate system centered on the sphere of interest as shown in Figure 9-4, the solution to Equation 9-2 is

$$\psi = -\vec{E}.\vec{r}cos\theta\left[1 - \frac{\beta a^3}{r^3}\right] \qquad \text{Equation 9-3}$$

where β is the particle dipole coefficient given as

$$\beta = \frac{\varepsilon_p - \varepsilon_s}{\varepsilon_p + 2\varepsilon_s} \qquad \text{Equation 9-4}$$

The dipole coefficient is a measure of the polarizability of the particle in an external electric field. If the particle and solvent has different dielectric constants, the dipole moment of the particle μ is $\varepsilon_o\varepsilon_s\beta a^3 E$ where ε_o is the permittivity of free space (8.854×10^{-12} Fm^{-1}).

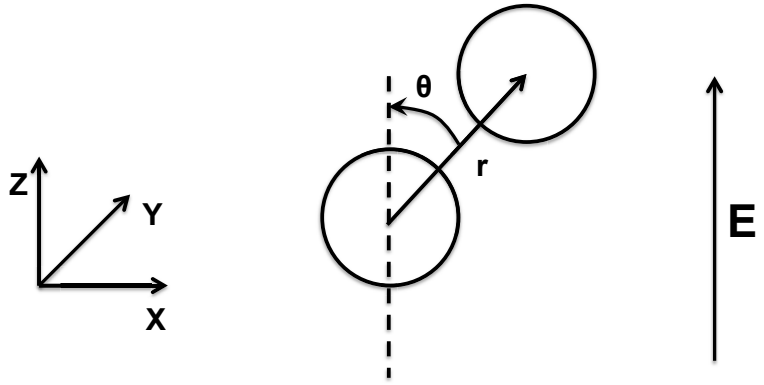

Figure 9-4. Coordinate system centered on a sphere with electric field in the z direction[21].

If θ is the angle between the direction of the applied field and the position of the second sphere for a spherical coordinate system centered on the first sphere, the dimensionless interaction energy between two point dipoles

$$\frac{U(r,\theta)}{k_bT} = -\frac{\lambda}{2}\left[\frac{3cos^2\theta - 1}{\left(\frac{r}{2a}\right)^3}\right] \qquad \text{Equation 9-5}$$

λ is a dimensionless parameter characterizing the relative importance of the polarization interaction energy to thermal energy, defined as

$$\lambda = \frac{Polarization}{Thermal} = \frac{\pi\varepsilon_o\varepsilon_s a^3(\beta E)^2}{k_bT} \qquad \text{Equation 9-6}$$

The interaction energy in Equation 9-5 is anisotropic, resulting in a force which can be decomposed into an attraction if the spherical particles line of center are aligned with the electric field, a repulsion for perpendicular alignments and a force acting to restore alignment with the electric field[21]. To achieve alignment of the SWNTs in the nanocomposite, the parameter λ must be greater than 1. The alignment occurs when the aligning dielectrophoretic force dominates the misaligning forces such as Brownian motion and electrophoretic force[14].

Figure 9-5 shows the schematic of the setup necessary to achieve the alignment. The setup consists of two electrodes, a Teflon plate, UV lamp enclosed in a white painted box and a voltage supply unit. The white surface of the inside of the box will reflect the UV light and ensure that the polymerization happens uniformly in the Teflon plate. SWNTs will be suspended in THF by sonication. Acrylic monomers and the UV initiator will be added to the suspension and sonicated/mixed for few hours. The mixture is poured into the Teflon plate and subjected to electric field. Simultaneously, the sample will be irradiated with UV light to complete the polymerization. Our previous work[22] suggested that nanocomposites using acrylates are defect free. Polymer from acrylates is rubbery at room temperature and hence do not introduce any interfacial defects in the membrane.

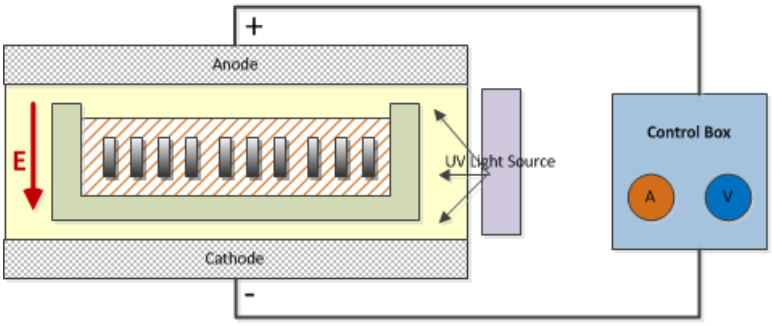

Figure 9-5. Schematic of the setup necessary to align SWNTs within the polymer matrix by electric field.

Below are some of the values, which can be employed for the alignment. The value of λ is calculated for these values. For relative dielectric constant $\varepsilon_s = 4.9$[14] and temperature T=40 ^{0}C, the condition for electric field strength obtained from Equation 9-6 and $\lambda > 1$ for alignment is

$$\lambda = \frac{\Pi \times (8.854 \times 10^{-12}\ F/m) \times 4.9 \times (0.29 \times 10^{-6}\ m)^3 \times E^2}{1.38 \times 10^{-23} J/K \times 313K} > 1 \qquad \text{Equation 9-7}$$

$$E > 36\ kV/m \qquad \text{Equation 9-8}$$

For a distance of 2 cm between the electrodes, the electric field strength is 720 V, which gives the $V_{p\text{-}p}$ (peak to peak voltage) to be 1440 V or 1.4 kV. Some ambiguity in this number is evident since higher strength electric field causes higher amount of heating in the nanocomposite system increasing its temperature T. This increase in turn affects the value of λ and therefore the alignment of the SWNTs. To optimize the parameter values, some preliminary experiments need to be performed. Based on these values, alignment of SWNTs in the nanocomposite membrane

will be studied and characterized using polarized Raman spectroscopy, which is discussed in the next section.

9.4. Characterization of SWNT Alignment

The alignment of the CNTs inside the separation layer of the membrane needs to be characterized. In this thesis work, attempts were made to characterize the alignment qualitatively by high resolution scanning electron microscopy (HRSEM). The micrographs from HRSEM were not very clear for any visual comparison of alignment of SWNTs within the separation layer among different membrane samples. To improve the performance of the TFN membranes for gas separations/desalination, it is equally important to have a reliable method of quantitatively characterizing the nanotube alignment just as much as improving the SWNT alignment itself.

Polarized Raman spectroscopy[14,23] is one such method that can be used to characterize the nanotube alignment in composite materials. Raman intensity of the tangential mode of SWNTs depends on the polarizer angle. The tangential mode intensity reaches a maximum when the polarized light is parallel to the nanotube axis and decreases gradually as the angle of the polarizer increases from 0^o (parallel to the nanotube axis) to 90^o (perpendicular to the nanotube axis). The intensity begins to increase again as the angle of the polarizer increases from 90^o to 180^o[14] as shown in Figure 9-6 and Figure 9-7. When the SWNTs are distributed over a range of angles, the total Raman intensity can be integrated to sum the contribution from nanotubes at each angle[23].

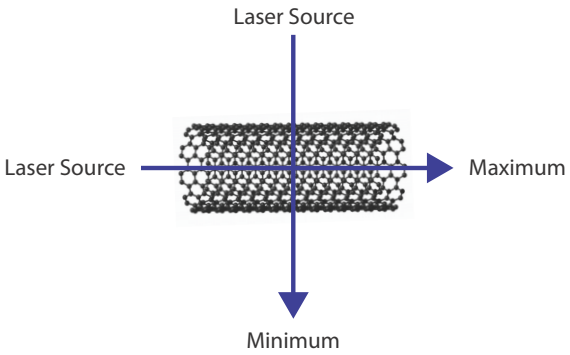

Figure 9-6. Polarized Raman spectroscopy showing a maximum and minimum in the intensity with the angle between the polarized light and the tube axis.

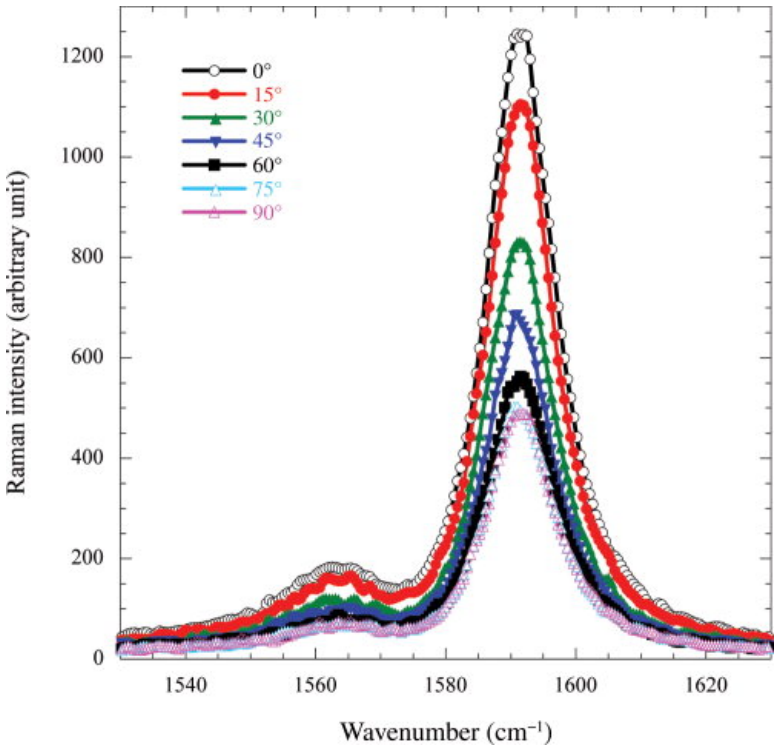

Figure 9-7. Polarized Raman spectroscopy showing the increase in the intensity of the peak at 1591 cm^{-1} with the angle between the nanotube axis and the polarizer angle[14] [used with permission].

The intensity of a Raman peak is

$$I(\psi) = \int_{\psi-\frac{\Pi}{2}}^{\psi+\frac{\Pi}{2}} cF(\theta-\psi,\Delta)\cos^4\theta d\theta \qquad \text{Equation 9-9}$$

where θ is the angle between the SWNTs axis and the incident excitation polarization, ψ is the angle of the sample with respect to the incident polarization as shown in

Figure 9-8, F(θ-ψ,Δ) is a distribution function of angular width characterized by the parameter Δ, and c is a parameter that gives the maximum intensity when θ=0. The degree of the SWNT alignment is determined by measuring I(ψ) for a convenient Raman peak at several sample angles and performing a least square fit to Equation 9-9. In the work by Hwang et. al.[23], they measured the alignment of SWNTs in a 1 wt% SWNT in a melt-spun PMMA fiber. They measured the breathing mode peak intensity (202 cm^{-1}) and plotted it as a function of the fiber angle Ψ. The best fit was found using Lorentzian angular distribution function to give c and Δ, where Δ is the full width at half maximum (FWHM) of the distribution. Two samples measuring $\Delta=4^o$ and 16^o were characterized. The sample exhibiting lower Δ indicates lower spread in the

distribution of the angle between the nanotube and the electric field and hence better SWNT alignment in the composite membrane.

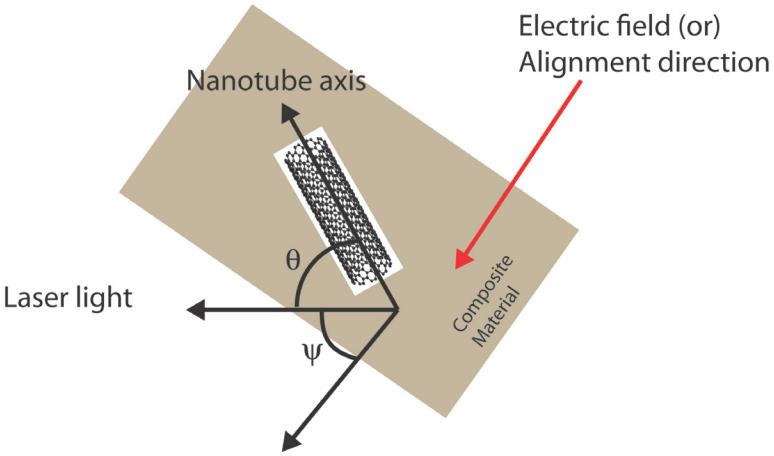

Figure 9-8. Schematic showing the CNT inside the matrix material, at an angle θ with the polarized light, and angle Ψ between laser light and the direction of electric field.

For our experiments, a small rectangular section of the nanocomposite membrane will be cut and used as the sample for polarized Raman spectroscopy. Intensity of the scattering will be recorded at different polarizer angles (between 0^o and 180^o). Different regions of the membrane will be analyzed by this technique to assess the uniformity of the alignment across the membrane cross-section. This data will help in understanding and improving the alignment of SWNTs, thereby enabling the fabrication of SWNT nanocomposite membranes with better gas separation properties.

9.5. Water Permeation and Salt Rejection in CNT membranes

Chapter 7 discussed the water permeation and salt rejection in CNT membranes with increasing weight percentage of SWNTs. Water flux increased by a factor of 3 in 20 wt% z-SWNT polyamide membrane compared to in neat polyamide, with a slight increase in salt rejection. However, the performance is not comparable to the commercial membranes[24]. For example, the water flux in 20 wt% TFN membrane is 37 L/(m^2 h) with salt rejection 98.6% at feed water pressure 530 psi and 1000 ppm salt concentration. Commercial membrane from Dow chemical company called Dow FilmTec TW30-4040 demonstrate water flux of 52 L/(m^2 h) with salt rejection 99.5% at transmembrane pressure difference of 225 psi and feed salt concentration of 2000 ppm. Hence there is a lot of scope for improvement in the performance of CNT membranes.

To achieve this improvement, it is very important to understand the water transport mechanism inside the CNT membranes. For this, along with the experimental studies already conducted in Chapter 7, more are necessary. Carbon nanotube/polyamide nanocomposite membranes will be fabricated using average CNT pore size ranging from 0.8 nm to 1.5 nm to examine the effect of pore size on water and ionic transport. The transport properties will be studied as a function of the electrolyte concentration, pH and ionic valence in order to distinguish between ion rejection based on size exclusion and that based on electrostatic repulsions. For example, higher rejection for divalent anionic salts (Na_2SO_4) compared to monovalent anionic salts (NaCl and $CaCl_2$), and decrease in salt rejection with feed concentration would suggest the operation of Donnan's ion exclusion phenomenon in which electrostatic interactions play an important role.

We will examine the membrane transport of aqueous solutions containing ions such as Na^+, Cl^-, K^+, OH^- and divalent ions such as Mg^{2+}, Ca^{2+}, CO_3^{2-}, which can be derived from common salts. The flux of laboratory de-ionized water and de-ionized water with the added salts will be tested for each membrane. The concentration of the salts will be varied from zero to 3000 ppm. Experimental flux and transport study experiments will be carried out on a laboratory-scale cross-flow membrane test unit, capable of pressures from 25 to 700 psi. In addition, the prolonged effects of using feed water containing sulphate and calcium salts on fouling will also be examined.

9.6. References

1. Louie, J. S., Pinnau, I. & Reinhard, M. Gas and liquid permeation properties of modified interfacial composite reverse osmosis membranes. *Journal of Membrane Science* **325**, 793–800 (2008).
2. Zhao, J., Wang, Z., Wang, J. & Wang, S. Influence of heat-treatment on CO_2 separation performance of novel fixed carrier composite membranes prepared by interfacial polymerization. *Journal of Membrane Science* **283**, 346–356 (2006).
3. Majumder, M., Chopra, N. & Hinds, B. . Mass Transport through Carbon Nanotube Membranes in Three Different Regimes: Ionic Diffusion and Gas and Liquid Flow. *ACS Nano* **5**, 3867–3877 (2011).
4. Corry, B. Water and ion transport through functionalised carbon nanotubes: implications for desalination technology. *Energy Environ. Sci.* **4**, 751–759 (2011).
5. Majumder, M., Stinchcomb, A. & Hinds, B. J. Towards mimicking natural protein channels with aligned carbon nanotube membranes for active drug delivery. *Life Sciences* **86**, 563–568 (2010).
6. Majumder, M., Chopra, N., Andrews, R. & Hinds, B. J. Nanoscale hydrodynamics: Enhanced flow in carbon nanotubes. *Nature* **438**, 44–44 (2005).
7. Hinds, B. J. *et al.* Aligned Multiwalled Carbon Nanotube Membranes. *Science* **303**, 62–65

(2004).
8. Majumder, M., Chopra, N. & Hinds, B. J. Effect of Tip Functionalization on Transport through Vertically Oriented Carbon Nanotube Membranes. *J. Am. Chem. Soc.* **127**, 9062–9070 (2005).
9. Kulprathipanja, S. *Zeolites in Industrial Separation and Catalysis*. (John Wiley & Sons: 2010).
10. Chan, W.-F. *et al.* Zwitterion Functionalized CNT-Polyamide Nanocomposite Membranes for Water Desalination. *Proceedings of the National Academy of Sciences*
11. Johnson, J. R. & Eubank, P. T. Intermolecular Interactions of Highly Polar Gases. *Ind. Eng. Chem. Fund.* **12**, 156–165 (2012).
12. Chen, X. Q., Saito, T., Yamada, H. & Matsushige, K. Aligning single-wall carbon nanotubes with an alternating-current electric field. *Appl. Phys. Lett.* **78**, 3714–3716 (2001).
13. Martin, C. A. *et al.* Electric field-induced aligned multi-wall carbon nanotube networks in epoxy composites. *Polymer* **46**, 877–886 (2005).
14. Park, C. *et al.* Aligned single-wall carbon nanotube polymer composites using an electric field. *J. Polym. Sci. B Polym. Phys.* **44**, 1751–1762 (2006).
15. Fischer, J. E. *et al.* Magnetically aligned single wall carbon nanotube films: Preferred orientation and anisotropic transport properties. *J. Appl. Phys.* **93**, 2157 (2003).
16. Smith, B. W. *et al.* Structural anisotropy of magnetically aligned single wall carbon nanotube films. *Appl. Phys. Lett.* **77**, 663 (2000).
17. Mauter, M. S., Elimelech, M. & Osuji, C. O. Nanocomposites of Vertically Aligned Single-Walled Carbon Nanotubes by Magnetic Alignment and Polymerization of a Lyotropic Precursor. *ACS Nano* **4**, 6651–6658 (2010).
18. Kim, J.-S. & Reneker, D. H. Polybenzimidazole nanofiber produced by electrospinning. *Polym. Eng. Sci.* **39**, 849–854 (1999).
19. Fang, X. & Reneker, D. H. DNA fibers by electrospinning. *J. of Macromolecular Sc., Part B* **36**, 169–173 (2012).
20. Farajian, A., Pupysheva, O., Schmidt, H. & Yakobson, B. Polarization, energetics, and electrorheology in carbon nanotube suspensions under an applied electric field: An exact numerical approach. *Phys. Rev. B* **77**, 205432 (2008).
21. Gast, A. P. & Zukoski, C. F. Electrorheological fluids as colloidal suspensions. *Advances in Colloid and Interface Science* **30**, 153–202 (1989).
22. Surapathi, A., Herrera-Alonso, J., Rabie, F., Martin, S. & Marand, E. Fabrication and gas transport properties of SWNT/polyacrylic nanocomposite membranes. *Journal of Membrane Science* **375**, 150–156 (2011).
23. Hwang, J. *et al.* Polarized spectroscopy of aligned single-wall carbon nanotubes. *Phys. Rev. B* **62**, R13310–R13313 (2000).
24. Xie, W. *et al.* Polyamide interfacial composite membranes prepared from m-phenylene diamine, trimesoyl chloride and a new disulfonated diamine. *Journal of Membrane Science* **403–404**, 152–161 (2012).

Appendix A

The following are the steps in performing a static gas sorption run in IGA for carbon nanotube sample.

1. Loading a sample
2. Decontamination
3. Removing the sample

A.1. Loading A Sample

1.1. Load Sample

File → New Sample or Basket → Yes

Authorization Code: Random

Small samples are a must 0-200 mg → Ideal range 0-100mg

→ <ok>

Put the basket on the IGA (with the lid)

→ Raise the draught shield

→ Once that is done hit <ok> **(Buoyancy setup)**

Set Name of the sample

→ Push the green basket

1.2 Click on empty pan reading

This step is related to the taring of the basket on the IGA

There will be a slight change of the basket weight

Hit <Yes> (Note: Do not press <Finished>)

1.3 Sample loading

→ Lower draught shield

→ Remove the basket

→ Weigh sample (cut sample in small pieces if polymer)

→ Put basket on balance

→ Put reactor up (Change the copper gasket every new run)

Once the reactor is in place, put the nuts and the washer in place.

(The nuts have to be tight; especially the nuts in the back)

Remember:

Static Mode: Copper gasket (use only once)

Humidity Mode: Viton Gasket (various uses)

1.4 Hit <Finished> button
Hit <Ok>

Hit <Ok> on the Lab book Window

1.5 Weight basket (with or without top)

Example: Basket with top = 0.1333 g

Weight range has to be within 80-100 mg of polymer

A.2. Outgas and Decontamination

2.1 Raise the pressure to 1000 mbar
(If decontamination follows outgas, purge the gas inlet line before starting Outgas step. If it is only outgas, no need to purge)

2.2 Go to Pressure set
→ Check that all the valves of the gas cylinders are closed.

→ Hit outgas (Ramp rate – 200 millibar/min, for CNT- 50 millibar/min)

→ Hit *Stop* when the pressure is between 100-200 millibar : usually its 150mbar.

→ Hit *Stop* again (In total stop (valves closed) clicked <u>two</u> times)

→ Hit DECONTAMINATE

→ Hit outgas again

→ the outgas block will be @ Green.

(Check: wait until the pressure at the vacuum pump is around 10^{-6} mbar)

When this color changes to red PIV1 becomes highlighted (~5 millibar) Hit PIV1

(If PIV1 is not highlighted, start chart and it will become highlighted)

→ Open green valve next to reactor (PIV1)

→ Set the temperature to 35 ^{o}C

2.3 After this
→ Start chart

→ set temperature – Degas temperature (time - 480 min)

→ Plug up heater to the temperature (200 ^{o}C)

→ Ramp rate – 10^{o} C/min and Hit <Ok>. It will freeze for some time.

Decontamination must go on for atleast 8 hrs. Set the timers for the heating process

After the 8 hours have passed

→ Decontamination **ENDS**

A.3. Start Isotherm

3.1 Close PIV1 (hit button) and after close the valve
→ End run →Chart (under run)

→ Stop decontamination

The first step will require opening the gas of choice

→ Hit stop again

→ Close

3.2 To set Temperature
In order to minimize the temperature time of the run, we can set the temperature first in the decontamination step and wait to stabilize at this temperature after the decontamination heating ends.

3.3 New Application Button
→ Pressure, flow, degas, water bath (static gas sorption)

*MFC keeps flow at maximum range

3.4 Pressure range → 20 bar
→ Hit Idle (Hand Symbol)

→ Setup → Static Isotherm → Turn gas ON

→ Setup → Isotherm → Static → Parameter → Edit Sequence → Set Temperature →ok → ok

→ Run → Isotherm → Static → [Name the run] →<Double check setup under [setup]>

3.5 End Status → must be @ outgas
Initial operation – begin sorption scans (Outgas temperature Set)

3.6 Double check setup → Temperature → continue → ok

A.4. Remove Sample

1. Run → End Chart
2. Change the temperature → 25^{o}C (rate 2^{o}C /min) → Start → Close
3. Change pressure to ambient → Stop outgas → Stop * 2 → Close
4. Remove sample (removing hand symbol) → Yes → Random → No
5. Go to atmospheric pressure → Open air admittance valve slowly (Takes a while)
6. Remove reactor → Ok

A.5. Obtain Data

1. Insert USB drive in the USB port
2. Explorer → My Computer → C: → IGAS → G200204 → Pull the last folders → Copy → flash drive

A.6. Data Analysis

1. Copy IGA run folder first on the computer for analysis
2. Put the same files and put them under the G200204 file
3. Open IGA software → Go to simulation
4. File → Verify all → Start verify → (Hit OK and Yes)
5. Hit Close
6. Start program in simulation mode
7. For static → Isothermal Replay → Find the sample → Check on Plot
8. We want the plot **weight vs. pressure** (weight = y axis, pressure = x axis)
9. Hit <Ok>
10. In static mode we need to account for the buoyancy mode
    Replay → reset sample mass → Automatic → Ok
11. File → Export → User Defined export → Add the following
    (min) Time

    (mg) Weight

    (mbar) Average pressure

    (^{o}C) Average Sample temperature

    --- % Mass

    (mmol/g) Concentration

    Hit export → Yes
12. Open from excel → Delimited → Spaces
13. Plot Concentration (mmol/g) as a function of pressure (mbar).

Appendix B (IGA Manual)

B.1. IGA Real Time Analysis

Isotherm determination requires measurement of the equilibrium uptake following a series of changes in the chemical potential (changes in gas pressure, humidity or the gas concentration). The time scale of the measurement depends on the molecular and thermal transport of the gas through the sample. We cannot directly measure the equilibrium uptake but rather must extrapolate this value or determine the best approximation.

The nature of the gas diffusion in the long time limit becomes a single exponential of the form $e^{-t/k}$ where k is a time constant. As the time scale increases it becomes less practical to wait long enough for the condition where the uptake is at equilibrium within the measurement accuracy. In this case, an analysis of the trend to derive the asymptote (e.g. of the long time limit exponential) is an appropriate method.

B.2. IGA Real Time Processor

The IGA real time processor uses least square regression of one of the two relaxation (diffusion) models in order to extrapolate a value of the asymptote and assess the time-scale of interaction. The measurement of the sorption-time curve involves inputting three parameters of run into the software (i) data logging interval (ii) minimum data collection time and (iii) maximum data collection time (timeout). Timeout is set by the practical constraints of the experimental run. For example, there is inevitably some time limit for a single isotherm point beyond which the experiment is using too much of machine time. When timeout expires, it can be either of the two situations (i) real time analysis has failed to make a prediction of the asymptote and (ii) the trend is analyzed at the timeout but the uptake has sufficiently not relaxed. In the next section, the two models used by IGA in making asymptotic uptake prediction are discussed.

B.2.1. The Linear Driving Force (LDF) Model

The LDF model of the relaxation u(t) is,

$$u(t) = u_o + \Delta u\left(1 - \exp\left(-\frac{[t - t_o']}{k}\right)\right) \qquad \text{Equation B-1}$$

B.2.2. Avrami's Model

$$u(t) = u_o + \Delta u(1 - \exp\left(-\frac{[t - t_o']^x}{k}\right)) \qquad \text{Equation B-2}$$

where u_0 is the uptake at the arbitrary time origin t_o', k is the exponential time constant and Δu is the change in uptake. The asymptotic uptake is then equal to $u_o + \Delta u$. Model curves using both the model are shown in Figure B-1. For x=1, the Avrami model reduces to LDF model.

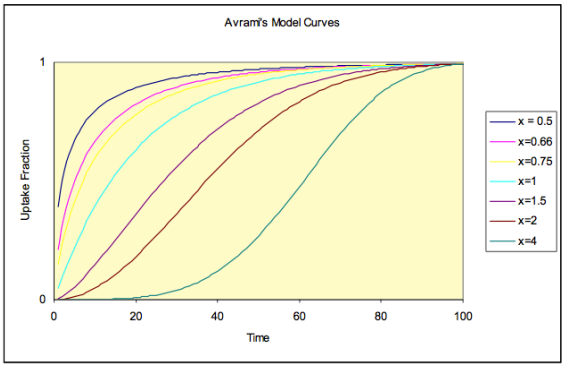

Figure B-1. Avrami's model curves for different x values. For x=1, it represents the uptake fraction predicted by LDF model.

Appendix C

C.1. Procedure to run a wet gas sorption test on IGA

(i) Loading of the sample and (ii) decontamination steps are similar to the steps reported for gas sorption isotherms in Appendix A.

C.2. Wet Gas Sorption Isotherm

1. Close PIV1. Then, end the chart
2. Stop the decontamination.
3. Increase the pressure to atmospheric pressure by opening the air admittance valve.
4. Close the air admittance valve.
5. Close the valve near the sample chamber
6. Now, open the green valve. (Do this very slowly. Keep checking for any increase in the pressure)
7. Now, slowly open the valve near the chamber (Also do this step very slowly. Keep checking for any increase in the pressure).
8. Set the pressure tab and pressure to 1000 mbar, set some flow rates, start and end it (the mass flow meters will kick in).
9. Open the nitrogen gas tank.
10. Start the chart.
11. Turn on the yellow heat transfer line.
12. Set the pressure to 1000 mbar using the pressure tab.
13. Set the total flow rate to 150 ml/min, RH = 20% (wet flow = 20%, dry flow= 80%).
14. Monitor the change in weight using the chart mode

C.3. Analysis of the Chart Data

The chart data collected at each RH is plotted as a scatter plot. The data points after the time where the pressure has reached to the set point are analyzed. The weight data points are averaged. The amount of wet gas absorbed in the sample is the difference in the average weight of the sample at 0% RH and that particular RH. This difference in average weight is converted into terms of concentration (mmol/g), which is plotted as a function of RH.

For example, in COOH functionalized SWNTs, the average weight of the sample at 0% RH is 55.9816247 mg (around 900 data points averaged) and at 20% RH is 56.8684949 mg

(around 900 data points averaged). The difference in weight is 0.88687021 mg, which in terms of concentration is 0.87964 mmol/g. Similarly, the values are calculated for 40%, 60%, 80% and 100% RH values, and plotted as an isotherm. Below is a plot obtained for water sorption in COOH functionalized SWNTs at 35 ^{0}C.

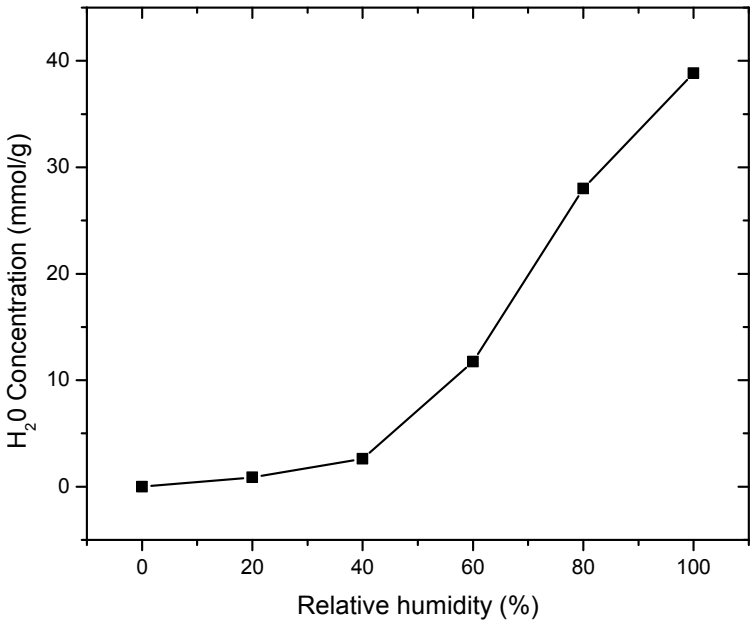

Figure C-1. Water Sorption in COOH functionalized SWNTs at 35 ^{0}C.

Appendix D

D.1. Estimation of the number of COOH groups on a functionalized SWNT

Let us consider a (11,11) SWNT for the estimation. For a (n,n) SWNT, following are the parameters of the nanotube[1]

Table D-1. Parameters of a (n,n) nanotube

Parameters	(n,n) nanotube	(11,11) nanotube
Diameter	$\sqrt{3}na/_{\pi}$	14.91 Å
Number of C atoms in a unit cell	4n	44
Length of a unit cell	a	2.46 Å
Circumference	$\sqrt{3}n$a	46.9 Å

Where a is the length of the unit vector, 2.46 Å.

The length of the CNT used in experiments is around 1000 nm. The diameter is around 1.5 nm, which is close to the diameter of (11,11) SWNTs. So, number of C atoms in one CNT is 44/0.246 nm×1000 nm = 1.79×10^{5} C atoms/CNT. Weight of the CNT is 12 amu×1.66×10^{-24}g/amu×1.79×10^{5} C atoms/CNT = 3.57×10^{-18} g/CNT.

The weight percentage of COOH groups = 5 wt% (2-7 wt% estimated from titration). Let the basis of the estimation be 100 g of CNTs. So, weight of COOH groups is 5 gm. Weight of only CNTs (excluding COOH groups) = 100 – 5 = 95 g. Number of CNTs in 100 g of functionalized COOH SWNTs = 95 g/ (3.57×10^{-18} g/CNT) = 2.66×10^{19} CNT per 100 g sample. Number of COOH molecules in 100 g sample = (5 g/(45 g/mol))×6.023×10^{23}molecules/mol = 6.69×10^{22} molecules of COOH per 100 g CNT sample. Hence number of COOH groups per CNT = 6.69×10^{22} molecules of COOH / 2.66×10^{19} CNT ≈ **2516 COOH groups per CNT**.

Number of C atoms on the circumference of an (n,n) nanotube end is 2n. A (11,11) CNT has 22 C atoms on the circumference and hence a maximum of 22 COOH groups on one end, totaling to **44 COOH groups** on both ends per CNT (assuming CNT is open on both ends). The previous number is well below the total number of COOH groups per CNT, which is 2516 groups per CNT. Hence the COOH groups are present not only on the open ends of the CNT but distributed all along the axial length of the CNT.

D.2. Estimation of the number of zwitterion groups on a functionalized SWNT

No titration reaction was performed to measure the weight concentration of zwitterion groups in functionalized SWNTs. However, XPS was performed measuring the atomic

percentages of C, O and N in the zwitterion functionalized SWNTs. These results were shown in Table 4-1. From the XPS results exclusively, the number of COOH and zwitterion functional groups in functionalized SWNTs is calculated in the following paragraphs.

In COOH functionalized SWNTs, for every 100 atoms of the sample, 87 are carbon atoms and 13 oxygen atoms (based on XPS atomic percentages). Each COOH group has two O atoms and hence 13/2 = 6.5 COOH groups for 87 C atoms. Total number of C atoms in a CNT from previous section is 1.79×10^5 C atoms/CNT. Let the number of COOH groups in a CNT is x. Number of C atoms in a CNT is 1.79×10^5 + x. Using proportionality, the value for x is calculated $\{87:6.5::(1.79\times10^5+x):x\}$. The number of COOH groups is **14×10^3 per CNT**. This number is larger than the value calculated in the previous section because XPS measures the concentration of atoms only in the top layer of the sample.

Similarly, the number of zwitterion functional groups in a CNT is calculated. In zwitterion functionalized SWNTs, for every 100 atoms of the sample, 77 are C atoms and 2 N atoms. Each zwitterion group has one nitrogen atom and hence 2 zwitterion groups per 77 C atoms. Let the number of zwitterion groups in a CNT be y. Using proportionality, the value of y is calculated. The number of zwitterion functional groups is **6×10^3 per CNT**. The number of zwitterion functional groups in a zwitterion functionalized SWNT is almost half of COOH groups in a COOH functionalized SWNT. This tells us that the yield of conversion of COOH groups in a COOH functionalized SWNT to zwitterions groups is lower than 100% (**around 43%**).

Appendix E : Journal Reuse Permissions

E.1. Figure 4 in Park, C. et al. Aligned single-wall carbon nanotube polymer composites using an electric field. J. Polym. Sci. B Polym. Phys. 44, 1751–1762 (2006).

JOHN WILEY AND SONS LICENSE TERMS AND CONDITIONS

Oct 17, 2012

This is a License Agreement between Anil Surapathi ("You") and John Wiley and Sons ("John Wiley and Sons") provided by Copyright Clearance Center ("CCC"). The license consists of your order details, the terms and conditions provided by John Wiley and Sons, and the payment terms and conditions.

All payments must be made in full to CCC. For payment instructions, please see information listed at the bottom of this form.

License Number	3011160582293
License date	Oct 17, 2012
Licensed content publisher	John Wiley and Sons
Licensed content publication	Journal of Polymer Science Part B: Polymer Physics
Book title	
Licensed content author	Cheol Park,John Wilkinson,Sumanth Banda,Zoubeida Ounaies,Kristopher E. Wise,Godfrey Sauti,Peter T. Lillehei,Joycelyn S. Harrison
Licensed content date	May 8, 2006
Start page	1751
End page	1762
Type of use	Dissertation/Thesis
Requestor type	University/Academic
Format	Print and electronic
Portion	Figure/table
Number of figures/tables	1
Number of extracts	
Original Wiley figure/table number(s)	Figure 4
Will you be translating?	No
Order reference number	
Total	0.00 USD
Terms and Conditions	

TERMS AND CONDITIONS

This copyrighted material is owned by or exclusively licensed to John Wiley & Sons, Inc. or one of its group companies (each a "Wiley Company") or a society for whom a Wiley Company has

E.2. Figure 1 in Graupner, R. Raman spectroscopy of covalently functionalized single-wall carbon nanotubes. Journal of Raman Spectroscopy 38, 673–683 (2007).

JOHN WILEY AND SONS LICENSE TERMS AND CONDITIONS

Oct 17, 2012

This is a License Agreement between Anil Surapathi ("You") and John Wiley and Sons ("John Wiley and Sons") provided by Copyright Clearance Center ("CCC"). The license consists of your order details, the terms and conditions provided by John Wiley and Sons, and the payment terms and conditions.

All payments must be made in full to CCC. For payment instructions, please see information listed at the bottom of this form.

License Number	3011170679328
License date	Oct 17, 2012
Licensed content publisher	John Wiley and Sons
Licensed content publication	Journal of Raman Spectroscopy
Book title	
Licensed content author	R. Graupner
Licensed content date	Feb 14, 2007
Start page	673
End page	683
Type of use	Dissertation/Thesis
Requestor type	University/Academic
Format	Print and electronic
Portion	Figure/table
Number of figures/tables	1
Number of extracts	
Original Wiley figure/table number(s)	Figure 1
Will you be translating?	No
Order reference number	
Total	0.00 USD
Terms and Conditions	

TERMS AND CONDITIONS

This copyrighted material is owned by or exclusively licensed to John Wiley & Sons, Inc. or one of its group companies (each a "Wiley Company") or a society for whom a Wiley Company has exclusive publishing rights in relation to a particular journal (collectively WILEY"). By clicking "accept" in connection with completing this licensing transaction, you agree that the following